

# **Study on Monitoring and Control of Cutting Processes Based on Sensor Information**

**Hiroo OZEKI**

**Study on Monitoring and Control of Cutting Processes Based on Sensor Information**

**Hiroo OZEKI**

**Nagoya University**  
**Graduate School of Engineering**

**Study on Monitoring and Control of Cutting  
Processes Based on Sensor Information**

**A dissertation submitted for the degree of Doctor of Philosophy**

**Development of Mechanical Science and Engineering**

**Hiroo OZEKI**



# Study on Monitoring and Control of Cutting Processes Based on Sensor Information

Hiroo OZEKI

## **Abstract**

This dissertation deals with monitoring and control technologies based on sensor information for milling and drilling processes, in order to provide bases for intelligent machining systems which can automatically recognize the state of the machining process and cope with unforeseen changes in the process or troubles in machining.

First, a sensor system based on the magnetostrictive effect which is installed in a tool holder for measuring cutting torque is proposed, in order to monitor the milling and drilling processes. Changes in the magnetic permeability of ferromagnetic alloy layers formed onto a rotating shaft due to torque are detected by coils as changes in impedance without contacting the rotating shaft. By mounting the magnetostrictive sensor on a tool holder, it has become possible to detect cutting torque as close to the cutting point as possible. The accuracy of the proposed sensor system is confirmed through static and dynamic evaluation tests. In order to investigate the relationship between tool failure and cutting torque, milling and drilling tests were carried out. As the results, the possibility of estimating flank wear during the milling process from cutting torque detected by the proposed sensor system has been recognized, as the maximum value of the cutting torque per revolution increased with increases in flank wear. Also, the possibility of estimating tool fracture during the milling process from cutting torque detected by the proposed sensor system has been recognized because the difference in the values of the maximum cutting torque generated by the two cutting edges consisting of a cutting tool increased when a tool fractured. In addition, a method for detecting tool fracture during drilling process is proposed using the frequency component caused by the spindle speed included in the cutting torque as an index. Also, a method for estimating abnormal drilling state caused by tool wear is proposed using the standard deviation and the mean value of the cutting torque as indexes, and the validity of the proposed method is confirmed through continuous drilling tests. In addition, we have proposed a monitoring system for cutting processes, which has not only monitoring

functions of cutting processes but also unique database functions to assist in developing the monitoring algorithms.

Next, to realize defect-free cutting of difficult-to-cut materials, namely, borosilicate glass and carbon fiber reinforced plastic (CFRP) composites, we propose to apply feedback control based on cutting force, because the degree of thrust force is directly related to the occurrence of machining defects. Therefore, we have developed a machining system which can be operated at a predetermined cutting force by changing the feed rate based on cutting force signals measured by a piezoelectric cutting dynamometer, and the basic performances of the developed system have been confirmed through evaluation tests. Subsequently, cutting tests with the developed system were performed, in order to consider the possibility of defect-free cutting of borosilicate glass and CFRP composites with feedback control based on cutting force. Based on the results of drilling tests when making through-holes on plates of borosilicate glass, we have verified that, under specific conditions, multistage thrust-force control can machine through-holes without significant cracks at the circular edge consists of the exit surface or at the side of the machined hole. We also have confirmed, under specific conditions through drilling tests of CFRP composites, that the feedback control process can machine through-holes without causing significant machining defects on CFRP composites. In the drilling tests, we used a conventional twist drill, and the work-piece was a quasi-isotropic laminate composite, which is a stack of unidirectional plies consisting of high-strength carbon fibers T800S and high-toughness matrix resin 3900-2b.

# Contents

<b>Abstract</b>	<b>1</b>
<b>List of figures and tables</b>	<b>7</b>
<b>1. Introduction</b>	<b>13</b>
1.1 Demands for machining	13
1.2 Intelligent machining system for cutting	14
1.2.1 Sensors for monitoring and control	16
1.2.2 Monitoring and control technologies	18
1.3 Machining of difficult-to-cut materials	20
1.3.1 Borosilicate glass	20
1.3.2 Carbon fiber reinforced plastic (CFRP) composites	22
1.4 Aim of this research	24
1.5 Overview of this dissertation	25

<b>2. Development of magnetostrictive torque sensors for cutting process monitoring</b>	<b>29</b>
2.1 Objectives	29
2.2 Magnetostrictive torque sensor	30
2.2.1 Magnetostrictive effect	30
2.2.2 Sensor structure	31
2.2.3 Development of sensor systems	33
2.3 Evaluation of the developed sensor systems	36
2.3.1 Experimental setup	36
2.3.2 Static evaluation of the sensor system	38
2.3.3 Dynamic evaluation of the sensor system	40
2.4 Summary of this chapter	45
<b>3. Monitoring of cutting processes with the developed sensor systems</b>	<b>47</b>
3.1 Objectives	47
3.2 Monitoring of end-milling process	48
3.2.1 Experimental methodology	48
3.2.2 Estimating tool wear from the sensor signals	49
3.2.3 Detecting tool fracture from the sensor signals	49
3.3 Monitoring of drilling process	54
3.3.1 Experimental procedure	54
3.3.2 Estimation of abnormal drilling state caused by tool wear	55
3.3.3 Detection of tool fracture	62
3.4 Development of a monitoring system for cutting processes	65

3.5 Summary of this chapter	69
<b>4. Development of a machining system with feedback control based on cutting force</b>	<b>71</b>
4.1 Objectives	71
4.2 System structure	72
4.3 System performance evaluation	75
4.4 Summary of this chapter	81
<b>5. Drilling of borosilicate glass with the developed machining system</b>	<b>83</b>
5.1 Objectives	83
5.2 Experimental methodology	84
5.3 Force control of cutting processes with the developed machining system	85
5.3.1 Drilling process with a twist drill	85
5.3.2 Drilling process with a ball-end mill	88
5.3.3 Milling process with a ball-end mill	93
5.4 Through-hole drilling with multistage force control	93
5.4.1 Investigation of crack generation during blind-hole drilling	95
5.4.2 Examination of through-hole drilling with multistage force control	100
5.6 Summary of this chapter	101
<b>6. Drilling of carbon fiber reinforced plastic composites with the developed machining system</b>	<b>105</b>

6.1 Objectives	105
6.2 Work-piece material	106
6.3 Experimental procedure	107
6.4 Examination to reduce machining defects on the exit surface	109
6.4.1 Methodology for controlling thrust force	109
6.4.2 Behavior of thrust force during the drilling process	114
6.4.3 Relationship between cutting speed and the quality of the machined hole	117
6.4.4 Effect of thrust force on the quality of the machined hole	118
6.4.5 Effect of thrust force on the quality of the machined hole	120
6.5 Investigation to prevent machining defects on the entry and exit surfaces	121
6.6 Summary of this chapter	125
<b>7. Conclusions</b>	<b>127</b>
7.1 Summary	127
7.2 Future work	130
<b>Acknowledgement</b>	<b>133</b>
<b>References</b>	<b>135</b>
<b>List of accomplishments</b>	<b>147</b>

## List of figures and tables

Figure 1.1	Key technologies and benefit	15
Figure 1.2	Expectations for intelligent machining systems	16
Figure 1.3	Machining process disturbances to be detected	17
Figure 1.4	Typical machining defects on CFRP laminates	22
Figure 1.5	Motivation – Needs from industry for monitoring and control of cutting processes	25
Figure 1.6	Overview of this dissertation	27
Figure 2.1	Magnetostrictive effect	31
Figure 2.2	Structure of the magnetostrictive torque sensor	32
Figure 2.3	Cancellation of the influence of axial force and radial force	33
Figure 2.4	Structure of the developed sensor system	35
Figure 2.5	Photograph of the developed sensor system	36
Figure 2.6	Experimental setup to evaluate the sensor system	37
Figure 2.7	Result of static calibration test	39
Figure 2.8	Influence of radial force on the sensor signal	39
Figure 2.9	Influence of axial force on the sensor signal	39
Figure 2.10	Behavior of the cutting torque during the spot facing as detected by the proposed sensor system and by the dynamometer	42

Figure 2.11	Setup for dynamic experiment	43
Figure 2.12	Result of dynamic torque evaluation experiments	43
Table 2.1	Machining conditions	44
Figure 2.13	Behavior of the cutting torque during the side-milling detected by the proposed sensor system	44
Figure 2.14	Result of side-milling experiments	45
Table 3.1	Cutting conditions	48
Figure 3.1	Behavior of the cutting torque during the process (Tool diameter = 15 mm)	50
Figure 3.2	Relationship between flank wear and the maximum value of the cutting torque	51
Figure 3.3	Fractured cutting edge of the end mill	52
Figure 3.4	Change in the behavior of the cutting torque caused by tool fracture (Tool Diameter = 15 mm)	53
Figure 3.5	Result of the measurements of the maximum cutting torque indicated by the two cutting edges using an artificially fractured tool and normal tool	54
Table 3.2	Characteristics of the sensor system	55
Figure 3.6	Examples of cutting torque in continuous drilling test	56
Figure 3.7	Standard deviation of cutting torque vs. hole No.	57
Figure 3.8	Mean value of cutting torque vs. hole No.	57
Figure 3.9	Distribution curve of cumulative frequency	59
Table 3.3	Coefficient of discrimination	59
Figure 3.10	Function $Y(x)$ of indexes	60
Figure 3.11	Relationship between final index $Z$ and hole No.	61
Table 3.4	Result of evaluation tests for the proposed method	61
Table 3.5	Drilling conditions	62
Figure 3.12	Fractured cutting edge of the drill	62

Figure 3.13	Change in the behavior of the cutting torque caused by tool fracture	63
Figure 3.14	Results of FFT analysis	64
Figure 3.15	Relationship between number of holes and power spectrum	64
Figure 3.16	Structure of the developed monitoring system for cutting processes	65
Figure 3.17	Software structure of the developed monitoring system	67
Figure 3.18	Conceptual diagram of interchangeable monitoring module	67
Figure 3.19	Graphical user interface of monitoring system for detecting tool fracture in the end-milling process	68
Figure 3.20	Graphical user interface of monitoring system for estimating tool fracture in the drilling process	68
Figure 4.1	Structure of the developed machining system	73
Figure 4.2	Appearance of the developed machining system	73
Figure 4.3	Comparison of the feedback loops between the developed system and conventional systems	74
Figure 4.4	Methodology for controlling the developed system	74
Figure 4.5	Measurement result of the natural frequency of the Z-axis drive mechanism	77
Figure 4.6	Result of the force operation test	77
Figure 4.7	Result of the transient response test	78
Figure 4.8	Evaluation of the system stability at a constant thrust force	79
Table 4.1	Results of the system stability evaluation under varying conditions	80
Figure 4.9	Relationship between the ratio of external force to controlled thrust force and the control error	81
Table 5.1	Specifications of the borosilicate glass	84
Figure 5.1	Experimental setup	85
Figure 5.2	Behaviors of thrust force and displacement in the drilling process when making a blind-hole with the drill	86

Figure 5.3	Machined blind-hole with the drill	87
Figure 5.4	Machined through-hole with the drill	88
Figure 5.5	Behaviors of thrust force in the processes when making through-holes with the ball-end mill	89
Figure 5.6	Machined through-holes with the ball end mill viewed from the bottom of the work-piece	91
Figure 5.7	Machined through-hole using feed control with the ball end mill viewed from the bottom of the work-piece (Feed rate at 3 mm/min, step-feed method)	91
Table 5.2	Results of drilling tests with ball-end mills	92
Figure 5.8	Behaviors of cutting forces in the milling process	94
Figure 5.9	Machined grooves with the ball-end mill	95
Figure 5.10	Result of the drilling test when the remaining thickness after the drilling was 0.10 mm	98
Figure 5.11	Result of the drilling test when the remaining thickness after the drilling was 0.05 mm	99
Table 5.3	Observational results of machined holes under varying conditions	99
Figure 5.12	Flow of multistage thrust-force control	101
Figure 5.13	Result of the drilling test with the multistage thrust-force control	102
Table 6.1	Mechanical properties of the work-piece material	107
Table 6.2	Drilling conditions	108
Figure 6.1	Experimental setup	108
Figure 6.2	Schematic view of delamination in CFRP composites due to drilling	112
Figure 6.3	Circular plate model for delamination analysis	112
Figure 6.4	Correlation between the uncut depth $h$ and the calculated critical thrust force $F_{crit}$	113

Figure 6.5	Minimum value of the thrust force to generate a hole (Cutting speed: 56.5 m/min.)	113
Figure 6.6	Flow of thrust force control in the drilling process	114
Figure 6.7	Behavior of thrust force during the drilling process (Cutting speed: 56.5 m/min.)	115
Figure 6.8	Schematic view of the cutting mechanism of CFRP composites per single ply	116
Table 6.3	Relationship between cutting speed and the quality of the machined hole	118
Figure 6.9	Optical micrographs and X-ray photographs of the machined holes viewed from the drill-exit surfaces	119
Figure 6.10	Machined hole viewed from the drill-exit surface (Thrust force for the fifth step: at a constant 20 N, Cutting speed: 169.6 m/min.)	120
Figure 6.11	Machined hole viewed from the drill-exit surface (Work-piece: Unidirectional laminate composites, Cutting speed: 56.5 m/min.)	121
Figure 6.12	Fig. 6.12 Influence of thrust force control on delamination factor $D_f$	123
Figure 6.13	Thrust force control for preventing machine defects on the entry and exit surfaces	123
Figure 6.14	Machined hole viewed from the both surfaces of CFRP composites	124
Figure 6.15	Relationship between the number of machined holes and cutting time	125
Figure 6.16	Machined holes viewed from the drill-exit surfaces	125



# **1. Chapter 1**

## **Introduction**

### **1.1 Demands for machining**

Machining is one of the most traditional and basic but yet important processes to manufacture goods not only for industrial use but also consumer use. In order to cope with recent changes in the needs from customers toward various products, it has been required for the manufacturers to improve the quality of products, to reduce the cost of manufacturing, to decrease the time for development and manufacturing of new products and to improve the efficiency of manufacturing. It is for such reasons that improvement in the machining process and also the machine tool functions is required these days [1].

The machines and tools for machining were invented originally to assist human operations to manufacture the artifacts. The machine tools have been given higher accuracy and greater power which are far beyond the ability of humans, and hence the

machine tools have been required to perform functions faithfully according to the order of the human operators. At present, the machine tools are required to have still higher abilities so that some of machine tools can take the place of the humans. The machine tools are required to possess the abilities which are peculiar to the human being, such as the intelligence. Human operators take actions in order to optimize their behaviors by utilizing the intelligence or the information processing functions based on the information sensed by their own sensors, namely, eyes, ears, hands and so on. The machine tools have been given motion performing functions technologically so far, and the machine tools now need reliable sensors to obtain necessary information and the intelligence to determine the actions on their own [2].

## **1.2 Intelligent machining system for cutting**

The importance of developing more efficient and accurate machining systems has been attracting growing interest. A shortage of skilled operators in recent years is accelerating the need to make machining systems more autonomous. In order to meet such demands, intelligent machining systems which can automatically recognize the state of the machining process and cope with unforeseen changes in the process or troubles in machining, have been proposed by Moriwaki [3, 4] and other engineers. To realize these systems, it is necessary to monitor the state of the machining process, which requires sensors that can provide information about the state of the machining process. In addition, signal processing strategies, which can detect disturbances in the machining process and can determine the best actions automatically based on signals from each sensor, are needed. The key technologies to realize the intelligent machining systems and the benefits when the systems are developed are summarized in Fig. 1.1 [5].

On the other hand, expectations for intelligent machining systems, based on the result of a survey, are shown in Fig. 1.2 [6]. The survey has been conducted on major machine tool builders and end users in Europe, the USA, Canada and Japan, and the number of responses is 49 in total. The responses to the questionnaires showed that the intelligent machining systems are in line with the current industrial needs in the different regions. Accordingly, the development of the intelligent machining systems is thought of as one of effective strategies for contributing to the future growth of the manufacturing industry.

The present study is aimed at establishment of advanced technologies related to the monitoring and the control of cutting processes, in order to provide a basis for the intelligent machining systems for cutting. This is because cutting takes an important role to manufacture various kinds of products. In the following subsections, therefore, the conventional researches related to the sensors and signal processing strategies for monitoring and/or for controlling cutting processes are presented.

Key Technologies	Benefits
<ul style="list-style-type: none"> <li>- Sensors for tool condition monitoring</li> <li>- Fusion of sensor information</li> <li>- Prediction and identification of machining processes</li> <li>- In-process control and intelligent response strategies</li> <li>- Storage and utilization of experience</li> </ul>	<ul style="list-style-type: none"> <li>- Accuracy, reliability and minimum malfunction</li> <li>- Maximum utilization of machine tool capacity</li> <li>- Multiplication of skilled operators' capability</li> <li>- Extension of unskilled operators' capability</li> <li>- Facilitate machining technology transfer</li> <li>- Comfortable working environments</li> <li>- Support environmental preservation</li> </ul>

Fig. 1.1 Key technologies and benefit

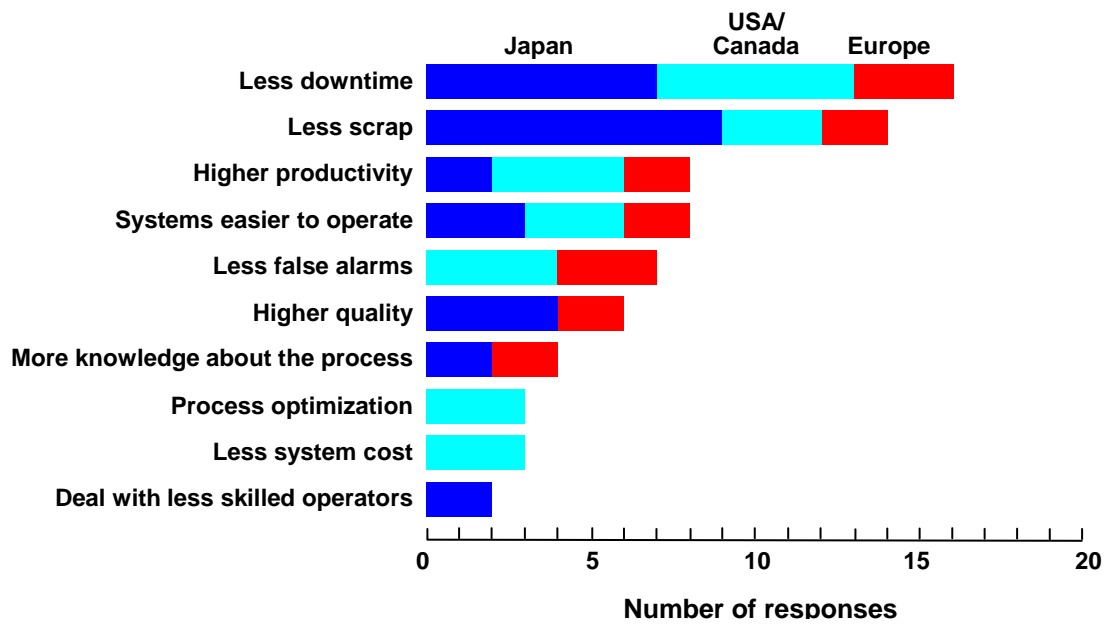


Fig. 1.2 Expectations for intelligent machining systems

### 1.2.1 Sensors for monitoring and control

The intelligent machining systems require sensors which can provide informative signals about the state of the machining process. According to the results of a survey regarding tool-condition monitoring, customers have especially demanded reliable sensors and signal transmission techniques in systems to detect tool wear and tool breakage, as shown in Fig. 1.3 [6]. In addition, the measurement accuracy, engineering adaptability and economic efficiency are required for the sensors [7].

Many researchers have been used various sensors for measuring cutting force, cutting torque, vibration, acoustic emission, tool temperature and so on for tool condition monitoring in cutting processes. In addition to the sensors, miscellaneous methods such as ultrasonic, optical and spindle motor current measurements have been proposed [8].

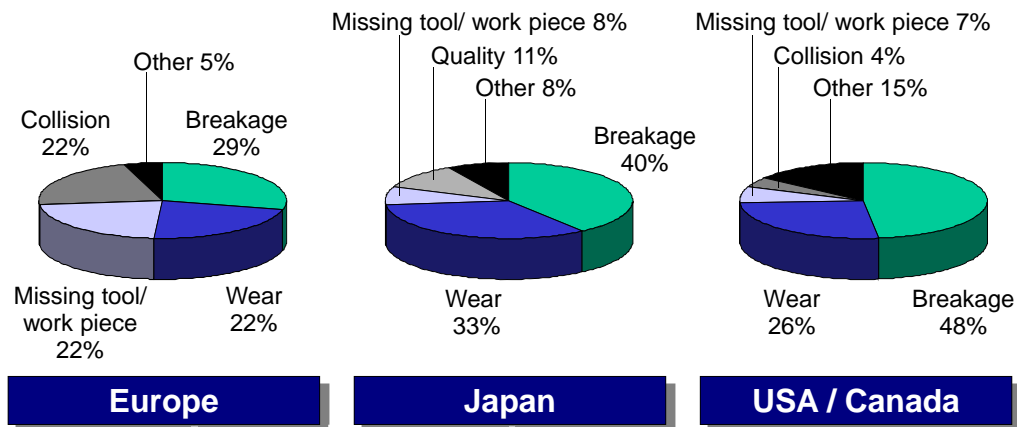


Fig. 1.3 Machining process disturbances to be detected

By mounting a sensor in a position which is located as close to the cutting point as possible, the reliability of detecting the information related to the state of the machining process will be improved. Hence, various methods have been proposed to directly detect the cutting forces of cutting tools in the milling and drilling processes: with a strain-gauge using FM wave transmission [9]; with a strain-gauge using optical data transmission [10]; with a piezoelectric sensor using electromagnetic data transmission [11, 12], etc. These methods are suited to laboratories. However they are difficult to use on practical production machine tools because sensor systems applying these methods become complicated by several built-in devices such as apparatus to receive electric power (or batteries), transmitters and signal-processing circuits.

Torque sensors that use coils to detect changes in the magnetic permeability of ferromagnetic alloy materials caused by torque have a great advantage because it is possible to detect torque in a rotating body without electronic contact. By utilizing this phenomenon, Brinksmeier suggested an eddy current torque sensor utilizing changes in

the magnetic permeability of the tool itself for monitoring the drilling process [13]. Since this type of sensor is very sensitive in respect to changes in the distance between the coils and the measured drill shank, it is necessary to average the output signals of the sensor in order to remove the influence of rotation eccentricity. In other words, the behavior of the cutting torque during one revolution cannot be dynamically observed by this sensor system. Sasada et al. proposed that torque could be detected by using magnetic anisotropy from the shape of a twist drill [14, 15]. This methods, however, has drawbacks to practical cutting torque measurement, since it is necessary to calibrate the output signal when the tool is changed.

### **1.2.2 Monitoring and control technologies**

In the 1950s, Massachusetts Institute of Technology had developed a numerical control (NC) milling machine, and the invention of the NC technique has provided rapid progress in manufacturing industry [16, 17]. NC machine tools can control own positions with a high degree of accuracy based on predetermined sequences, but cannot adjust the movement generally when unforeseen changes in the process or troubles in machining occur. Consequently, monitoring technologies to recognize the state of the machining process and control technologies to cope with unforeseen changes in the process or troubles in machining are being required as mentioned above.

Aiming to realize tool condition monitoring, various effective approaches with acoustic emission (AE) sensors have been done in turning processes [18 – 21], in milling processes [21 – 25] and in drilling processes [25, 26]. These approaches, however, are not suitable for the tool condition monitoring when unforeseen states such as the tangle of chips on a cutting tool, chip packing, etc. occur. This is because the AE

sensor can measure the wideband frequency of elastic waves due to material deformation and crack generation in materials [27], but both the occurrence of tool failure and the deformation of chips emit the elastic waves. So that, it is difficult to monitor tool failure while the tangle of chips on a cutting tool and chip packing exist. Other approach is to use the current or power measurement of driving motors current. For example, Szecsi proposed a DC motor based cutting tool condition monitoring system. However, the developed and trained monitoring system is able to define the average flank wear of the cutting tools with an accuracy of  $\pm 0.2$  mm in about 80% of the situations [28]. In addition, various types of vision-based tool condition monitoring systems are proposed, but current vision sensors, namely, CCD cameras can only be used between cutting cycles [29].

To regulate the state of cutting process, many past works on control of cutting force have been conducted [30, 31]. For example, Ibaraki proposed a long-term control scheme of cutting forces to regulate tool life in end milling processes [32]. The cutting force is monitored only at every "check point" set on the tool path, and the cutting force is controlled based on the point-to-point cutting forces. But the effectiveness of the proposed control approach is only for homogeneous materials such as hardened steel. Kim presented a control system that increases the metal-removal rate, while maintaining a constant cutting force using motor currents as indirect force sensors [33]. The control methodology with fuzzy-logic algorithm is simple design, but the overshoot of the controlled cutting force is large when the area of cutting cross-section is changed. Kakinuma studied the cutting force control method using information of both current reference and position encoder, to realize monitoring and adaptive control of cutting process without force sensor [34]. The proposed method can control cutting force

accurately, but this method needs high-accuracy position encoder.

To achieve the monitoring and/or control of cutting processes based on the information about the state of the process, one of the most effective and reliable sensors are force and torque sensors, since the degrees of cutting force and torque are directly related to the mechanics of the cutting process [35]. From the results of previous researches, it has been widely established that cutting force and/or torque can be correlated to tool failure [36 – 56].

## **1.3 Machining of difficult-to-cut materials**

In this dissertation, we propose to apply feedback control based on cutting force, in order to realize defect-free cutting of difficult-to-cut materials. As work-pieces to examine the effectiveness of the proposed approach, we used two kinds of difficult-to-cut materials, namely, borosilicate glass and carbon fiber reinforced plastic (CFRP) composites. The reason why we selected the materials for the investigation and the previous studies which deal with the machining of glass and CFRP are described below.

### **1.3.1 Borosilicate glass**

Borosilicate glass is becoming an important material for lab-on-a-chip devices, which are a subset of micro-electrode mechanical systems (MEMS) devices and often indicated by micro total analysis systems (TAS). This is because of properties like its high thermal and chemical resistance, its excellent transparency and its good surface quality. In addition, it is possible to connect between a silicon wafer and the borosilicate glass by using the anodic bonding technique [57 – 59]. The flow channels on the

substrate of lab-on-a-chip device consist of holes and grooves on a glass plate that are generally fabricated by a chemical etching process [60 – 62] or powder blasting process [63]. Recently, hole-making methods with laser ablation have been demonstrated [64 – 66]. However, these processes are unsuitable for making highly accurate flow channels with cross-sections of three-dimensional geometry, because it is difficult to control the cross-sectional shape in depth direction. Moreover, from the point of view of environmental protection, the chemical etching process is not recommended.

Many engineers agree that the cutting process is one of the most effective methods for manufacturing flow channels on a glass plate, since the cutting process can make flow channels of three-dimensional geometry without any chemicals. Also, flow channels are produced by the cutting process with high form accuracy and surface quality in a short machining time. However, it is difficult to machine glass under stable cutting conditions at all times because glass, being a hard and brittle material, is sensitive to such problems as progressive tool wear. In addition, machining defects, such as cracks at the machined surface occur frequently during this kind of process. This is because the fracture-toughness value of glass is low compared to that of other hard and brittle materials such as ceramics and so on [67, 68]. In fact, the fracture-toughness value  $K_{IC}$  of borosilicate glass is only approximately  $1.1 \text{ MPa}\sqrt{\text{m}}$  [69].

Various effective methods have been proposed to machine holes and grooves on glass plates with cutting tools. For example, ultrasonic vibration aided cutting was proposed by Moriwaki, Shamoto, et al., [70, 71] and Lee et al. [72]. In addition, a machining method that combines electrical-discharge machining (EDM) and ultrasonic vibration machining was suggested by Yan et al. [73]. Matsumura et al., proposed glass cutting

with a tilted ball-end milling cutter made from carbide with a ceramic coat [74 – 77]. Iizuka discussed the possibility of ductile-mode cutting for glass by utilizing a fly cutting technique [78, 79]. Mizobuchi et al. suggested helical drilling to fabricate through-holes on glass plates using an electroplated diamond tool, which has a special shape to grind from the bottom side of the glass plate [80, 81]. These methods, however, are not suitable for unusual states of tool condition, such as when tool wear has occurred.

### 1.3.2 Carbon fiber reinforced plastic (CFRP) composites

Due to such unique properties as high-specific strength, high-specific stiffness, and so on, carbon fiber reinforced plastic (CFRP) composites are becoming more and more widely used in the aerospace industry [82 – 85]. Holes must be drilled on component parts made of CFRP composites, to allow for riveting and fastening structural assemblies [86]. Currently, drilling with the use of a cutting tool is one of the most commonly applied processes [87, 88]. However, as shown in Fig. 1.4, machining

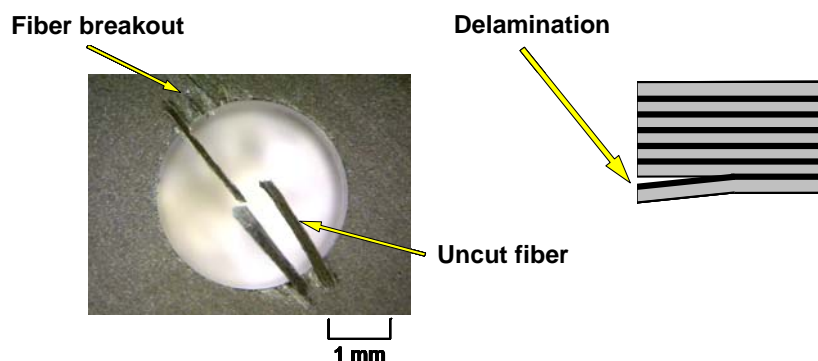


Fig. 1.4 Typical machining defects on CFRP laminates

defects caused by delamination occur frequently during this kind of process [89]. These machining defects bring about strength reduction of the CFRP composites and the use of fastener components adversely affects assembly [90]. Therefore, such machining defects must be avoided in the drilling process.

Aiming to reduce the occurrence of delamination in the drilling processes and to obtain satisfactory machined surfaces, tool geometry/material and cutting parameters are the key factors [91]. Many researchers have proposed various types of tool geometry and the cutting tests have been carried out under different cutting parameters. Hocheng and Tsao presented drilling of CFRP composites with the use of twist drill, saw drill, candle stick drill, core drill, step drill [92 – 95] and various compositely-shaped tools—which are combinations of two types of drills—namely, step-core-twist drill, step-core-saw drill and step-core-candlestick drill [96]. In addition, Hocheng and Tsao analyzed the effects of the eccentricity of drills [97, 98], pilot hole [99] and exit back-up [100] on the occurrence of the delamination. Durão et al.[101] and Gaitonde et al. [102] studied different drill point geometries and feed rates for CFRP composite drilling. Davim and Reis discussed a new comprehensive approach for selecting cutting parameters in order to achieve damage-free drilling based on a combination of Taguchi's techniques and on the analysis of variance [103, 104]. One of the other approaches is to apply a vibration-assisted drilling technique that has been presented by Wang et al. [105, 106]. All of the above studies have focused attention on the reduction of the thrust force during the drilling processes. This is because the size of the delamination zone has been shown to be related to the thrust force developed during the drilling process and it is believed that there is a "critical thrust force" below which no damage occurs [86, 107].

## 1.4 Aim of this research

Various types of effective monitoring and control technologies based on sensor information for cutting processes have been proposed by many researchers as mentioned above. In spite of having useful strategies, the technologies are not being utilized generally. This is because the technologies including sensors, which provide informative signals about the state of the process, still have disadvantages in terms of the reliability and the economic efficiency [1\_16].

The present study is aimed at establishment of more efficient technologies for monitoring and controlling cutting process, which is playing the major role in the general machining processes, in order to improve the quality of products, to reduce the cost of manufacturing and to improve the efficiency of manufacturing, as shown in Fig. 1.5.

First, a sensor system based on the magnetostrictive effect which is installed in a tool holder for measuring cutting torque has been proposed, in order to monitor the milling and drilling processes. The torque sensor that uses coils to detect changes in the magnetic permeability of ferromagnetic alloy materials caused by torque has a great advantage because it is possible to detect torque in a rotating body without electronic contact. By mounting the magnetostrictive sensor on a tool holder, it has become possible to detect cutting torque as close to the cutting point as possible. Subsequently, to investigate the possibility of tool failure monitoring from cutting torque measured by the proposed sensor system, we have performed milling and drilling tests.

Next, we have proposed to apply feedback control based on cutting force, in order to realize defect-free cutting of difficult-to-cut materials. This is because the degree of cutting force is directly related to the occurrence of machining defects on the

difficult-to-cut materials. Therefore, we have developed a machining system which can be operated at a predetermined cutting force by changing the feed rate based on cutting force signals measured by a piezoelectric cutting dynamometer. In addition, in order to consider the possibility of the difficult-to-cut materials with feedback control based on cutting force, cutting tests with the developed system have been carried out. As work-pieces to examine the effectiveness of the proposed approach, we use two kinds of difficult-to-cut materials, namely, borosilicate glass and carbon fiber reinforced plastic (CFRP) composites.

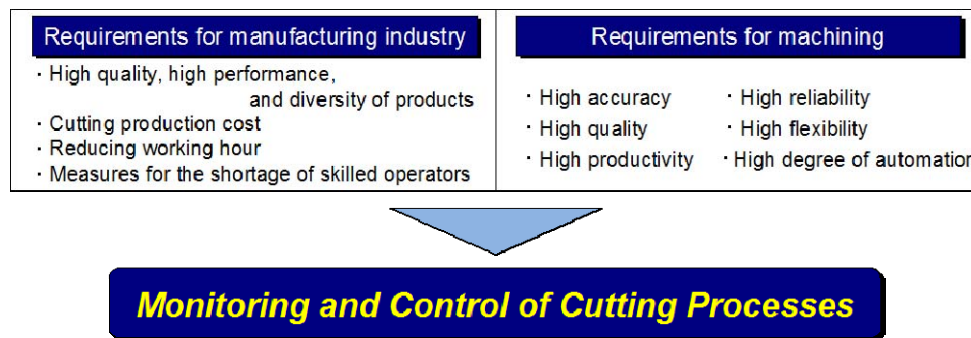


Fig. 1.5 Motivation – Needs from industry for monitoring and control of cutting processes

## 1.5 Overview of this dissertation

This dissertation consists of seven chapters as shown in Fig. 1.6, in order to provide the bases of monitoring and control technologies based on sensor information for cutting processes. The outline of this dissertation is described as follows.

In chapter 2, a method for detecting cutting torque by utilizing the magnetostrictive

effect and a sensor system to realize the method are proposed. In addition, the proposed sensor system installed a magnetostrictive torque sensor in a tool holder is developed, and the performance of the sensor system is confirmed through static and dynamic evaluation tests.

In chapter 3, the possibility of estimating tool wear and tool fracture detection from the cutting torque measurement with the developed sensor system is discussed. Also, methods to detect tool fracture and to estimate abnormal drilling state caused by tool wear according to cutting torque obtained from the developed sensor system are proposed. In addition, we have proposed a monitoring system for cutting processes, which has not only monitoring functions of cutting processes but also unique database functions to assist in developing the monitoring algorithms.

In chapter 4, we have developed a machining system which can be operated at a predetermined cutting force by changing the feed rate based on cutting force signals measured by a piezoelectric cutting dynamometer. In addition, the basic performances of the developed system have been confirmed through evaluation tests.

In chapter 5, to realize defect-free cutting of borosilicate glass, we propose to apply feedback control based on cutting force, since cutting force is directly related to the mechanics of the cutting process [28]. By conducting drilling and milling tests with the developed machining system, we have investigated the possibility of borosilicate-glass cutting with feedback control based on cutting force.

In chapter 6, we propose an approach to apply feedback control based on thrust force, in order to realize defect-free drilling of CFRP composites. In addition, by conducting drilling tests with the developed machining system, we have investigated the possibility of defect-free drilling of CFRP composites with feedback control based on thrust force.

In the drilling tests, we used a conventional twist drill, and the work-piece was a quasi-isotropic laminate composite, which is a stack of unidirectional plies consisting of high-strength carbon fibers T800S and high-toughness matrix resin 3900-2b.

In chapter 7, this dissertation is concluded with a brief summary and the future work is discussed.

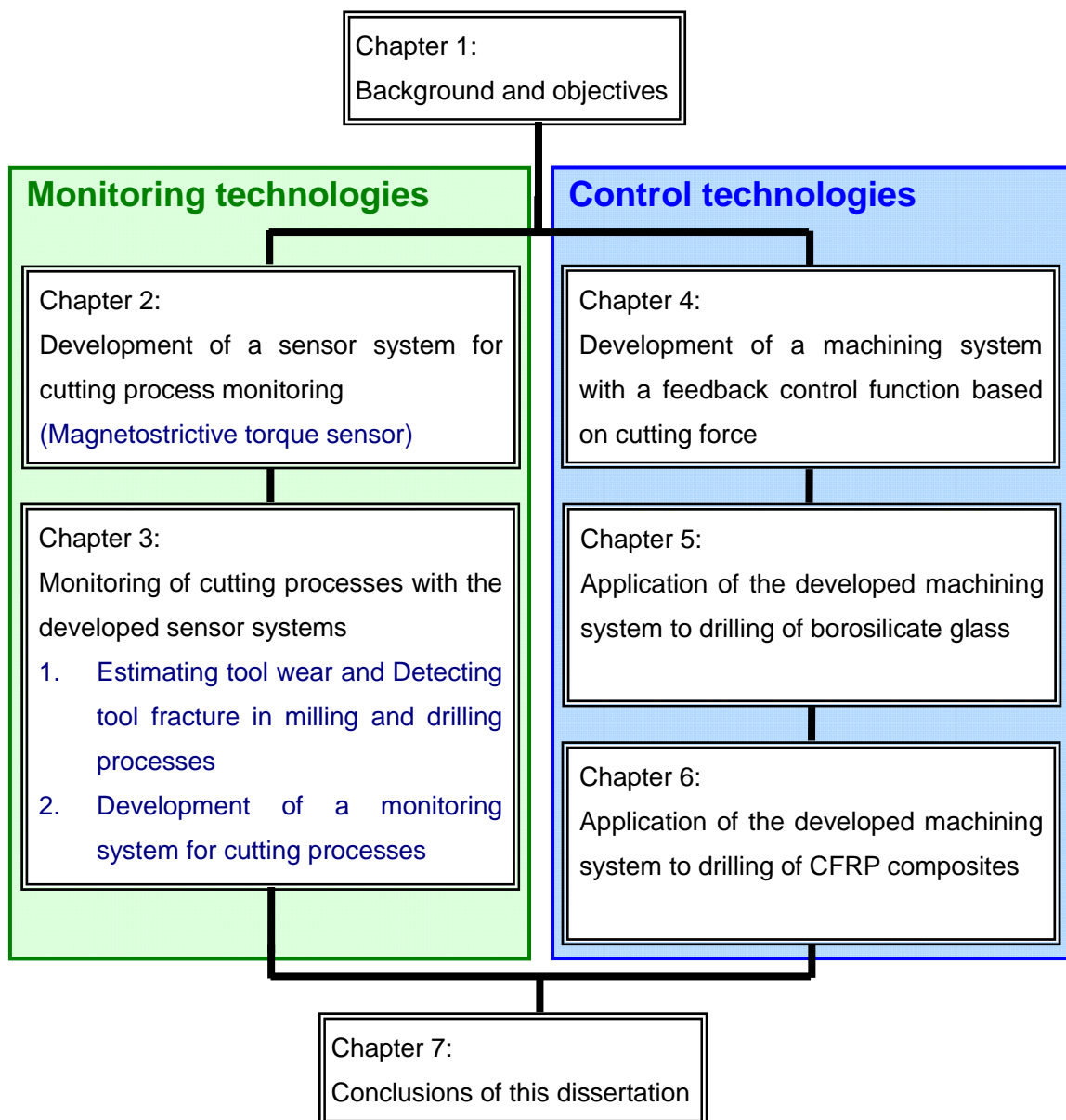


Fig. 1.6 Overview of this dissertation



## **Chapter 2**

# **Development of magnetostrictive torque sensors for cutting process monitoring**

### **2.1 Objectives**

To realize the intelligent machining systems described in section 1.2, it is necessary to monitor tool conditions during the machining process. These tasks require sensors which can provide informative signals about the state of the machining process. From the results of a survey regarding tool-condition monitoring, it is clear that many engineers have required reliable sensors and signal transmission techniques in systems to detect tool wear and tool breakage, as mentioned in chapter 1 [2].

To recognize tool wear and tool breakage, one of the most effective and reliable methods is to detect cutting forces because they can be directly related to the mechanics of the cutting process [35]. In addition, by mounting a sensor in a position which is

located as close to the cutting point as possible, the reliability of detecting the cutting force will be improved.

On the other hand, torque sensors that use coils to detect changes in the magnetic permeability of ferromagnetic alloy materials caused by torque have a great advantage because it is possible to detect torque in a rotating body without electronic contact. By utilizing this phenomenon, we have suggested a more efficient approach by developing a sensor system based on the magnetostrictive effect, which is installed in a tool holder to measure cutting torque, in order to provide a basis for the intelligent machining systems.

Therefore, the objective of the present work is to propose a method for detecting cutting torque by utilizing the magnetostrictive effect and a sensor system to realize the method. Subsequently, the proposed sensor system installed a magnetostrictive torque sensor in a tool holder is developed, and the performance of the sensor system is confirmed through static and dynamic evaluation tests.

## **2.2 Magnetostrictive torque sensor**

### **2.2.1 Magnetostrictive effect**

As shown in Fig. 2.1, when tensile stress is applied to a ferromagnetic material that consists of many magnetic domains, the direction of easy magnetization of each magnetic domain turns along the tensile axis. But when compressive stress is applied to the material, the direction of each magnetic domain turns perpendicular to the tensile axis. Consequently, the magnetic permeability of the material changes in proportion to the stress. This phenomenon is known as the magnetostrictive effect [108], and it can be used to detect torque.

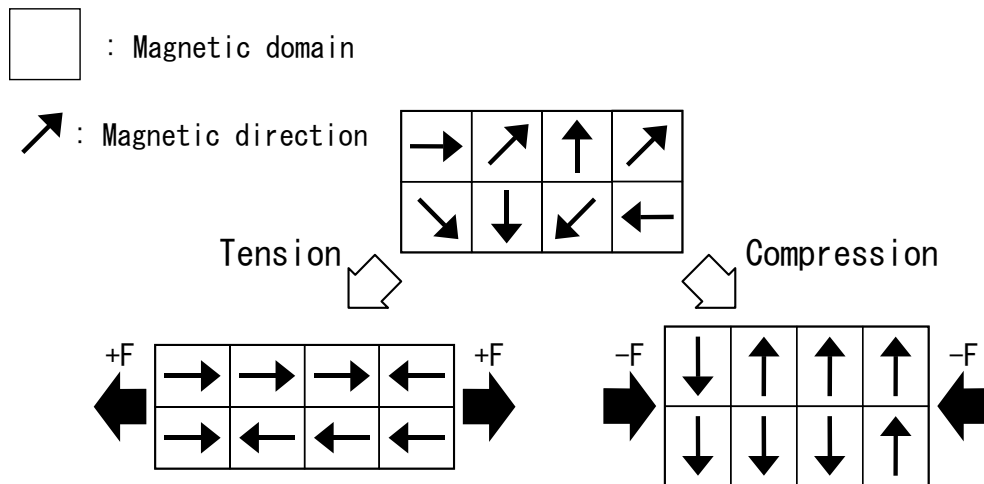


Fig. 2.1 Magnetostrictive effect

### 2.2.2 Sensor structure

In order to detect torque, we have adopted the structure as shown in Fig. 2.2. Two groups of strips of ferromagnetic alloy layers are formed onto a sensor shaft at helical angles of 45 degrees and  $-45$  degrees to the shaft axis, with two circular coils located around them. When torque is applied to the sensor shaft, the magnetic permeability of the upper strips and lower strips of ferromagnetic alloy layers change symmetrically with the torque due to the effect of shape magnetic anisotropy. As the impedance of each circular coil varies in proportion to the permeability, the value and the direction of torque are simultaneously obtained from the output of the differential amplifier.

To measure cutting torque in the cutting process, a cutting tool has to be connected to the sensor shaft. Therefore, the sensor shaft is loaded not only with torque but also with axial force and radial force. These force components inevitably apply stress on the ferromagnetic alloy layer and so affect the magnetic permeability of the ferromagnetic

alloy layers. In order to measure only cutting torque, the influences of the axial force and the radial force on the ferromagnetic alloy layers must be eliminated. The sensor structure, which consists of two pairs of ferromagnetic alloy layers and the circular coil, is designed to cancel the influence of the axial force and the radial force.

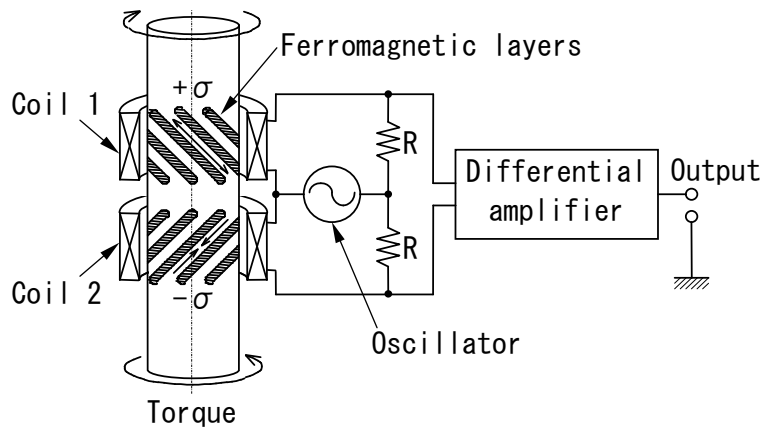


Fig. 2.2 Structure of the magnetostrictive torque sensor

When axial force is applied to the sensor shaft, the ferromagnetic alloy layers on both sides receive the same compressive stress as shown in Fig. 2.3(a). In this case, the values for the impedance change of both circular coils are the same, and the direction of change of both circular coils is the same. Therefore, the influence of the axial force can be eliminated by obtaining the difference of impedance change in these circular coils by using the differential amplifier shown in Fig. 2.2.

When radial force is applied to the sensor shaft, one side of the sensor shaft, which is bounded by a neutral plane parallel to the shaft axis, receives tensile stress and the

opposite side receives compressive stress as shown in Fig. 2.3 (b). Since the circular coils for detecting the change of magnetic permeability surround the sensor shaft, the change in magnetic permeability caused by the radial force can be canceled in the sensor, where the gap between the ferromagnetic alloy layers on the sensor shaft and the circular coils around them has been kept at a constant distance.

Consequently, as described above, it is clear that the sensor structure has the ability to cancel the influence of axial force and radial force.

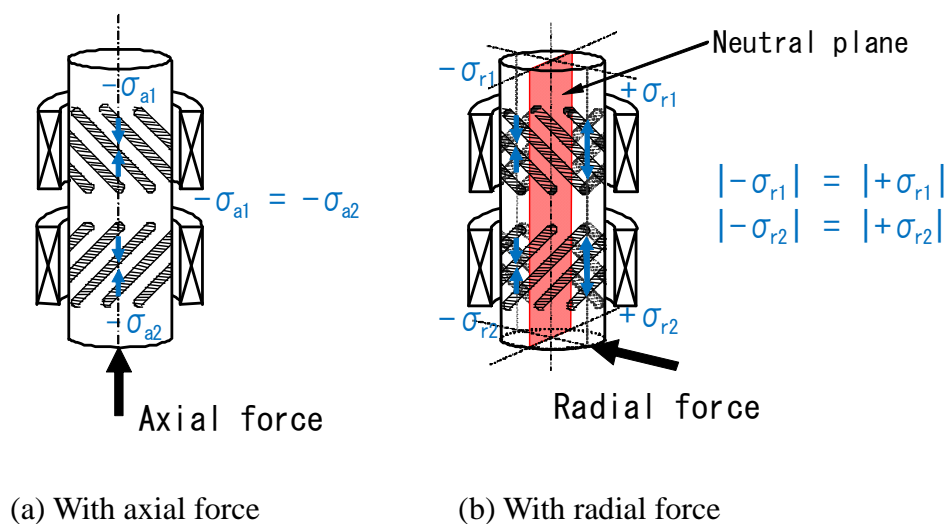


Fig. 2.3 Cancellation of the influence of axial force and radial force

### 2.2.3 Development of sensor system

By mounting a sensor on a tool holder, it becomes possible to detect changes in sensor signals depending on the tool condition of the cutting point as closely as possible.

Accordingly, we installed the magnetostrictive torque sensor in a tool holder which is an ISO No. 40 tool shank with a 7/24 taper. In this work, we have developed three types of sensor system described below, but the developed sensor systems have a same design concept as follows. In order to maintain the gap between the ferromagnetic alloy layers on the sensor shaft and the circular coils at a constant distance, and to restrain bending of the sensor shaft caused by radial force, we have adopted the structure shown in Fig. 2.4, where a cylindrical housing of the tool holder is used to carry the radial load of the sensor shaft through both angular contact bearings and the coil case around the sensor shaft. The coil case with two circular coils is fixed to the spindle head of a machining center with a connector for mechanical and electrical connection. When the tool holder is detached by a tool changing arm of the machining center, the coil case with the connector is locked to the cylindrical housing by means of a positioning lever in order to keep a position of the connector for inserting the tool holder into the spindle again. Consequently, the proposed sensor system can be applied to the automatic tool changer (ATC). Figure 2.5 shows a photograph of the developed sensor system which has the collet holder to hold a rotating tool at the end of a sensor shaft and the measuring range is 9.8 Nm.

As mentioned above, we designed three types of tool holders which had sensors installed. One is an experimental product mainly designed for evaluating the ability of detecting the cutting torque in the milling process. This type combines the sensor shaft with an end-milling cutter. The end-milling cutter has a diameter of 10 mm at the cutting edge and a diameter of 12 mm at the sensor shaft, and has one cutting insert made of cemented carbide. The others are tool holders designed in consideration of practical application, because static and dynamic evaluation tests using the first product

showed that the sensor system had the ability to detect cutting torque. The results of the evaluation tests will be given in chapter 3. The latter types have the collet holder to hold a rotating tool at the end of a 16mm-diameter sensor shaft.

In these products, we used a Fe-Ni-based alloy containing Mo and B for the ferromagnetic layer material and a non-magnetic Fe-based alloy containing Mn and Cr for the shaft material because our investigation revealed that the combination of these materials was suitable not only for hysteresis error and linearity but also for sensitivity. The ferromagnetic alloy layers were formed with a plasma spray coating method. The exciting frequency of the circular coils, which allows the evaluation of torque dynamics, was 40 kHz and the exciting current was 25 mA.

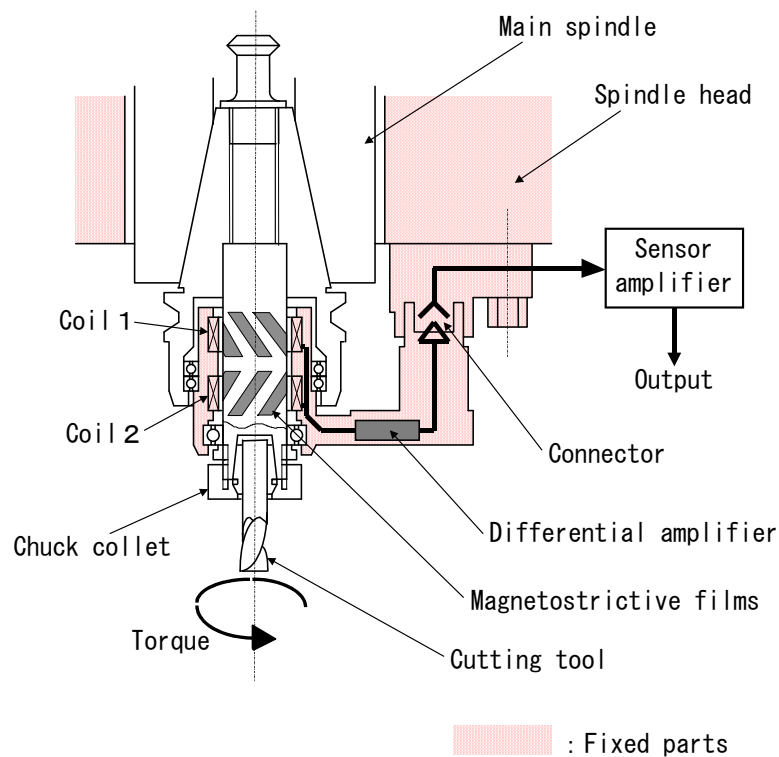


Fig. 2.4 Structure of the developed sensor system

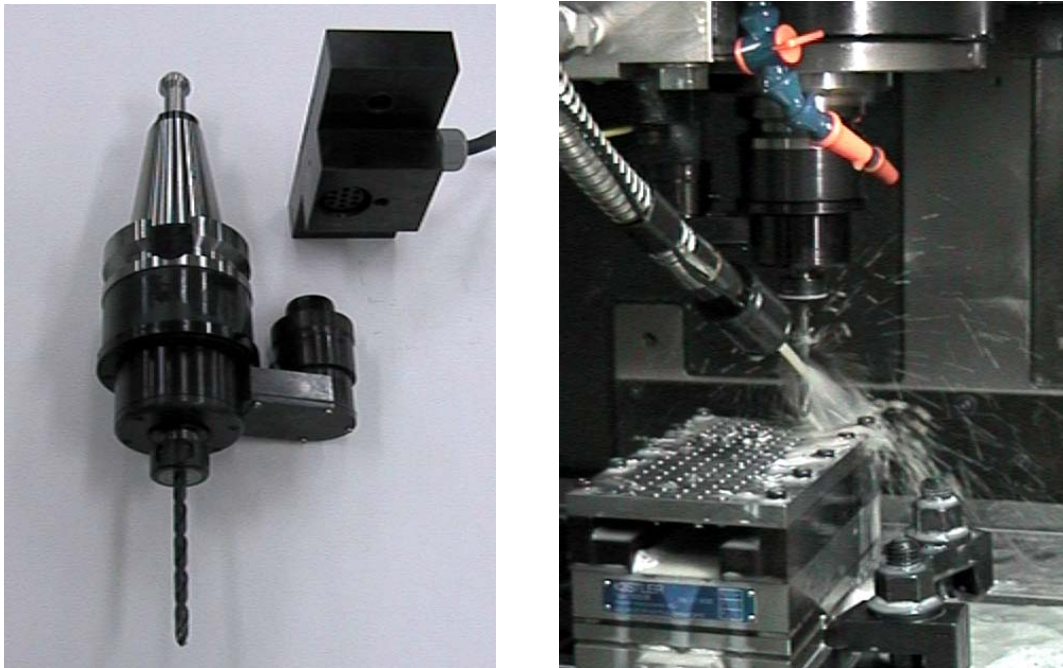


Fig. 2.5 Photograph of the developed sensor system

## 2.3 Evaluation of the developed sensor systems

At first, evaluation tests are necessary in order to determine the performance of the sensor system and to evaluate the sensor system's ability to cancel axial and radial forces. This section describes the results of static and dynamic evaluation tests which used the type of sensor shaft combined with an end-milling cutter.

### 2.3.1 Experimental setup

Figure 2.6 shows the experimental setup used to evaluate the developed sensor system. A tool holder, in which the magnetostrictive torque sensor has been installed, is mounted on the main spindle of a machining center. The sensor signal is derived by subtracting one coil output from the other coil output using a differential amplifier. This signal is amplified and input into a personal computer through a main sensor

amplifier, a low pass filter and an analog-to-digital converter.

In order to obtain calibrated data and to compare the signal from the proposed sensor system with another reliable sensor, a piezoelectric type of dynamometer (Kistler, Type 9272), which had been installed between a workpiece and the table, was used to measure the force components in x, y and z directions, and the dynamic cutting torque. In static torque calibration tests, a strain-gauge type of torque sensor was used to measure static torque. The signals from the dynamometer and the strain-gauge torque sensor were also input into the personal computer via the low pass filter and the analog-to-digital converter in synchronization with the signal of the proposed sensor system.

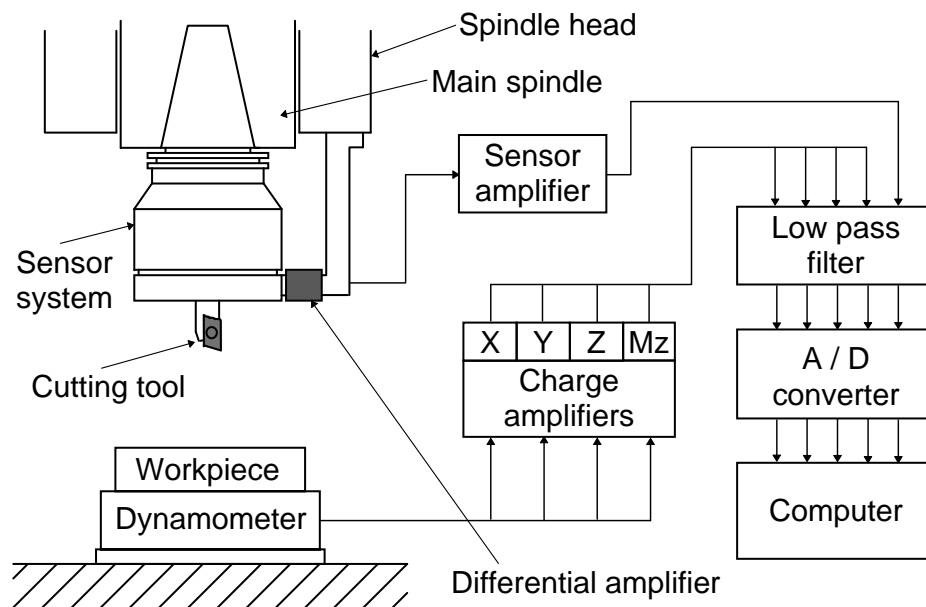


Fig. 2.6 Experimental setup to evaluate the sensor system

### 2.3.2 Static evaluation of the sensor system

Figure 2.7 shows the relationship between torque acting on the cutting edge and the sensor signal. This relationship is obtained from a static torsion test using the strain-gauge torque sensor as the standard. The output signal from the sensor system indicates a proportional dependence on the torque loading. In this case, the hysteresis error of this sensor system is less than 2 % of the full-scale output (F.S.), where F.S. means the increment in voltage caused by changing the torque from 0 to 9 N·m at room temperature. The linearity error is below 2 % F.S. The static torsion tests were performed five times, and the tests showed reproducible results.

During the cutting process, the sensor shaft connected with a cutting tool is subject not only to torque but also to axial force and radial force. Axial force and radial force also cause stress in the magnetostrictive layers. Although the influence of these forces on the sensor signals is theoretically canceled as described in subsection 2.2.2, this issue should be experimentally confirmed. Figure 2.8 shows the result of a static bending test which was carried out by applying force to the cutting edge in a horizontal direction. The output signals from the sensor system exhibit slight deviations from the zero point in the radial force range of 0 to 600 N, where the maximum value of the output signal deviation is 1.8 % F.S. Figure 2.9 represents the result of a static compression test which was done by applying force on the axis of the sensor shaft. The maximum value of the output signal deviation is 1.3% F.S. in the axial force range of 0 to 700 N. We repeated five times for the static bending tests and the static compression tests, and the both tests showed reproducible results.

From these results, it was confirmed that torque can be estimated from the sensor signals of the proposed sensor system.

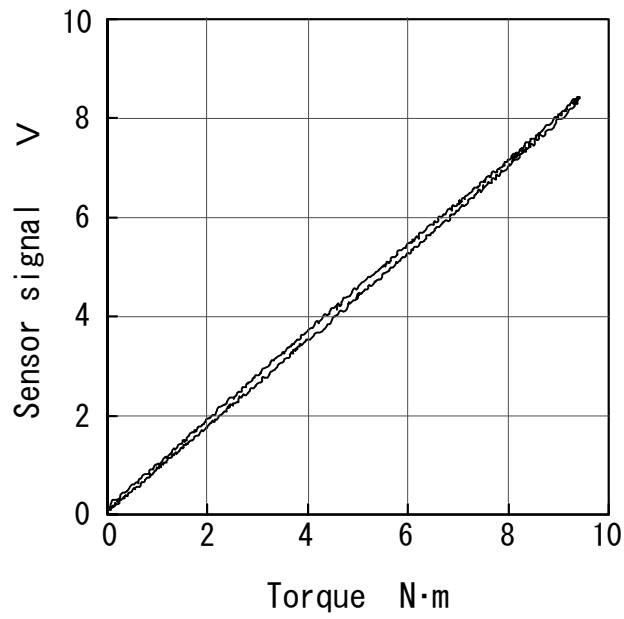


Fig. 2.7 Result of static calibration test

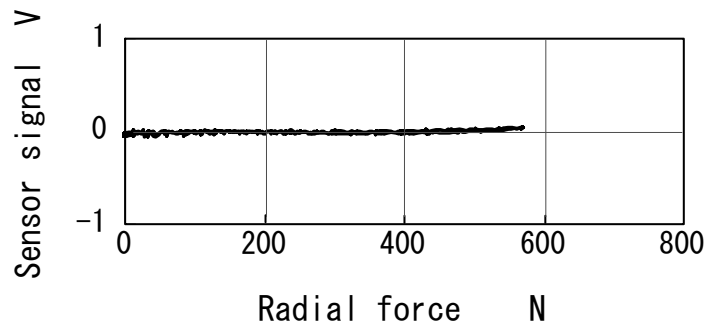


Fig. 2.8 Influence of radial force on the sensor signal

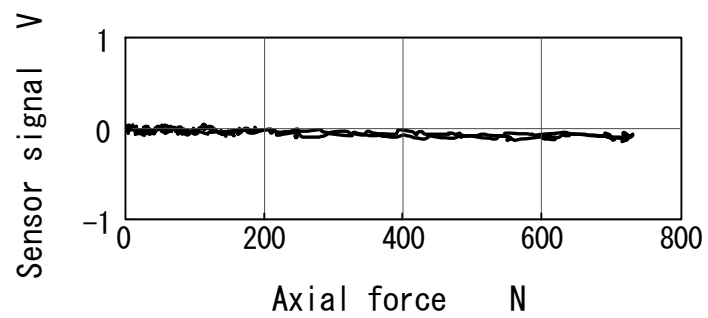


Fig. 2.9 Influence of axial force on the sensor signal

### 2.3.3 Dynamic evaluation of the sensor system

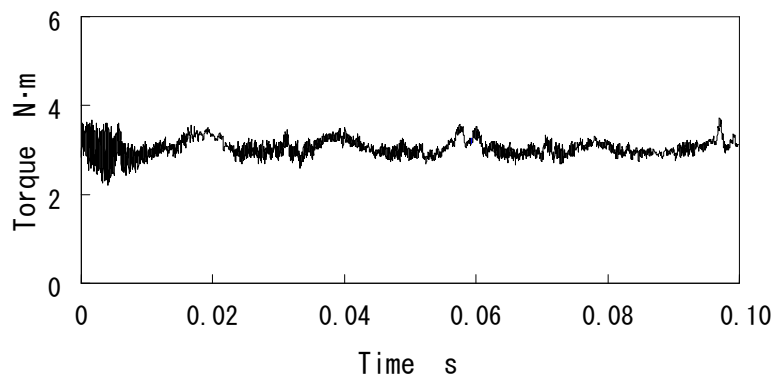
In order to dynamically evaluate the performance of the sensor system, the cutting torque detected by the proposed sensor system was compared with the cutting torque acting on a workpiece measured by the piezoelectric dynamometer in the spot facing which is a process to form a cylindrical hole with a flat face at the end of the hole. The spot facing test was carried out under the following conditions: the spindle speed was 3,000 r.p.m.; the feed rate was 0.05 mm per revolution; the workpiece material was JIS S45C steel (S45C is iron with a carbon content of 0.45 %). Figures 2.10 (a) and (b) show the behavior of the cutting torque during the spot facing as detected by the proposed sensor system and by the dynamometer respectively. As shown in Figs. 2.10 (a) and (b), each signal has significant frequency components. Accordingly, each output signal was analyzed by fast Fourier transformation to identify the frequency component which had been included in each signal. As a result, it became clear that the torque signal obtained from the proposed sensor system involved the frequency component of 4.3 kHz, and the torque signal from the dynamometer involved the frequency components of 50 Hz and 4 kHz. The frequency component of 50 Hz included in the torque signal from the dynamometer is the influence of the spindle speed, because the frequency component of 50 Hz is in agreement with the frequency caused by the spindle speed and is due to the action that one peripheral cutting edge moves in a circle with the radius of 5 mm round the center of the dynamometer where torque is determined accurately. On the other hand, the torque signal from the proposed sensor system is independent of the spindle speed, because the sensor shaft connected with the end-milling cutter directly receives torque. The frequency components of 4.3 kHz and 4 kHz are in agreement with the natural frequency of torsional direction of each system.

Since the natural frequency of each system is included in each output signal and the frequency of 50 Hz caused by the spindle speed is included in the output signal from the dynamometer, the results cannot be directly compared. However, the value and behavior of the cutting torque which was detected by the proposed sensor system and by the dynamometer are similar to each other. Next, in order to quantitatively confirm the accuracy of the cutting torque and to investigate the influence of which the spindle speed exerts on the torque signals detected by the proposed sensor system, dynamic experiments were carried out. The experimental setup used is illustrated in Fig. 2.11. The end-milling cutter installed in the sensor system is connected to the dynamometer with an overload coupling which can give dynamic torque load of the same value to the sensor system and the dynamometer, and that value can be adjusted. The main spindle was rotated at 1,000, 2,000, 3,000 and 4,000 r.p.m. Figure 2.12 shows the torque signals detected by the proposed sensor system plotted against the dynamic torque measured by the dynamometer. The maximum value of torque signal deviation from the dynamic torque measured by the dynamometer is less than 2 % F.S. Therefore, it became clear that the proposed sensor system could measure the cutting torque.

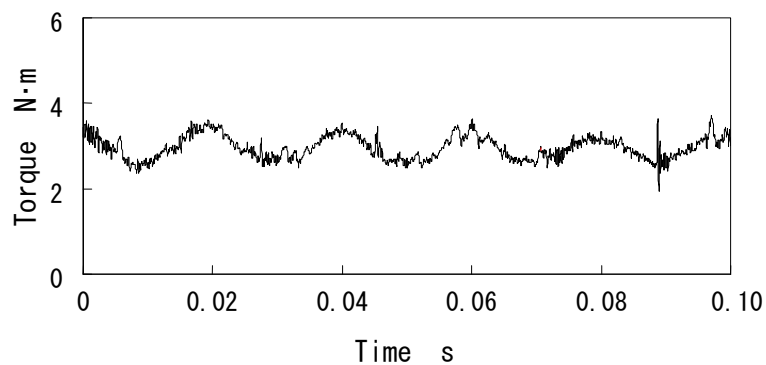
The side-milling tests were carried out under the machining conditions shown in Table 2.1. Figures 2.13 (a) and (b) show examples of cutting tests measured by the proposed sensor which was done under the following cutting parameters: the main spindle was rotated at 3,000 r.p.m.; the axial depth of cut was 2.0 mm; the width of cut was 2.0 mm. These results show that the behavior of the cutting torque measured by the proposed sensor system represents the difference in the cutting cross-section during the milling process between down-cut milling and up-cut milling. By way of another example, Fig. 2.14 shows the results of the side-milling experiments in which the

plotted marks represent the maximum value of the cutting torque per revolution measured by the proposed sensor system at down-cut milling. As is obvious from Fig. 2.14, the maximum values of the cutting torque increase as the width of the cut increases. In addition, the maximum values of the cutting torque are almost the same if the feed rate per tooth is kept constant.

From the above results it may be concluded that the proposed sensor system can measure the cutting torque.



(a) Magnetostrictive sensor



(b) Dynamometer

Fig. 2.10 Behavior of the cutting torque during the spot facing as detected by the proposed sensor system and by the dynamometer

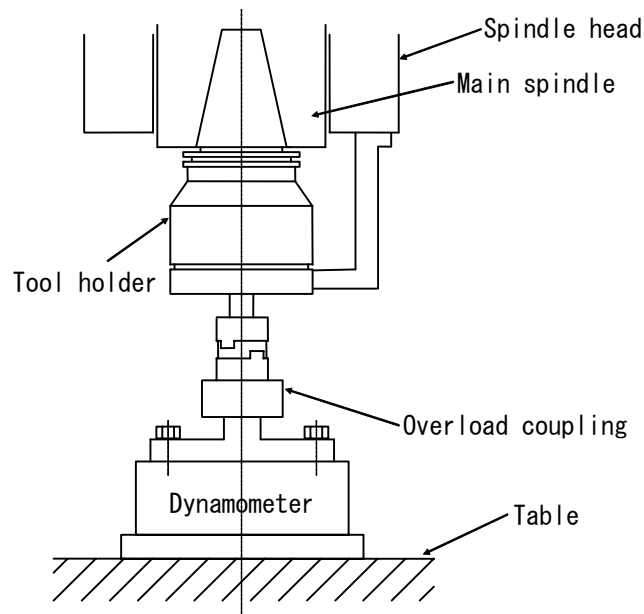


Fig.2.11 Setup for dynamic experiment

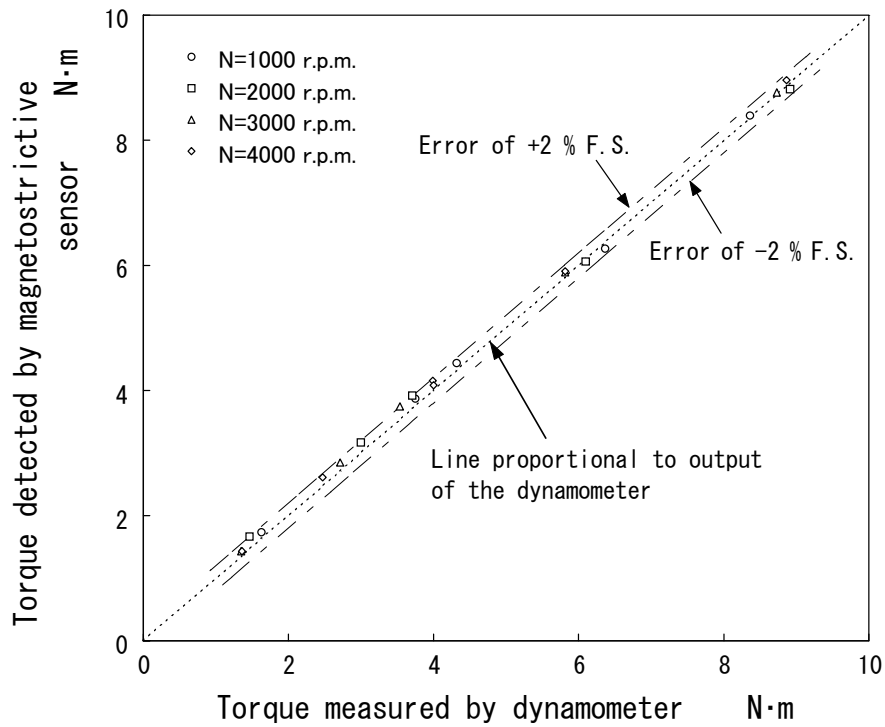
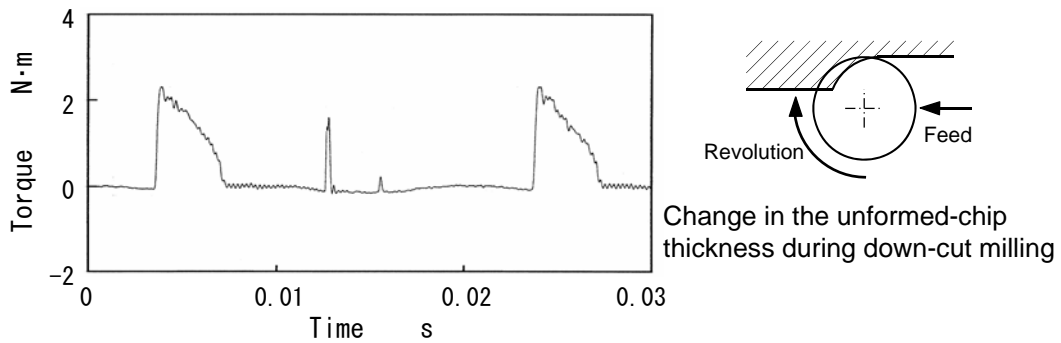


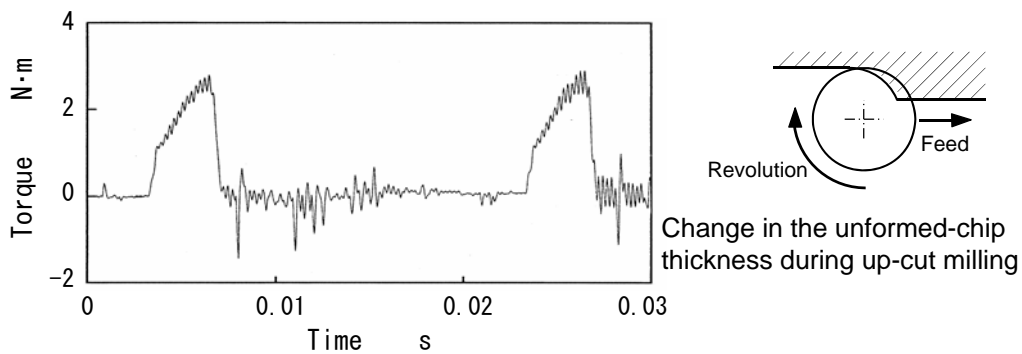
Fig.2.12 Result of dynamic torque evaluation experiments

Table 2.1 Machining conditions

Tool	End mill
	Diameter : 10 mm
	Number of teeth : 1
	Cutting insert : Carbide
Cutting Parameters	Spindle speed : N = 2500, 3000, 3500 r.p.m.
	Feed : f = 0.05 mm/tooth
	Axial depth of cut : t = 2.0, 4.0 mm
	Width of cut : Wc= 0.5, 1.0, 1.5, 2.0 mm
	Lubrication : Dry
Workpiece material	Carbon steel (Iron with Carbon content of 0.45 %, JIS S45C)



(a) Down-cut milling



(b) Up-cut milling

Fig.2.13 Behavior of the cutting torque during the side-milling measured by the proposed sensor system

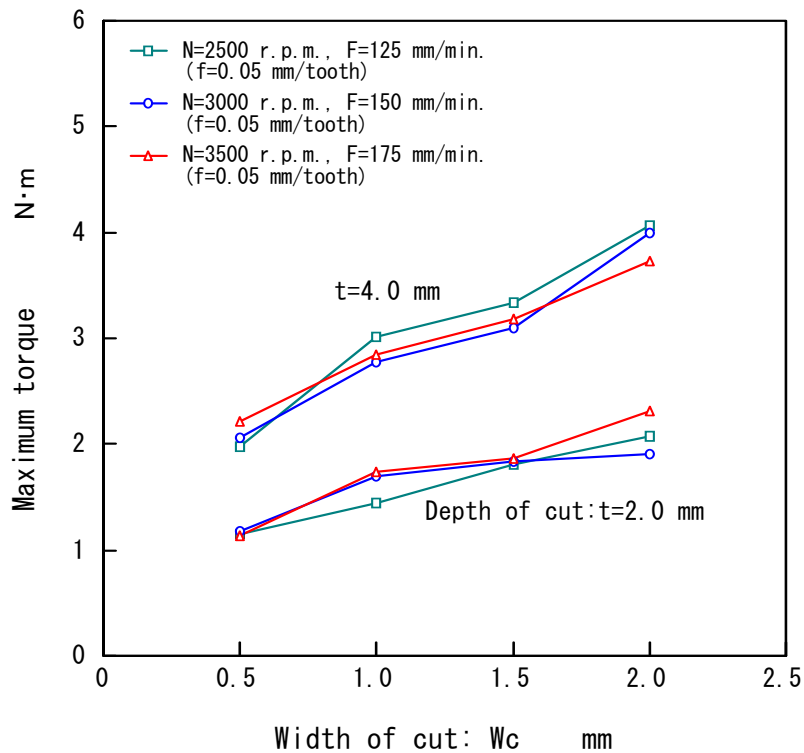


Fig. 2.14 Result of side-milling experiments

## 2.4 Summary of this chapter

The present research developed a sensor system based on the magnetostrictive effect, which was installed in a tool holder, for measuring cutting torque in order to monitor the milling process. The results obtained are summarized as follows;

- (1) A method for detecting cutting torque by utilizing the magnetostrictive effect and a sensor system for realizing the method were proposed.
- (2) Three sensor systems based on the proposed method, in which a magnetostrictive torque sensor was installed in a tool holder, were developed.

- (3) Static evaluation tests, including a calibration test and investigations of the influence of radial force and axial force, confirmed that the proposed sensor system had the ability to detect torque.
- (4) Dynamic evaluation tests showed that the proposed sensor system had the ability to detect cutting torque, through comparison with the dynamic torque measured by a piezoelectric type of dynamometer acting on a workpiece as a standard.

## **Chapter 3**

# **Monitoring of cutting processes with the developed sensor systems**

### **3.1 Objectives**

Machining processes need to be made more autonomous due to the shortage of skilled operators in recent years, to reduce the production cost and so on. To realize such demands, signal-processing strategies, which can detect disturbances in the machining process based on signals from each sensor as well as sensors that can provide information about the state of the machining process, are needed. According to the results of a survey regarding tool-condition monitoring, engineers related to machining have especially demanded to detect tool wear and tool breakage in machining processes, as described in chapter 1 and 2 [2].

In this chapter, therefore, the possibility of estimating tool wear and tool fracture

Table 3.1 Cutting conditions

Tool	End mill
	Diameter : 10, 15 mm
	Number of teeth : 2
	Material : High speed steel
Cutting Parameters	Cutting speed : N = 30 m/min
	Feed : f = 0.10 mm/tooth
	Axial depth of cut : t = 4.0 mm
	Width of cut : Wc= 2.0 mm
	Lubrication : Dry
	Cut-down milling
Workpiece material	Carbon steel (Iron with Carbon content of 0.45 %, JIS S45C)

detection in milling and drilling processes from the cutting torque measurement with the developed sensor system, which has been fully mentioned in chapter 2, has been investigated. In addition, we have proposed a monitoring system for cutting processes, which has not only monitoring functions of cutting processes but also unique database functions to assist in developing the monitoring algorithms.

## 3.2 Monitoring of end-milling process

### 3.2.1 Experimental methodology

In order to investigate the relationship between tool failure and torque signals, cutting tests were carried out under the cutting conditions shown in Table 3.1, using a tool holder designed in consideration of practical application that was provided with the collet holder to hold a cutting tool on the end of the sensor shaft. This sensor system with a measuring range of 30 N·m has the following performance: both the hysteresis error and the linearity are less than 2 % F.S. in the torque range of 0 to 30 N·m; the

influences of axial force and radial force are both less than 2 % F.S.; the natural frequency of torsional direction is approximately 800 Hz.

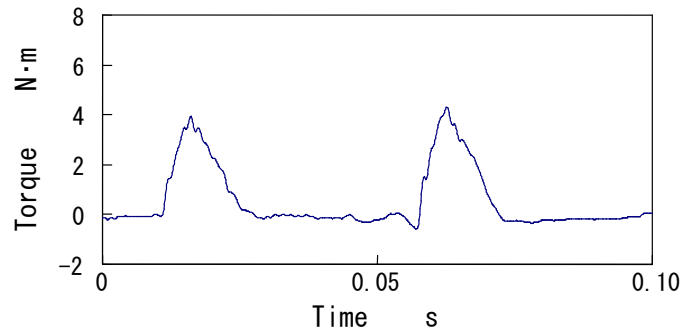
### **3.2.2 Estimating tool wear from the sensor signals**

Continuous cutting tests were performed in order to clarify changes in the behavior of cutting torque with progressive tool wear. The behaviors of the cutting torque during the process in which the width of the flank wear is 0 mm, 0.07 mm and 0.18 mm are shown in Figs. 3.1 (a), (b) and (c), respectively. In these results, the tool diameter was 15 mm. As is obvious from these figures, the cutting torque increases with increased tool wear.

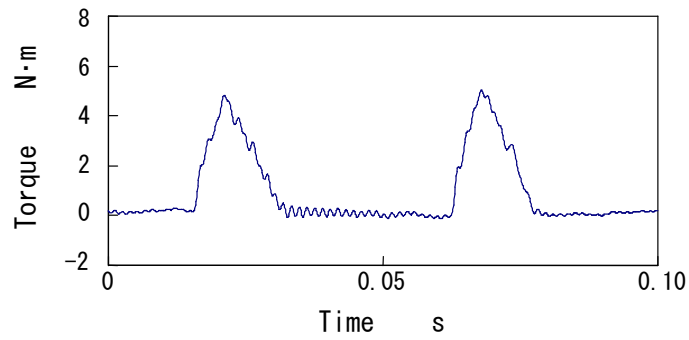
In order to investigate the possibility of identifying the width of flank wear from the cutting torque signal, the maximum values of the cutting torque detected by the proposed sensor system are plotted. Figure 3.2 shows the relationship between the width of flank wear and the maximum value of the cutting torque. As shown in Fig. 3.2, it is expected that flank wear can be estimated by the maximum value, due to the fact that the maximum cutting torque increase with increased flank wear.

### **3.2.3 Detecting tool fracture from the sensor signals**

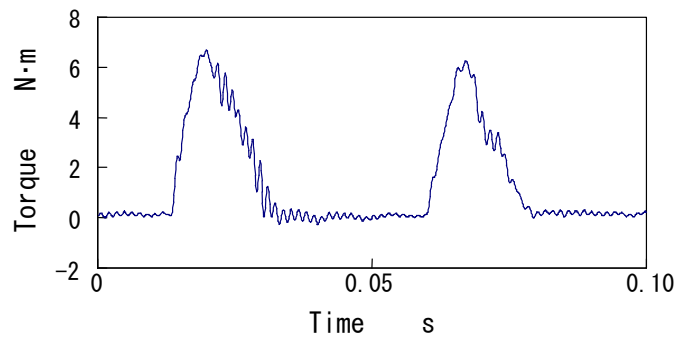
In order to clarify changes in the behavior of the cutting torque caused by tool fracture, continuous cutting tests were carried out. Tool fracture occurred during the cutting test when the cutting time reached 54 minutes. Figure 3.3 shows the photograph of the fractured cutting edge. The breakage of the fractured cutting edge was a three-cornered shape 1.3 mm long in the axial direction and 0.4 mm wide in the radial



(a) Flank wear = 0 mm



(b) Flank wear = 0.07 mm



(c) Flank wear = 0.18 mm

Fig. 3.1 Behavior of the cutting torque during the process (Tool diameter = 15 mm)

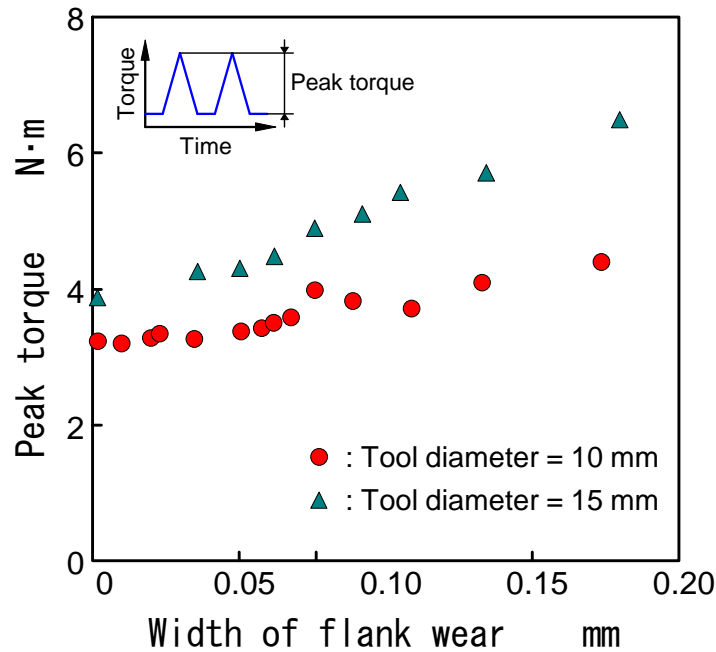


Fig. 3.2 Relationship between flank wear and the maximum value of the cutting torque

direction. In this experiment, the tool diameter was 15 mm. The behavior of the cutting torque when one of the cutting edges was fractured is shown in Fig. 3.4 (a). For comparison with the above data, the behavior of the cutting torque before fracturing is shown in Fig. 3.4 (b). As is obvious from Figs. 3.4 (a) and (b), the difference in the values of the maximum cutting torque generated by the two cutting edges consisting of a cutting tool increases due to tool fracture. Since the proposed sensor system has enough dynamic sensitivity for detecting cutting torque given by each cutting edge, tool fracture can be identified by observing the value of the maximum cutting torque generated by each cutting edge.

Next, in order to confirm that the difference in the value of the maximum cutting torque generated by the two cutting edges increases due to tool fracture can be

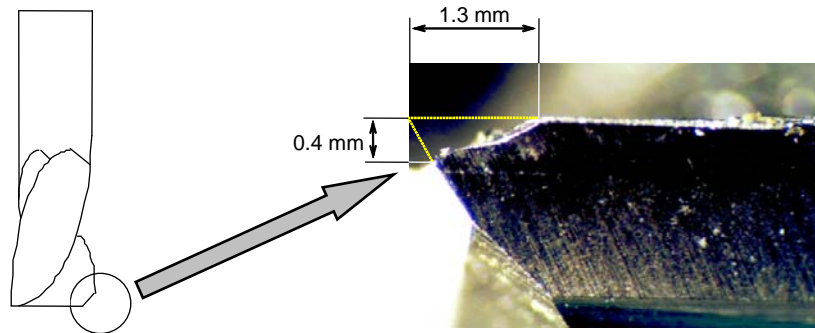
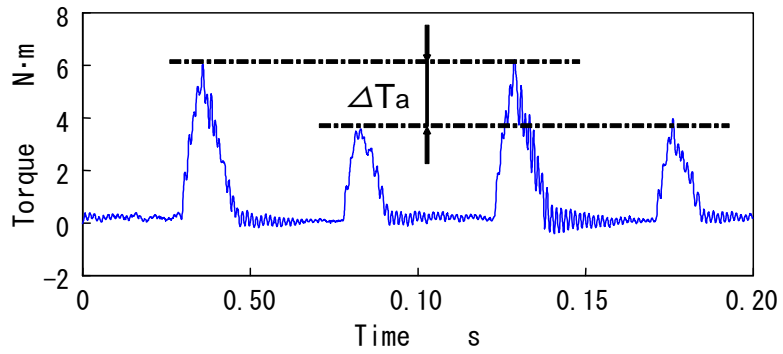


Fig. 3.3 Fractured cutting edge of the end mill

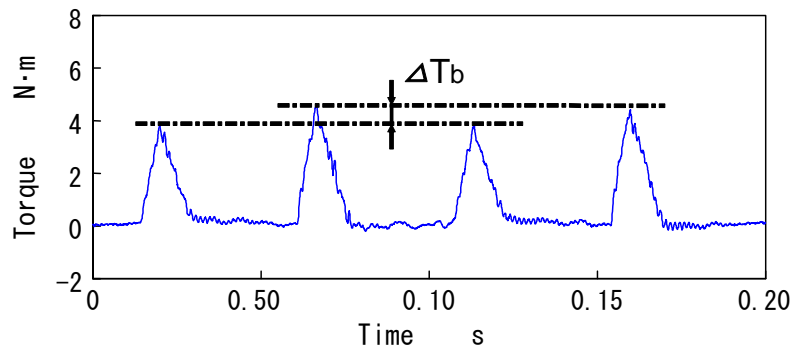
reproduced, an artificially fractured tool was prepared for a cutting test. The artificially fractured tool was shaped as follows: an isosceles triangle shape 0.5 mm long in the axial direction and 0.5 mm long in the radial direction was removed from the cutting edge. These experiments were carried out under the following cutting parameters: the tool diameter was 10 mm; the width of cut was 3 mm; the axial depth of cut and the feed rate were varied from 1 to 4 mm and from 0.07 to 0.13 mm/tooth respectively. The results of the measurements of the maximum cutting torque generated by the two cutting edges are summarized in Fig. 3.5. In this figure,  $\Delta T_b$  represents the difference in the value of the maximum cutting torque generated by the two cutting edges of an un-chipped tool, and  $\Delta T_a$  represents the difference of the artificially fractured tool. In these results,  $\Delta T_a$  is larger than  $\Delta T_b$  over the whole area of the cutting cross-section measured.

As is obvious from Figs. 3.4 and 3.5, the difference in the value of the maximum cutting torque generated by the two cutting edges increases due to tool fracture. Therefore, it is expected that tool fracture can be detected by the difference in the value

of the maximum cutting torque detected by the developed sensor system.



(a) After tool fracture



(b) Before tool fracture

Fig. 3.4 Change in the behavior of the cutting torque caused by tool fracture

(Tool Diameter = 15 mm)

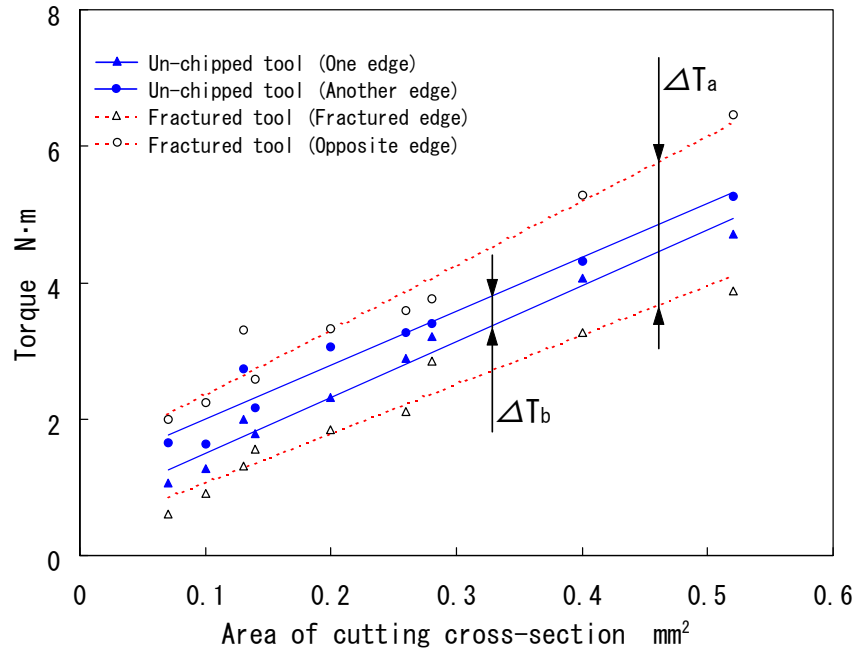


Fig. 3.5 Result of the measurements of the maximum cutting torque indicated by the two cutting edges using an artificially fractured tool and normal tool

### 3.3 Monitoring of drilling process

#### 3.3.1 Experimental methodology

In order to investigate the relationship between tool failure and cutting torque, we carried out continuous drilling tests. Cutting torque was measured by a tool holder designed in consideration of practical application, which was provided with the collet holder to hold a cutting tool on the end of the sensor shaft. In the production of the sensor shaft, we have improved the heat fusing treatment after the plasma spray coating of ferromagnetic alloy layers based on our investigation to minimize the hysteresis and linearity errors. The temperature and the time of the heat fusing treatment were 1085 °C

and 5 min., respectively. The measuring range of this sensor system is 9.8 N·m. The results of the static evaluation tests for the sensor system are summarized in Table 3.2. The linearity, the hysteresis and the cross talk of the sensor system are less than  $\pm 1\%$  of the full-scale output (F.S.), where F.S. means the increment in voltage caused by changing the torque from 0 to 9.8 Nm at room temperature. The cross talks ( $F_{x,y} \rightarrow M_z$ ) and ( $F_z \rightarrow M_z$ ) mean the influence of radial force and axial force on the torque signal. From the results, the linearity, the hysteresis and the cross talk of the sensor system are improved because of the modification of the heat fusing treatment.

Table 3.2 Characteristics of the sensor system

Measuring range	9.8 N·m
Linearity	- 0.7 %F.S.
Hysteresis	0.5 %F.S.
Cross talk ( $F_x, y = 500 \text{ N} \rightarrow M_z$ )	$\leq \pm 1 \text{ %F.S.}$
Cross talk ( $F_z = 1000 \text{ N} \rightarrow M_z$ )	$\leq \pm 1 \text{ %F.S.}$
Natural frequency ( $M_z$ )	3,800 Hz

### 3.3.2 Estimation of abnormal drilling state caused by tool wear

A continuous drilling test was performed under the following conditions: the cutting tool was a high-speed steel drill with the diameter of 3 mm, the cutting speed was 20 m/min, the feed was 0.06 mm/rev. and the workpiece was a carbon steel with the thickness of 10 mm. Figures 3.6 a) and b) show examples of the cutting torque measured by the sensor system in continuous drilling tests. As is obvious from these

figures, the cutting torque during drilling of the 700th hole shows a violent variation as compared with that during drilling of the 50th hole. In addition, the value of the cutting torque during drilling of the 700th hole is higher than that during drilling of the 50th hole at a rough estimate. It is noted that the widths of flank wear at the outer corner after drilling of the 50th hole and 700th hole are 0.06 mm and 0.24 mm, respectively. The data points of cutting torque obtained by the drilling tests were subjected to statistical analysis. For the statistical analysis, we used the data points from 1 sec. to 4 sec. after starting actual drilling, and sampling rate is 400 Hz. Figure 3.7 shows the relationship between the number of holes and the standard deviation of the cutting torque for each hole. The standard deviation of the cutting torque  $\sigma_{mz}$  is given by:

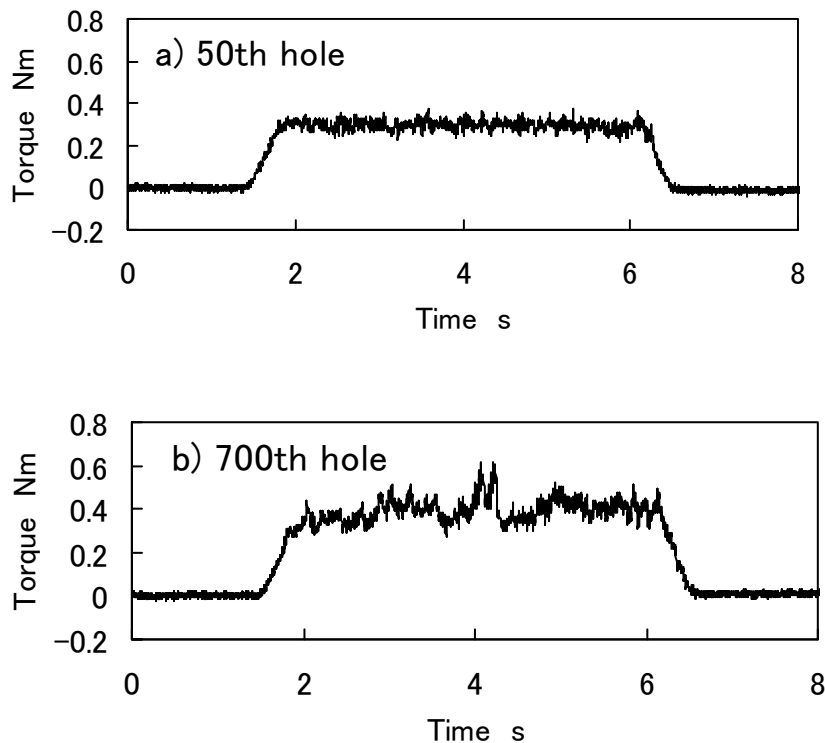


Fig. 3.6 Examples of cutting torque in continuous drilling test

$$\sigma_{mz} = \sqrt{\frac{\sum a^2 - (\sum a)^2}{n(n-1)}} \quad (3.1)$$

In equation (3.1),  $a$  and  $n$  represent the value of the cutting torque obtained from each sampling and the total number of samplings, respectively. In the drilling tests, the total number of samplings  $n$  is 1200. As shown in Fig. 3.7, the standard deviation of the cutting torque increases almost linearly up to approximately the 600th hole, above which it increases remarkably. In addition, the mean value of the cutting torque shows a

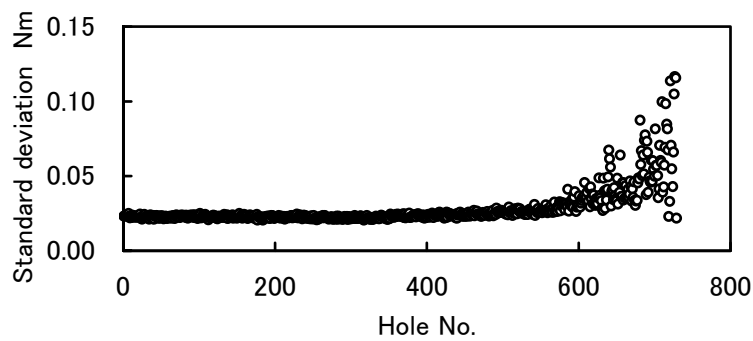


Fig. 3.7 Standard deviation of cutting torque vs. hole No.

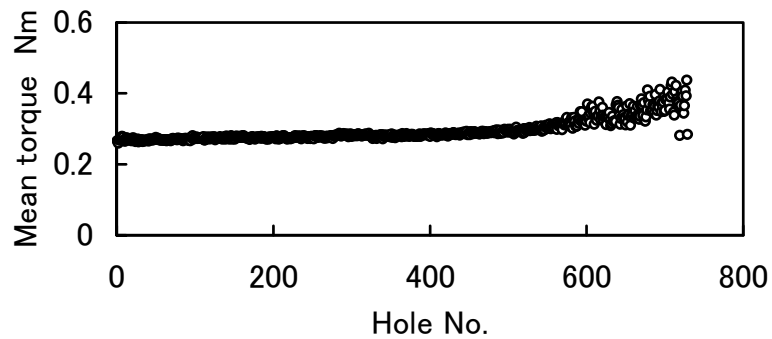


Fig. 3.8 Mean value of cutting torque vs. hole No.

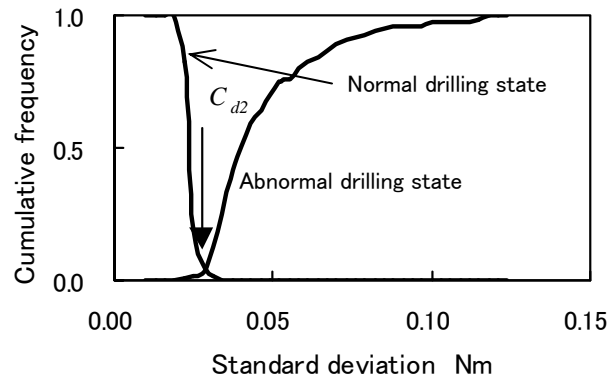
gradual increase up to approximately the 600th hole and then an abrupt increase as shown in Fig. 3.8. Corresponding to these phenomena, cutting sound that has the frequency range of over 5 kHz often occurred from the 592nd hole onward. It is thought that the cutting sound is mainly due to increased tool wear.

A method for estimating the abnormal drilling state caused by tool wear is proposed using the result obtained from the drilling test. The standard deviation and the mean value of the cutting torque were used as indexes for estimating the abnormal drilling state caused by tool wear. In the proposed method, the abnormal drilling state caused by tool wear was defined by the occurrence of cutting sound which has the frequency range of over 5 kHz i.e. the normal drilling state is up to the 591st hole and the abnormal drilling state is from the 592nd hole. Figure 3.9 shows distribution curves of cumulative frequency for the mean value and the standard deviation of the cutting torque. The overlap expressed by two distribution curves cannot clearly discriminate between the normal drilling state and the abnormal drilling state. Accordingly, the coefficient of discrimination  $C_d$  that shows the ability to judge the abnormal drilling state is defined by:

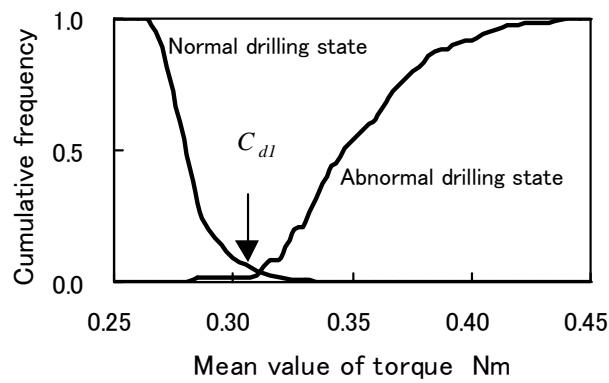
$$C_d = 1 - 2 \times F_{in} \quad (3.2)$$

where  $F_{in}$  is the value of the intersection of two lines as shown in Fig. 3.9. The calculated results for  $C_d$  are shown in Table 3.3. Then, the function  $W(a)$ , which transforms the standard deviation and the mean value of the cutting torque into probability of the abnormal drilling state, is defined by:

$$W(a) = \frac{F_{ab}(a)}{F_{nor}(a) + F_{ab}(a)} \quad (3.3)$$



(a) Standard deviation of cutting torque

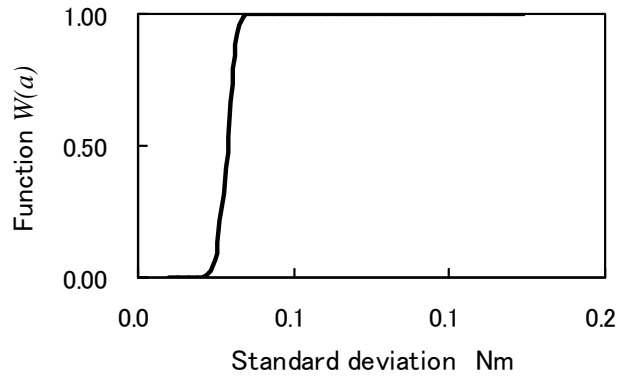


(b) Mean value of cutting torque

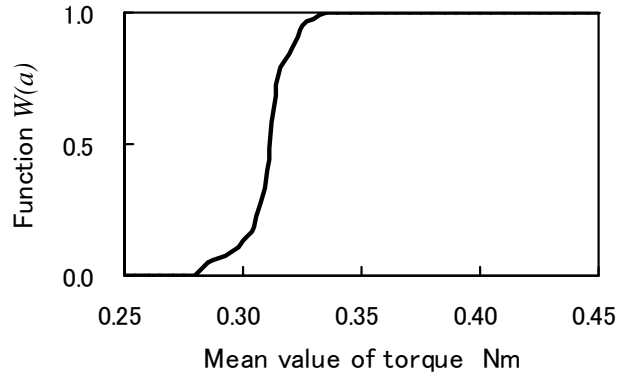
Fig. 3.9 Distribution curve of cumulative frequency

Table 3.3 Coefficient of discrimination

	Coefficient of discrimination: $C_d$
Mean value of torque	0.915
Standard deviation of torque	0.879



(a) Standard deviation of cutting torque



(b) Mean value of cutting torque

Fig. 3.10 Function  $W(a)$  of indexes

where  $F_{nor}(a)$  and  $F_{ab}(a)$  are the cumulative frequencies of the normal drilling state and the abnormal drilling state, respectively. The calculated results for the function  $W(a)$  are shown in Fig. 3.10. Finally, the index of final judgment  $J$  is defined by equation (3.4). In this equation, the output  $W_1$  and  $W_2$  obtained from Fig. 3.10 is weighted using the coefficient of discrimination shown in Table 3.3.

$$J = \frac{W_1 \times C_{d1} + W_2 \times C_{d2}}{C_{d1} + C_{d2}} \quad (3.4)$$

If the index of final judgment  $J$  is more than 0.5, the proposed method judges the state as the abnormal drilling state.

In order to confirm the validity of the proposed method, continuous drilling tests were carried out twice under the same drilling conditions. Figure 3.11 shows the relationship between the number of holes and the index of final judgment  $J$ . The results of estimating the abnormal drilling state are shown in Table 3.4. Judging from the results, it may be concluded that the proposed method can estimate the abnormal state caused by tool wear.

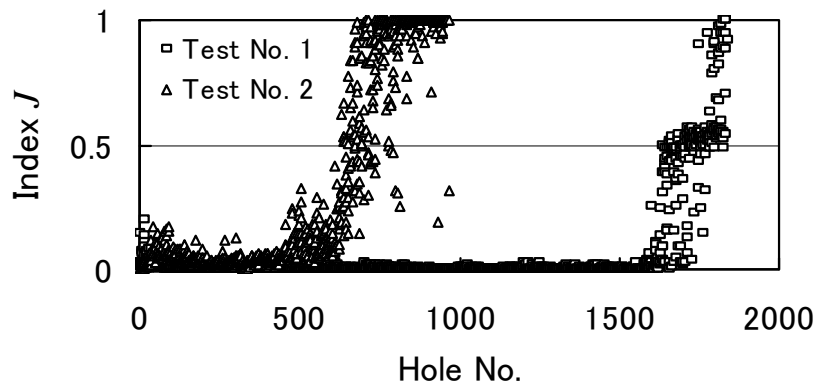


Fig. 3.11 Relationship between final index  $J$  and hole No.

Table 3.4 Result of evaluation tests for the proposed method

	Test No. 1	Test No. 2
Actual value (Hole No.)	1,636	689
Estimated value (Hole No.)	1,653	631
Error (Hole No.)	+17	-58

### 3.3.4 Detection of tool fracture

A continuous drilling test was performed under the conditions shown in Table 3.5. In this drilling test, tool fracture occurred during drilling of the 841st hole. Figure 3.12 shows the fractured cutting edge of the drill. The cutting torque when one of the cutting edges was fractured is shown in Fig. 3.13 a). For comparison with the above data, the cutting torque before fracturing is shown in Fig. 3.13 b). As shown in these figures, the cutting torque during drilling of the 842nd hole shows an increase of significant frequency components included in the torque signal as compared with that during the

Table 3.5 Drilling conditions

Tool	Twist drill	
	Diameter	5 mm
	Point angle	118°
	Material	High-speed steel
Cutting parameters	Cutting speed	20 m/min
	(Spindle speed)	1300 rpm
	Feed	0.10 mm/rev.
	Coolant	Emulsion
Workpiece material	Carbon steel (Iron with carbon content of 0.45%, JIS S45C)	
	Thickness	10 mm

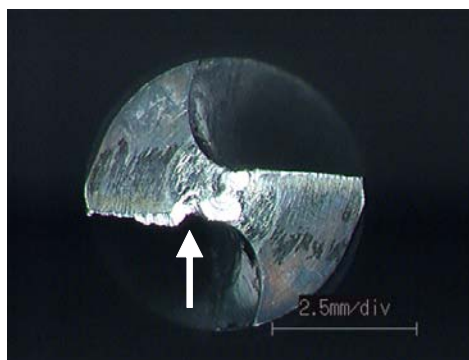


Fig. 3.12 Fractured cutting edge of the drill

drilling of the 840th hole. The data points of the cutting torque were subjected to Fast Fourier transformation (FFT). Figure 3.14 shows the results of FFT analysis during drilling of the 840th hole and 842nd hole. The frequency component of 21.7 Hz included in the torque signal of the 842nd hole is increased in comparison with that of the 840th hole. The frequency component of 21.7 Hz included in the cutting torque is the influence of the spindle speed, because it matches the frequency caused by the spindle speed. In order to clarify the change due to tool fracture, the peak value of the power spectrum of 21.7 Hz is plotted against the number of holes in Fig. 3.15. From the figure, the frequency component of 21.7 Hz increased remarkably when the drill fractured.

Therefore, a method for detecting tool fracture by using a rigid threshold as shown in Fig. 3.15 is proposed, because the frequency component caused by the spindle speed included in the cutting torque shows a sharp rise when the drill fractures.

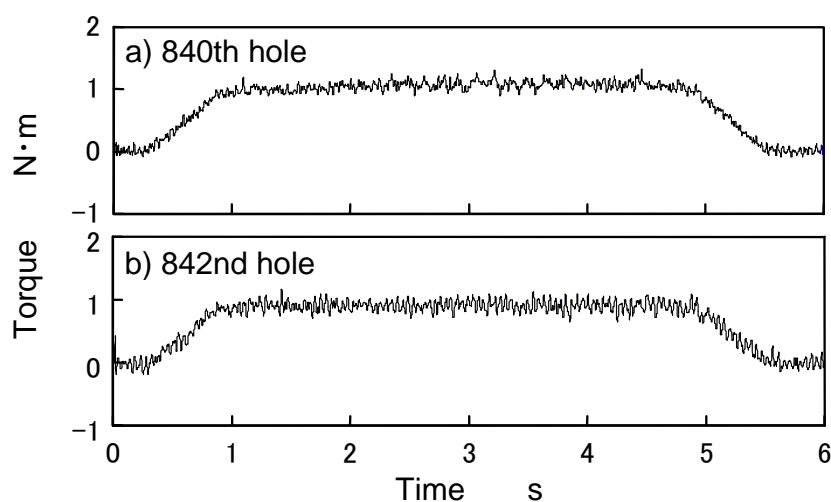


Fig. 3.13 Change in the behavior of the cutting torque caused by tool fracture

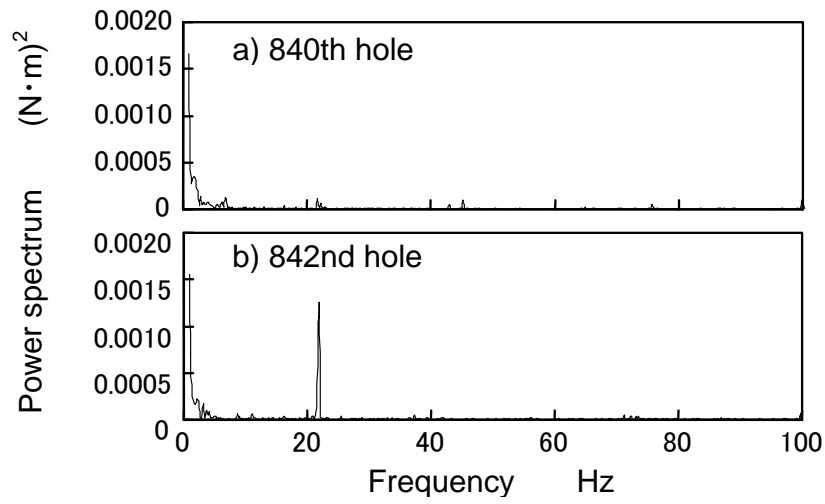


Fig. 3.14 Results of FFT analysis

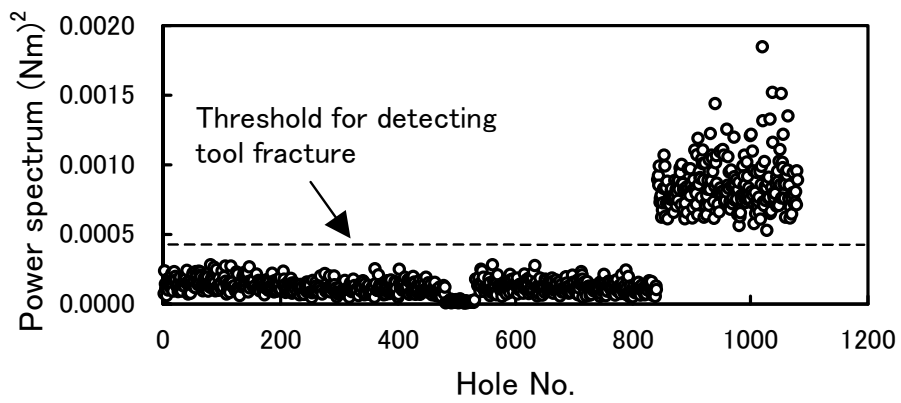


Fig. 3.15 Relationship between number of holes and power spectrum

### 3.4 Development of a monitoring system for cutting processes

We have developed a monitoring system for cutting processes, and the structure is shown in Fig. 3.16. In the system, a magnetostrictive torque sensor, which is installed in a tool holder, is used as a sensing device to provide information related to the state of the cutting process. Monitoring algorithm in the digital signal processor (DSP) processes the signals measured by the magnetostrictive torque sensor, in order to estimate the state of the cutting process. The DSP (Chubu Electric, type ADSP324) is equipped with analogue-to-digital (A/D) and digital-to-analogue (D/A) converters, and programmed input-output (PIO) interfaces. When tool failure is detected by the monitoring algorithm, an alarm signal is transmitted to the control unit of the machine tool through the interfaces of the PIO and the control unit.

In addition to the monitoring function, we have added database functions to the monitoring system. Figure 3.17 illustrates the software structure of the developed

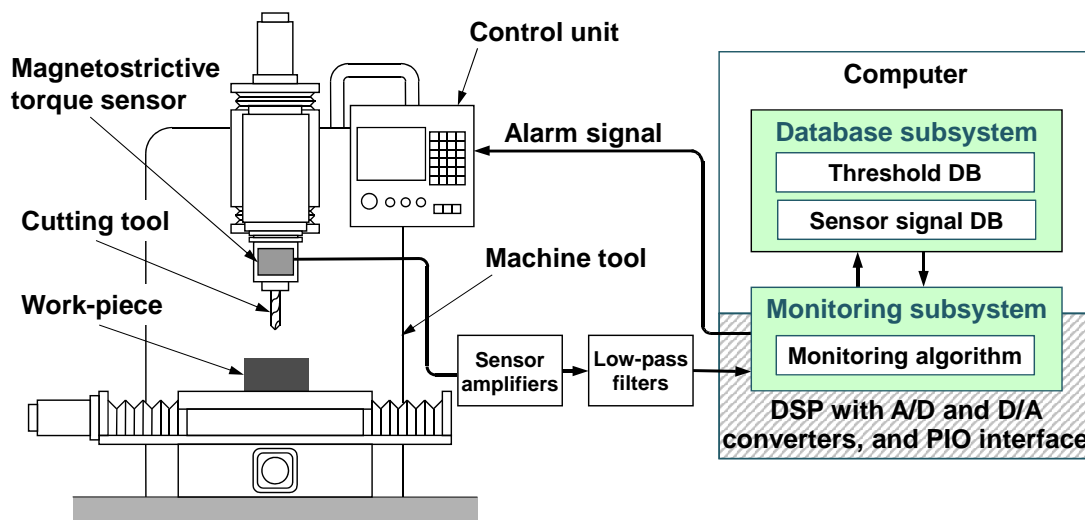


Fig. 3.16 Structure of the developed monitoring system for cutting processes

monitoring system. The system structure is composed mainly of a monitoring subsystem that has the monitoring algorithm and a database subsystem. The database subsystem stored on the computer consists of a threshold database, a sensor signal database and so on. The threshold database records thresholds, which are used for diagnosis of the state of the cutting process in the monitoring algorithm. The users of the monitoring function can search the standard threshold by cutting conditions from the threshold database, and can set the threshold for the monitoring algorithm when the data is available. The sensor signal database can record raw sensor signals obtained from cutting tests along with the attribute information such as the cutting conditions, the measurement conditions and the state of the cutting process, in order to assist in developing monitoring algorithms. Subsequently, the developers of monitoring algorithms can easily obtain data from the sensor signal database for investigating the relationship between sensor signals and the state of the cutting process. In addition, the developed monitoring system can simulate the signal processing of the monitoring algorithm by utilizing the recorded sensor signals. Therefore, the developers can efficiently evaluate the developed monitoring algorithm on the basis of the results of the simulations. Various monitoring modules, which are combinations of a monitoring algorithm with the threshold database, can be installed in the developed monitoring system, and the monitoring modules are interchangeable as shown in Fig. 3.18.

We have developed two monitoring modules for detecting tool fracture in the end-milling and drilling processes based on the results of our investigations as described in subsections 3.2.3 and 3.3.3. Figures 3.19 and 3.20 show the graphical user interfaces of the developed monitoring modules for end-milling process and for drilling process, respectively. We carried out verification tests of the developed monitoring modules by

utilizing the simulation function and the recorded sensor signals. The results of the verification tests showed that the monitoring algorithms could identify tool fractures in the end-milling and drilling processes.

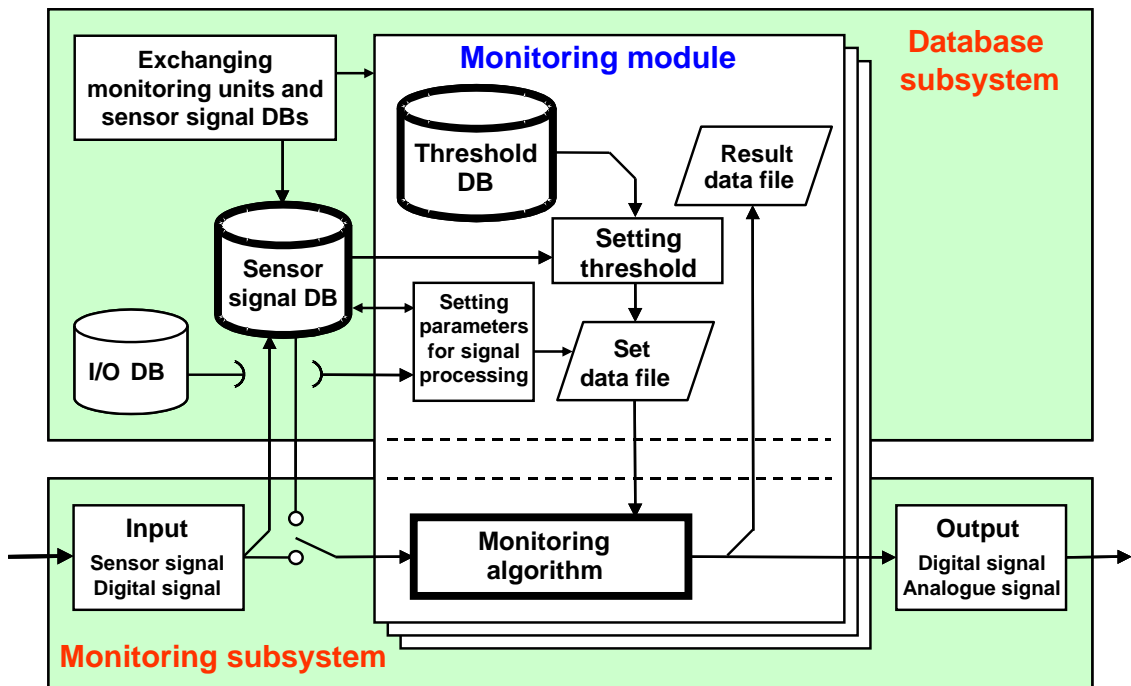


Fig. 3.17 Software structure of the developed monitoring system

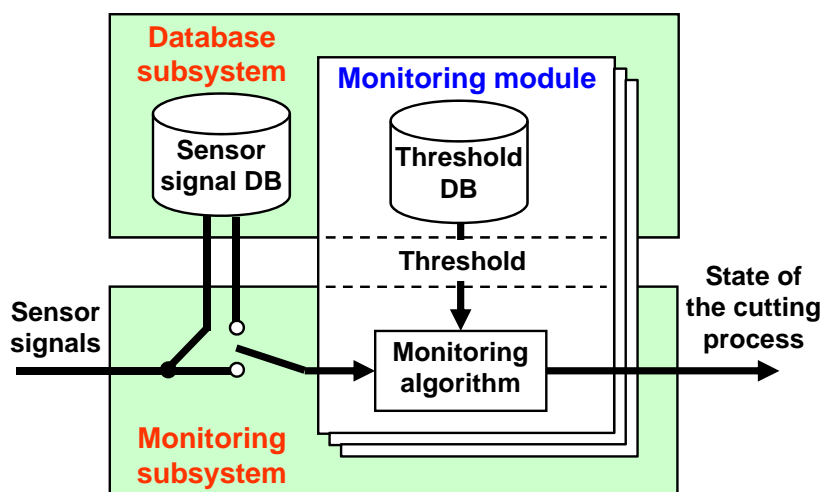


Fig. 3.18 Conceptual diagram of interchangeable monitoring modules

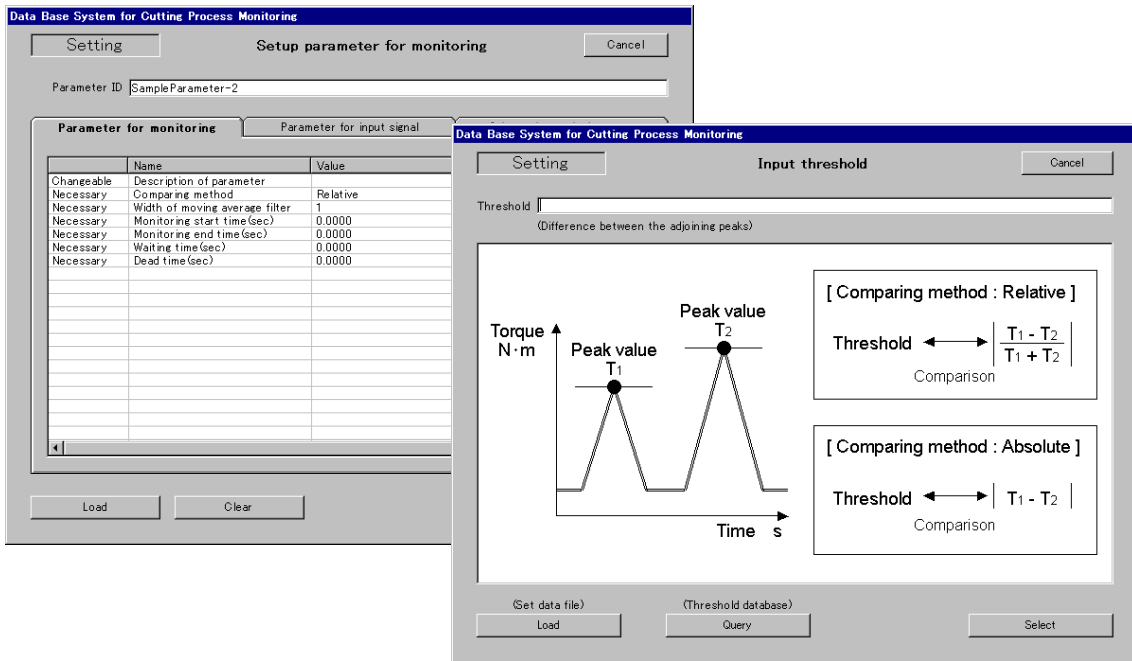


Fig. 3.19 Graphical user interface of monitoring system for detecting tool fracture in the end-milling process

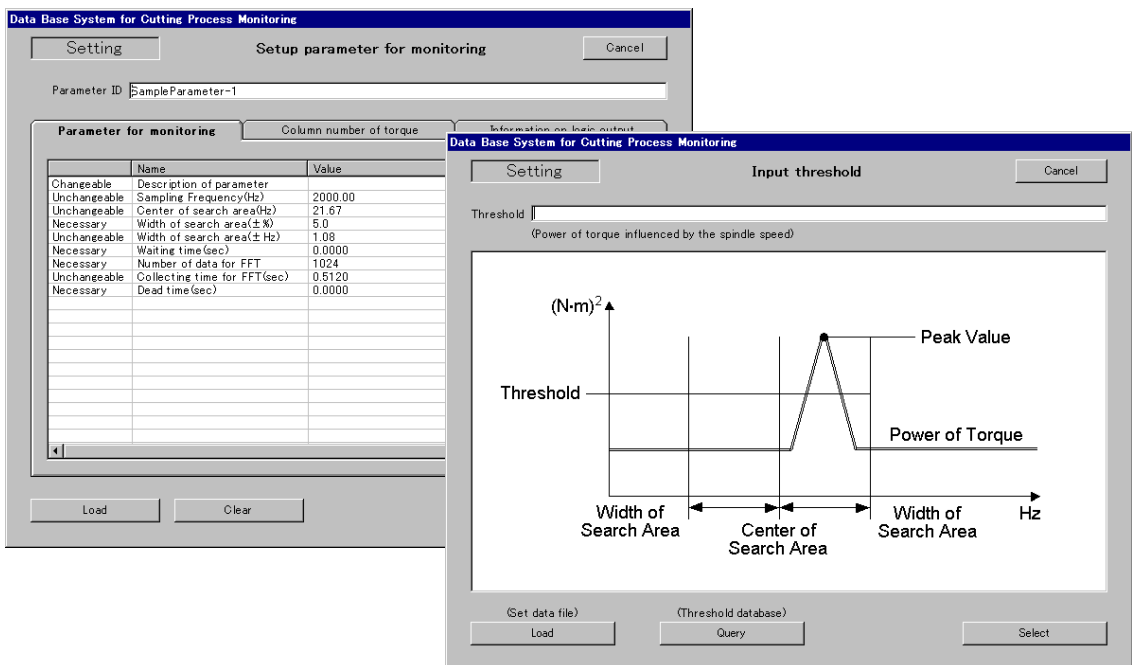


Fig. 3.20 Graphical user interface of monitoring system for estimating tool fracture in the drilling process

### 3.5 Summary of this chapter

In this chapter, we have discussed the possibility of estimating tool wear and tool fracture detection in milling and drilling processes from the cutting torque signals measured by the developed sensor system. In addition, we have proposed a monitoring system for cutting processes, which has not only monitoring functions of cutting processes but also unique database functions to assist in developing the monitoring algorithms. The results of the present study are summarized as follows:

- (1) The possibility of estimating flank wear in the milling process from cutting torque detected by the developed sensor system was recognized through continuous cutting tests, as the maximum value of the cutting torque per revolution increased with increases in flank wear.
- (2) The possibility of estimating tool fracture in the milling process from cutting torque detected by the developed sensor system was recognized through cutting tests because the difference in the values of the maximum cutting torque generated by the two cutting edges consisting of a cutting tool increased when a tool fractured.
- (3) In the drilling process, the standard deviation and the mean value of the cutting torque showed an abrupt increase when the abnormal drilling state caused by tool wear occurred. A method for estimating abnormal drilling state caused by tool wear was proposed using the standard deviation and the mean value of the cutting torque as indexes. The validity of the proposed method was confirmed through continuous drilling tests.
- (4) In the drilling process, the frequency component caused by the spindle speed included in the cutting torque showed a sharp rise when the drill fractured. A method

for detecting tool fracture during drilling was proposed using the frequency component caused by the spindle speed included in the cutting torque as an index.

(5) We have developed a monitoring system for cutting processes, which has not only monitoring functions but also database functions to assist in developing monitoring algorithms. The database functions are twofold such as the functions of a threshold database and a sensor signal database. The threshold database records thresholds, which are used for diagnosis of the state of the cutting process in the monitoring algorithm. The sensor signal database can record raw sensor signals obtained from cutting tests along with the attribute information. In addition, the developed monitoring system has a simulation function for the monitoring algorithm by utilizing the recorded sensor signals, in order to examine the propriety of the monitoring algorithm.

## **Chapter 4**

# **Development of a machining system with feedback control based on cutting force**

### **4.1 Objectives**

To realize defect-free cutting of difficult-to-cut materials, one of the most effective and reliable methods is to control the feed rate or spindle speed based on cutting force or torque, because the cutting force and torque are directly related to the mechanics of the cutting process.

Therefore, we have proposed and developed a machining system which can be operated at a predetermined cutting force by changing the feed rate based on cutting force signals measured by a piezoelectric cutting dynamometer. Subsequently to the development, the basic performances of the developed system have been confirmed through evaluation tests.

## 4.2 System structure

Figure 4.1 and 4.2 show the structure and the appearance of our newly developed machining system, respectively. AC servo systems are utilized for the motor-driven feed of the developed system. The AC servo amplifier (Panasonic, MINAS A4T) has an analog-to-digital converter for acquiring signals from a sensor in order to control the force on an object. The analog-to-digital converter has a resolution of 16 bits and a sampling time of 0.166 msec., and the servo amplifier controls the feed rate based on the acquired sensor signals. Therefore, the AC servo system can be operated at a predetermined force on the object. The control in the servo amplifier is based on a proportional-integral-derivative (PID) algorithm. Figure 4.3 shows a comparison of the feedback loops between the developed system and conventional systems [109]. The feedback loop of the AC servo system we utilized is shorter than that of conventional systems. Consequently, the AC servo system can act within the cycle time of 0.166 msec. when the maximum allowable performance is enabled. To provide force signals to the AC servo amplifiers, a piezoelectric cutting dynamometer (Kistler, 9256C2) is used. Via a three-channel charge amplifier (Kistler, 5019B131), the cutting force signals are inputted in the analog-to-digital converter of the AC servo amplifiers and a data acquisition system. In addition, a motion controller (ACCEL, MPC-2000) is utilized for switching between a position control mode and a force control mode because of the following reason: When utilizing the force control mode, the AC servo system cannot control its positioning, even though it is essential to control the positioning in cutting processes. Hence, the position signals obtained from rotary encoders are used as a trigger to switch to the other mode, as shown in Fig. 4.4. Also, information regarding the displacements of the three axes is inputted in the data acquisition system from the

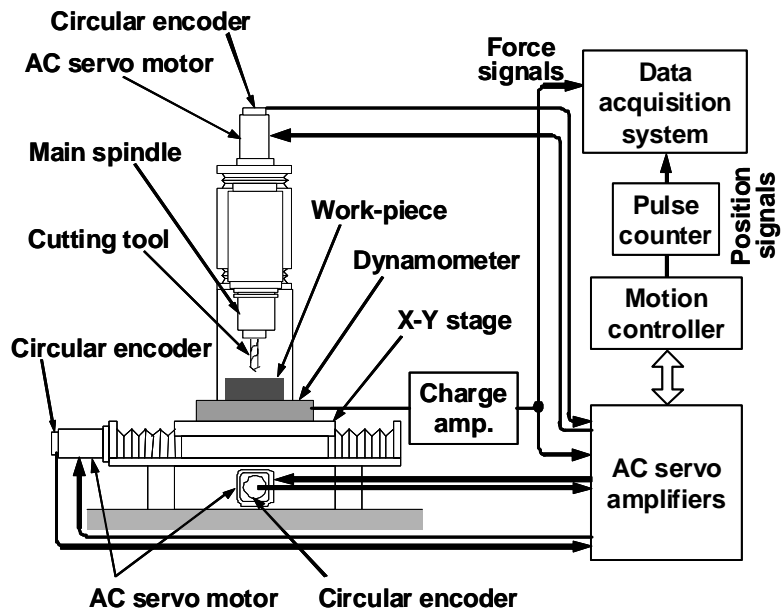


Fig. 4.1 Structure of the developed machining system

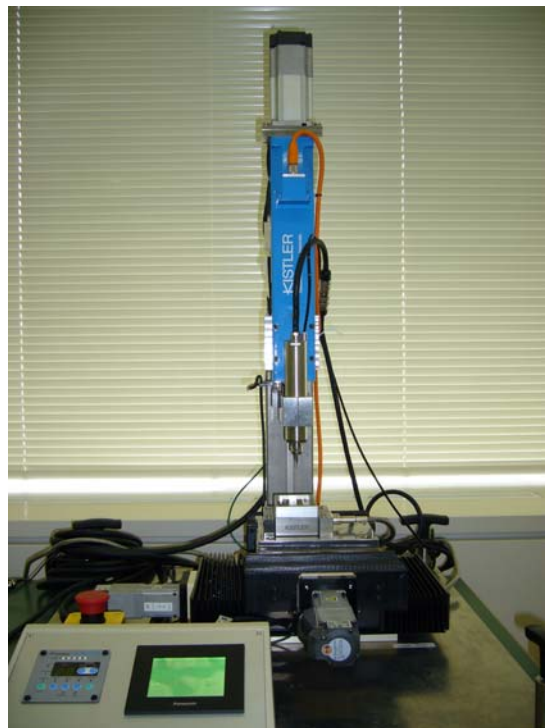


Fig. 4.2 Appearance of the developed machining system

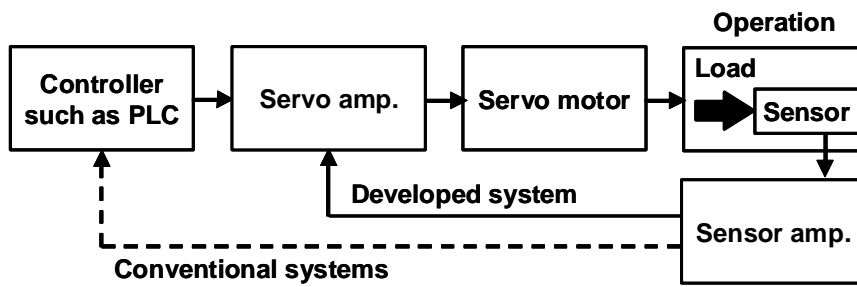


Fig. 4.3 Comparison of the feedback loops between the developed system and conventional systems

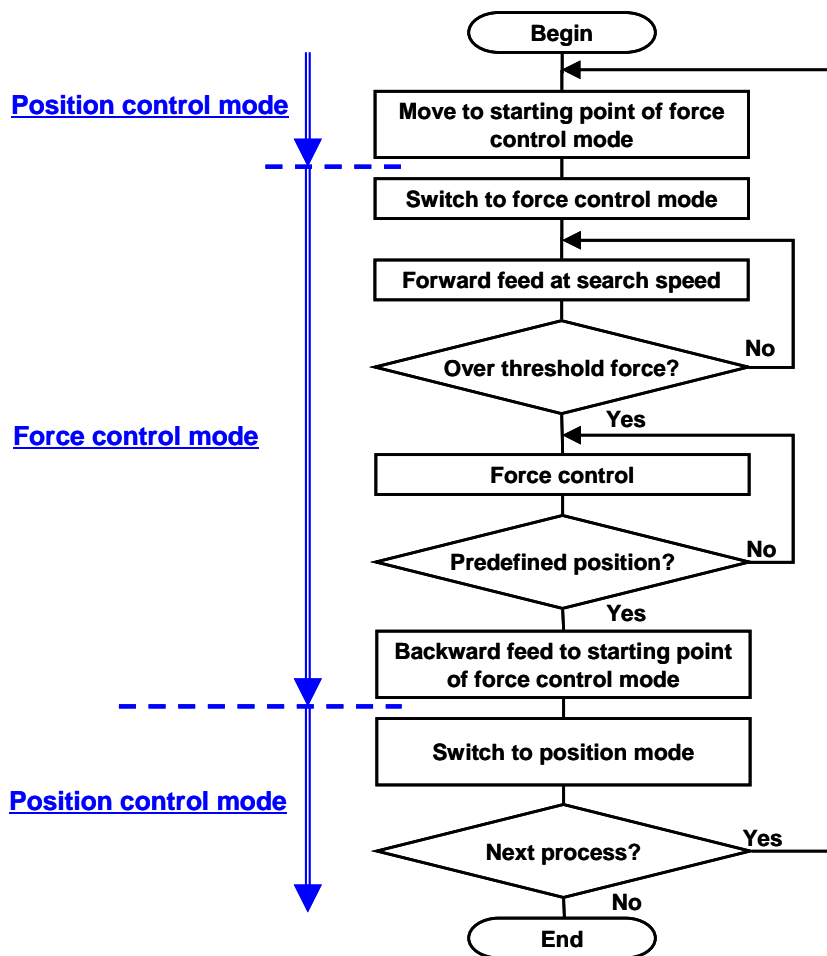


Fig. 4.4 Methodology for controlling the developed system

rotary encoders through pulse counters.

The advantages of the system we developed are twofold. Not only can we directly control the feed rate based on the signals from the cutting dynamometer—i.e., the system can be operated at a predetermined force on the object—but we can also alternately switch between the position control mode and the force control mode based on the position signals.

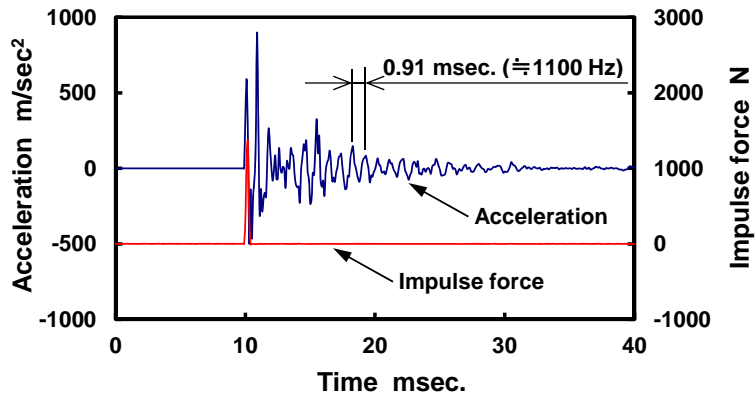
### **4.3 System performance evaluation**

To confirm the basic performance of the developed system, evaluation tests of the Z-axis were carried out under the following conditions. The thrust force to the cutting dynamometer is applied through a ball-end mill with a diameter of 1.0 mm (which is clamped to a main spindle), and the search speed (which means the preset value of the feed rate until a thrust force signal crosses the threshold to begin force feedback control) is adjusted to 5 mm/sec. Recorded sensor signals by the data acquisition system were acquired as raw signals. But the thrust force signals for the feedback control were processed by a low-pass filter in the AC servo amplifier for Z-axis, and the cutoff frequency was set at 500 Hz for the following reason.

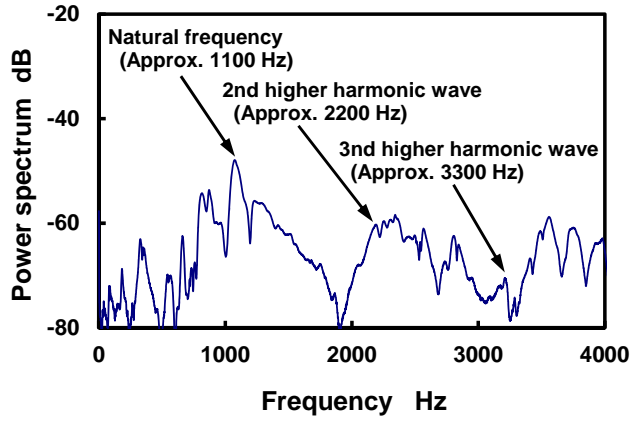
Figure 4.5 shows the measurement result of the natural frequency of the Z-axis drive mechanism. In this measurement, a piezoelectric accelerometer (Kistler, Type 8702B100) was attached at the axial end of the Z-axis drive mechanism, and then the axial end was excited by a piezoelectric impulse hammer (Kistler, Type 9726A20000) in the direction of the Z-axis. From Figs. 4.5 (a), the period of the periodic vibration included in the acceleration signal is 0.91 msec. which means that the frequency is approximately 1100 Hz. From Figs, 4.5 (b), the result of fast Fourier transformation

(FFT) analysis shows the peak of the power spectrum of approximately 1100 Hz. In addition, the peak of the second and third higher harmonic waves, which are approximately 2200 and 3300 Hz respectively, are observed. Accordingly, it is clear that the natural frequency of the Z-axis drive mechanism is approximately 1100 Hz [110]. To avoid the resonantly-generated control error, it is necessary to eliminate the influence of the natural frequency of the Z-axis drive mechanism [111]. Therefore, the cutoff frequency of the low-pass filter should be set at 500 Hz or less. In fact, when the cutoff frequency was set at 600 Hz or more, the thrust force controlled by the developed machining system fluctuated abnormally in sympathetic vibration with the natural frequency of the Z-axis drive mechanism.

Figure 4.6 shows the result of the force operation test that was done under the following procedures. First, the threshold to begin force feedback control is 8 N and the rate of increase in thrust force is 40 N/sec.; second, after the thrust force exceeds the threshold, the thrust force is controlled to proportionally increase at 40 N/sec., and then the thrust force is kept at a constant 40 N; third, the fall of the thrust force from 40 to 0 N is controlled by step response after keeping it at a constant 40 N for 0.8 seconds; fourth, the sequence from step one to step three is repeated four times; fifth, after the thrust force crosses over the threshold, the thrust force is controlled at 40 N/sec. and then the thrust force is kept at a constant 20 N; sixth, the decrease of the thrust force from 20 to 10 N is controlled by step response after keeping it at a constant 20 N for 1.3 seconds; finally, the fall of the thrust force from 10 to 0 N is controlled by step response after keeping it at a constant 10 N for 0.8 seconds. As is obvious from Fig. 4.6, the behavior of the thrust force is accurately controlled at the predetermined value, and the overshoot of the thrust force is very small.



(a) Output signals from the accelerometer and the impulse hammer



(b) Result of FFT analysis

Fig. 4.5 Measurement result of the natural frequency of the Z-axis drive mechanism

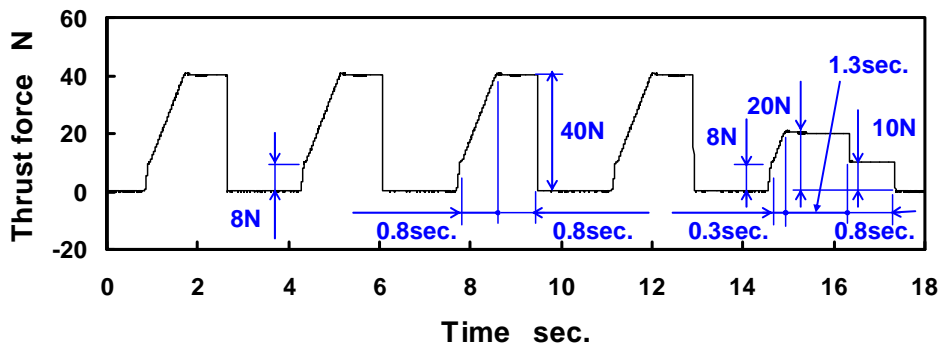


Fig. 4.6 Result of the force operation test

Next, a transient response test of the Z-axis was performed under the following conditions. The thrust force applied to the cutting dynamometer is constantly controlled at 10 N first, and then the controlling value is changed to 11 N. The rise is controlled by step response. Figure 4.7 shows the result of the transient response test. The stabilization time from 10 N to 11 N, with a margin of error of 11 N plus or minus 2%, is 7.35 msec., and the overshoot is 0.3 N. The stabilization time consists of the delay time of the analog-to-digital converter (0.166 msec.) and the low-pass filter (2 msec.), the control delay of the PID compensation, and the effect of the inertial force of the mechanism. Consequently, it is contemplated that the typical time-constant of the developed machining system is approximately 7.35 msec. under the same conditions. The maximum spindle speed of the developed machining system is 60,000 rpm (= 1.0 msec./rev.). The stabilization time of 7.35 msec. can control the predetermined force by adjusting the feed rate within 8 revolutions of a cutting tool when the main spindle is rotated at 60,000 rpm and the cutoff frequency of the low-pass filter in the AC servo amplifier for Z-axis is set at 500 Hz. Therefore, it would appear that the developed machining system has enough response characteristics to apply cutting processes.

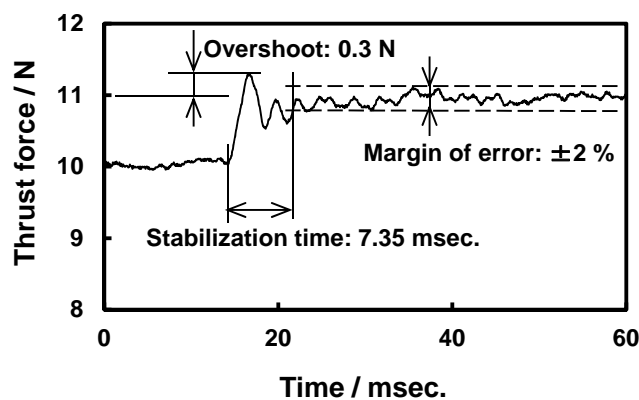


Fig. 4.7 Result of the transient response test

When the developed system was controlled at a constant thrust force, the system stability was investigated under the following procedures. First, a weight equivalent to 1 N, in which a piezoelectric force sensor (Kistler, type 9323AA) has been installed, is placed on the table of the cutting dynamometer; second, the output signals of the cutting dynamometer and the force sensor are reset to zero; third, the thrust force applied to the table is constantly controlled at 10 N; finally, the thrust force of 1 N as an external force is reduced by removing the weight by a human hand. The result of the experiment is shown in Fig. 4.8. The falling time from 0 to 1 N of the external force is approximately 40 msec, and most of the falling time is caused by the motion speed of the human hand since the frequency response of the force sensor including its charge amplifier (Kistler, type 5015A) is up to 200 kHz (-3 dB) [112]. During the falling time, the thrust force controlled by the developed system is restored to 10 N with a margin of error of plus or minus 2.0 %. And then, the thrust force is controlled at a constant 10 N with a margin of error of plus or minus 1.0 %. In addition, we also carried out the evaluation tests under varying the controlled thrust force and the external force, and the results are

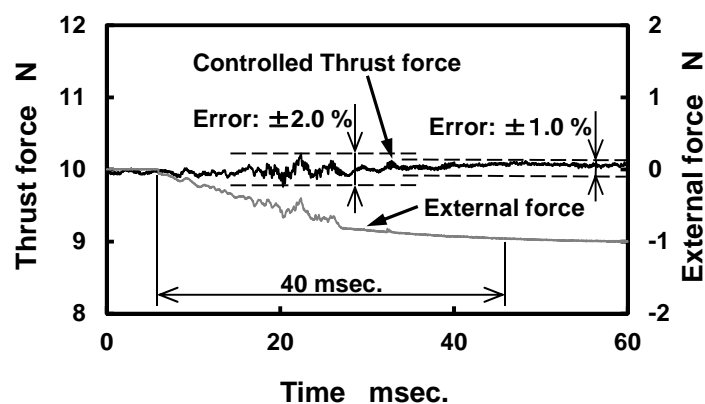


Fig. 4.8 Evaluation of the system stability at a constant thrust force

summarized in Table 4.1. Based on the results shown in Table 4.1, the relationship between the ratio of external force to controlled thrust force and the maximum control error during the falling time of the external force was examined, and the result is shown in Figure 4.9. The maximum control error increases in correlation with an increase in the ratio of external force to controlled thrust force. In addition, the maximum control error increases with decrease in the external force. Consequently, it is necessary to ensure the further development of the system as our future work. In the evaluation tests, however, all of the maximum control errors are within plus or minus 3.0%. After the falling time of the external force, all of the test results showed that the developed machining system controlled the thrust force at predetermined values with a margin of error of plus or minus 1.0 %.

Judging from the results of these tests, it may be concluded that the system we developed can adequately control the predetermined force by changing the feed rate based on thrust force measured by the cutting dynamometer.

Table 4.1 Results of the system stability evaluation under varying conditions

Controlled thrust force [N]	Maximum control error during the variation of external force [ $\pm$ %]	
	External force: -0.5 N	External force : -1.0 N
5	3.0	2.7
10	2.3	2.0
15	1.9	1.7
20	1.6	1.5

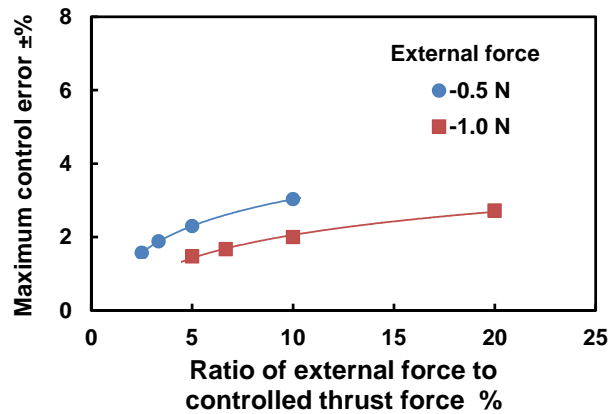


Fig. 4.9 Relationship between the ratio of external force to controlled thrust force and the maximum control error

## 4.4 Summary of this chapter

The key points of our work in this chapter are summarized as follows:

- 1) We have proposed an approach of applying feedback control based on thrust force, in order to realize defect-free cutting of difficult-to-cut materials.
- 2) We have developed a machining system that can be operated at a predetermined cutting force by changing the feed rate based on cutting force signals measured by a piezoelectric cutting dynamometer.
- 3) By conducting evaluation tests, the basic performance of our newly developed system has been confirmed. As the results, it has been verified that our system can adequately control the thrust force.



## **Chapter 5**

# **Drilling of borosilicate glass with the developed machining system**

### **5.1 Objectives**

To fabricate flow channels, which consist of holes and grooves, on the substrate of a lab-on-a-chip device made of glass, the cutting process is one of the most effective methods. This is because holes and grooves are produced with high form accuracy in a short machining time. However, it is difficult to machine glass under stable cutting conditions at all times because glass, being a hard and brittle material, is sensitive to the occurrence of cracks at the cutting portion during this kind of process.

In this chapter, we propose to apply feedback control based on cutting force, in order to realize defect-free cutting of borosilicate glass. We carried out drilling tests with our newly developed machining system that is fully described in chapter 4, in order to

confirm the possibility of borosilicate-glass cutting with feedback control based on cutting force.

## 5.2 Experimental methodology

As work-pieces in the cutting tests, we used plates of borosilicate glass with a thickness of 1.1 mm. The chemical composition and mechanical properties of the borosilicate glass are shown in Table 5.1 [113].

Figure 5.1 shows the experiment setup for drilling. As shown in this figure, a jig to fix and to immerse the work-piece in lubricating pure water was mounted on the dynamometer. A backing plate of borosilicate glass (of the same type as the work-piece) was placed under the work-piece in the drilling tests, in order to prevent chippings and cracks at the exit surfaces on the work-piece.

In the milling tests using ball-end mills to fabricate grooves on glass plates, cutting at the center of a rotating tool should be avoided in order to obtain a fine machined surface, since the cutting speed at the center is zero. Accordingly, in the milling tests, the ball-end mills were tilted at plus 45 degrees to the vertical axis as Matsumura et al.

Table 5.1 Specifications of the borosilicate glass

Chemical composition [wt%] 81%SiO <sub>2</sub> , 13%B <sub>2</sub> O <sub>3</sub> , 4%Na <sub>2</sub> O/K <sub>2</sub> O, 2%Al <sub>2</sub> O <sub>3</sub>	
Thickness: 1.1 mm	
Material properties:	
Density at 20 °C	2.2 g/cm <sup>3</sup>
Young's modulus at 20 °C	64GPa
Knoop hardness	480 HK <sub>0.1/20</sub>
Poisson's modulus	0.2
Bending strength	25 MPa

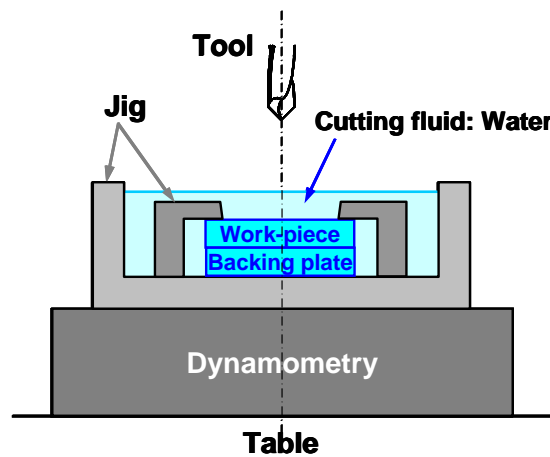


Fig. 5.1 Experiment setup for drilling

suggested [75 - 77]. Feed direction of the milling tests was plus 45 degrees to the tilted ball-end mills.

After the cutting tests, machined surfaces on the work-piece were observed by an optical microscope equipped with a CCD camera.

### 5.3 Force control of cutting processes with the developed machining system

Drilling tests with the developed machining system were performed under the following conditions: the spindle speed was 20,000 rpm; the feedback control was based on thrust force signals; and the cutoff frequency of low-pass filters in the AC servo amplifiers was 160 Hz to eliminate the influence caused by the spindle speed as well as the influence of the natural frequency of the Z-axis drive mechanism.

#### 5.3.1 Drilling process with a twist drill

Drilling tests with the developed system were carried out using twist drills of

diamond-coated carbide with a diameter of 1.0 mm. Figure 5.2 shows an example of behaviors of thrust force and displacement in the drilling process when making a blind-hole. The photographs of the machined hole obtained by the test are shown in Fig. 5.3. In Fig. 5.2, the displacement of 0 mm indicates the upper surface of the work-piece. At first, the thrust force was controlled to proportionally increase from 0 to 5 N over a span of five seconds, and then the thrust force was kept at a constant 5 N. Consequently, when the depth of the cut at the pointed end of the cutting edge reached 0.9 mm, the thrust force was steadily and proportionally decreased from 5 to 0 N over a span of five seconds. The fluctuation component included in the thrust force caused by the cutting mechanics is observed, but the average of the thrust force in the process is controlled as a predetermined value. On the other hand, the change in the displacement is not regular because our newly developed system controlled the thrust force by changing the feed rate based on cutting force signals. From the results, it has been verified that our recently developed system can control the thrust force in the drilling process. From the photograph focused on the upper surface of the machined hole as shown in Fig. 5.3(a),

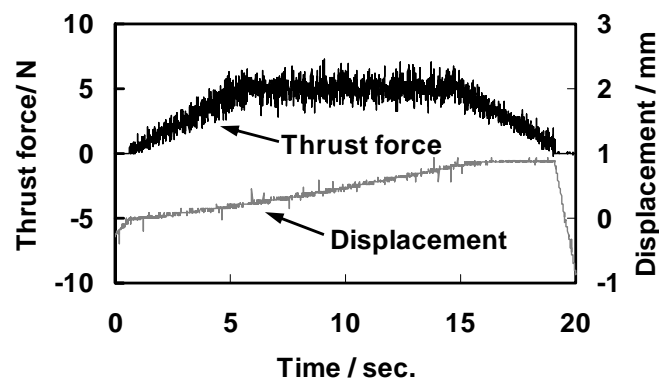
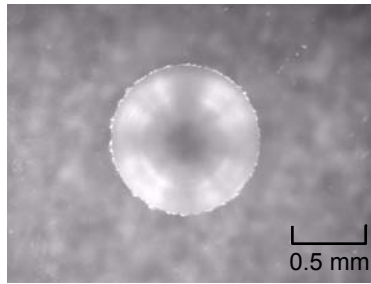
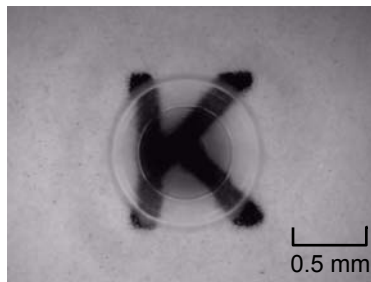


Fig. 5.2 Behaviors of thrust force and displacement in the drilling process when making a blind-hole with the drill



(a) Focused on the upper surface



(b) Focused on the bottom face of the machined hole

Fig. 5.3 Machined blind-hole with the drill

chippings at the circular edge consists of the upper surface and the side of the machined hole are observed, but the width of chippings is very small, less than 3% of the machined hole diameter. In addition, the bottom face of the machined hole is very transparent, as shown in Fig. 5.3(b), since the letter “K,” printed on a paper that was placed under the glass plate, can be seen very clearly through the machined glass plate. This result implies that the process was done under ductile cutting.

Figure 5.4 shows an example of another machined hole, which is observed from the lower surface. This machined hole was made under the same conditions as in the above-mentioned test, but with a different depth of cut. The depth of cut was 1.5 mm, which included drilling of the backing plate. As is obvious from the photograph, the circular edge consists of the lower surface and the side of the machined hole has a lot of

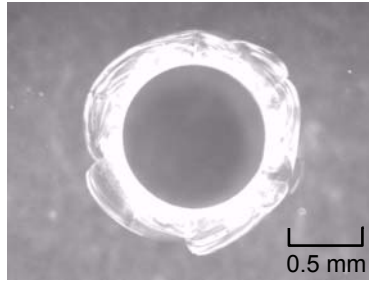
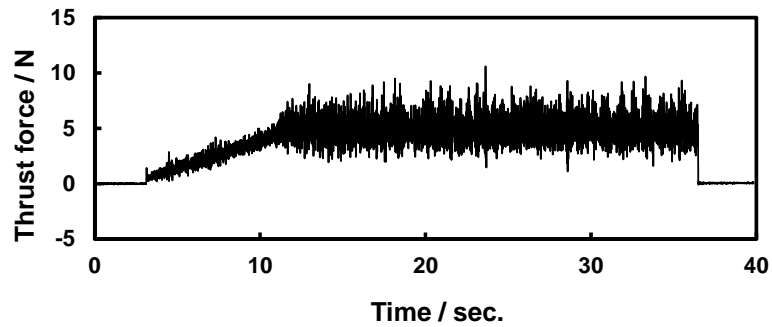


Fig. 5.4 Machined through-hole with the drill

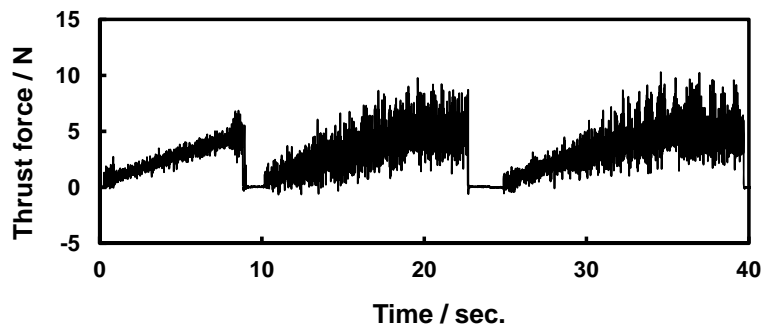
chippings and cracks, and these flaws are very large in comparison with those in Fig 5.3(a). In addition to this test, other drilling tests with drills were performed to fabricate through-holes under various conditions including the application of the step-feed method described in the next subsection. However, it was impossible to machine any through-hole with high quality. It would appear that the outer corner of the drill affects the crack and chipping initiation when the remaining thickness of the glass plate is reduced, since the cutting force is larger than that at other parts of cutting edges due to the differences in the volume of material removed per unit time.

### 5.3.2 Drilling process with a ball-end mill

In place of the above-mentioned drills, we carried out drilling tests with ball-end mills to make through-holes. The ball-end mills were made of diamond-coated carbide, where the diameter was 1.0 mm with a 0.5 mm nose radius. The tests were carried out under the following conditions. Thrust force was at first controlled to proportionally increase from 0 to 5 N over a span of 10 seconds, and then kept at a constant 5 N. When the depth of the cut at the pointed end of the cutting edge reached a set value, the feedback control was stopped and then switched to a backward feed control. The depth



(a) Continuous feed method



(b) Step-feed method

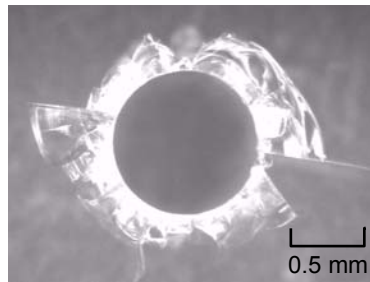
Fig. 5.5 Behaviors of thrust force in the processes when making through-holes with the ball-end mill

of the cut in total was 1.5 mm, which included drilling of the backing plate. In the case of the step-feed method, the feed was divided into three different depths of cut at the pointed end of the cutting edge, namely 0.40, 0.95, and 1.50 mm in series.

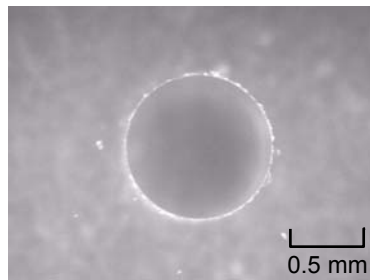
Figures 5.5(a) and (b) show the behaviors of thrust force in the drilling processes with continuous feed and step-feed methods, respectively. And the machined holes viewed from the lower surface of the work-pieces are shown in Figs. 5.6(a) and (b), corresponding to Figs. 5.5(a) and (b). As is obvious from these photographs, the

machined hole made by the step-feed method is of much higher quality compared to the machined hole made by the continuous feed method. In figure 5.6(b), chippings at the circular edge consists of the lower surface and the side of the machined hole are observed, but the width of chippings is very small, less than 3 % of the machined hole diameter. From observation of the ball-end mill after the drilling tests using the continuous method, chip packing is seen at flutes of the ball-end mill. The fluctuation component included in the thrust force with the step-feed method is slightly larger than that of the continuous feed method, as shown in Figs. 5.5(a) and (b). On the other hand, the average of the thrust force of the step-feed method is smaller than that of the continuous feed method, because the first step of the control pattern is the increase in proportion from 0 to 5 N over a span of 10 seconds, and the durations of each step are nearly equal to the span of the first step. What is especially important is that when the pointed end of the cutting edge reaches the lower surface of the glass plate, the thrust force is controlled by the first step of the step-feed pattern. The cutting time is around 30 sec. in Fig. 5.5(b), obtained from the displacement information. Therefore, it is believed that the occurrence of significant cracks and chippings at the circular edge consists of the lower surface and the side of the machined hole was avoided by the force feedback control.

For comparison, drilling tests using conventional feed control were done. In the tests, the feed rate was 3 mm/min., which was nearly equal to the average of the feed rate calculated from the displacement information of Figs. 5.5(a) and (b). Other cutting conditions were the same as in the above test. Results of the drilling tests with ball-end mills are summarized in Table 5.2. In the case of using feed control with continuous feed and step-feed methods, we were not able to machine any fine through-holes in the



(a) Continuous feed method



(b) Step-feed method

Fig. 5.6 Machined through-holes with the ball end mill viewed from the bottom of the work-piece

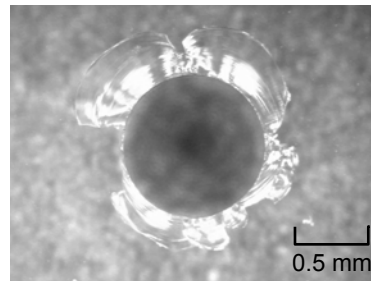


Fig. 5.7 Machined through-hole using feed control with the ball end mill viewed from the bottom of the work-piece (Feed rate at 3 mm/min, step-feed method)

tests as shown in Fig. 5.7.

Based on observation of the results of the drilling tests with ball-end mills, it would appear that the step-feed method is necessary in order to prevent the occurrence of chip

Table 5.2 Results of drilling tests with ball-end mills

Force/Feed control	Step/Continuous feed method	Width of chippings and cracks to the hole diameter
Thrust force at 5 N	Step-feed	less than 3 %
	Continuous feed	over 20 %
Feed rate at 3 mm/min.	Step-feed	over 20 %
	Continuous feed	over 20 %

packing at the flutes of tools. In addition, the force feedback control is effective for machining through-holes on glass, since the control avoids the occurrence of significant cracks and chippings when the pointed end of the cutting edge has reached the lower surface of the glass plate. Also, the shape of ball end mills is suitable for glass drilling processes, because the cutting force at the outer side of the end cutting edge is smaller than that at other parts of the end cutting edges caused by the differences in the volume of material removed per unit time. However, this methodology for controlling thrust force is not effective when the cutting state is abnormal due to progressive tool wear etc. This is because the controlling methodology does not consider controlling the correct value of thrust force synchronized with the tool position when the pointed end of the cutting edge reaches near the lower surface of the glass plate. Accordingly, we will propose an improved methodology for controlling thrust force synchronized with a tool position in section 5.4.

### **5.3.3 Milling process with a ball-end mill**

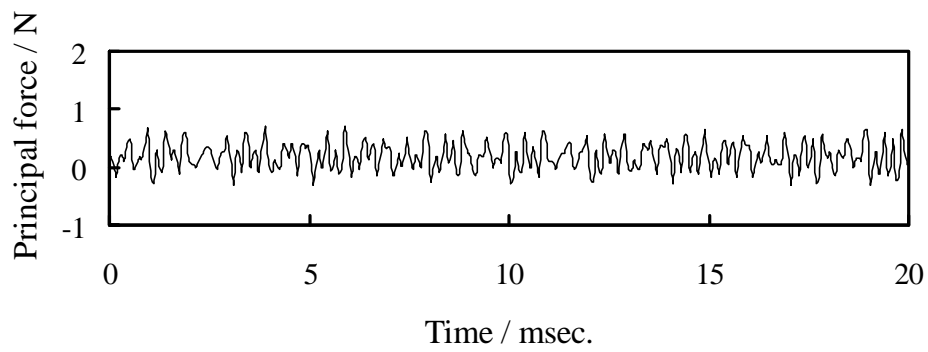
Milling tests with the developed system were performed to fabricate grooves on glass plates under the following conditions: the tools were ball-end mills of (Al,Ti)N-coated carbide, where the diameter was 0.2 mm with a 0.1 mm nose radius; the spindle speed was 60,000 rpm; the axial depth of cut was 0.05 mm; principal force was used for controlling the feed rate of feed direction; and the principal force was controlled at 0.5 N.

Figures 5.8(a), (b) and (c) show the behaviors of principal force, feed force, and thrust force, respectively. After this test, the feed rate of feed direction was calculated. As the result, the mean value of the feed rate was 23.0 mm/min. For comparison, we carried out milling test with feed control and the feed rate was set at constant 20.0mm/min. (which means that the feed rate was lower than that of the calculated mean value from the milling test with force control). The surfaces of the machined groove, as compared to the surface for which the principal force was controlled at 0.5 N are shown in Figs. 5.9 (a) and (b), respectively. As is obvious from the photographs, when the principal force is controlled at 0.5 N, the quality of the machined surface is improved and the occurrence of chipping is reduced.

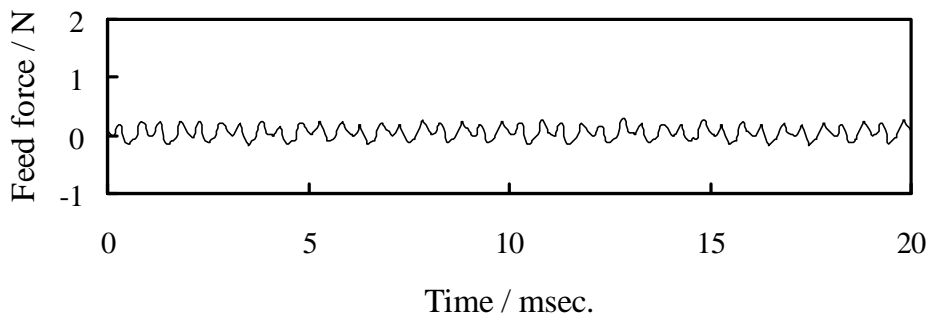
From the results, it would appear that the force feedback control shown in our newly developed system has the potential to be used for glass cutting in milling processes.

## **5.4 Through-hole drilling with multistage force control**

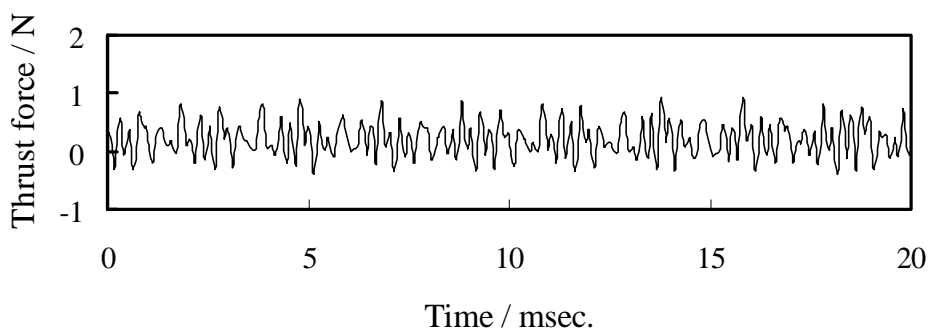
In this section, we propose an improved methodology for controlling thrust force synchronized with a tool position, in order to drill through holes on plates of borosilicate glass without significant cracks on the exit surfaces.



(a) Principal force

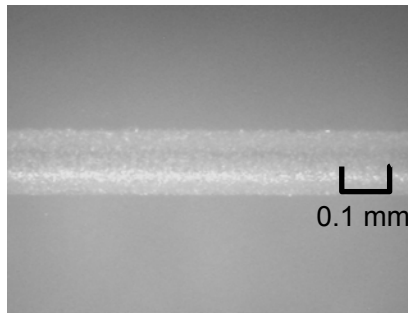


(b) Feed force

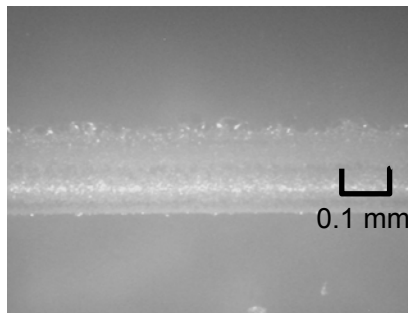


(c) Thrust force

Fig. 5.8 Behaviors of cutting forces in the milling process



(a) Force control (Principal force at 0.5 N)



(b) Feed control (Feed rate at 20 mm/min.)

Fig. 5.9 Machined grooves with the ball-end mill

#### 5.4.1 Investigation of crack generation during blind-hole drilling

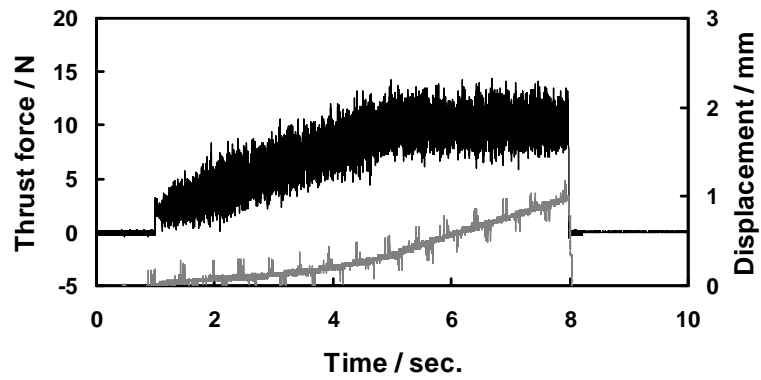
In the mechanical drilling processes of glass plates, cracks occur frequently at the back side of the work-piece when the remaining thickness of the work-piece is reduced. Until that time, however, the glass plate is machined without any significant cracks under certain conditions [67, 68]. Accordingly, we divided the drilling process into two stages for force feedback control. The first stage of the process is to make a blind-hole with a view to enhancing the productivity, and the second stage is to manufacture a through-hole without significant cracks on the exit surface of the work-piece after the

first stage. In the drilling tests, we used ball-end mills of diamond-coated carbide having a diameter of 1.0 mm with a 0.5 mm nose radius, based on positive results from our study described above. The spindle speed was 20,000 rpm. The thrust force signals for the feedback control were processed by a low-pass filter in the AC servo amplifier for z-axis, and the cutoff frequency was set at 500 Hz to eliminate the influence of the natural frequency of the Z-axis drive mechanism. This is because, based on the results of cutting tests in subsection 5.3.2, the fluctuation component included in thrust force cause by the spindle speed in the drilling of borosilicate glass is negligible small compared with the influence of the natural frequency of the Z-axis drive mechanism.

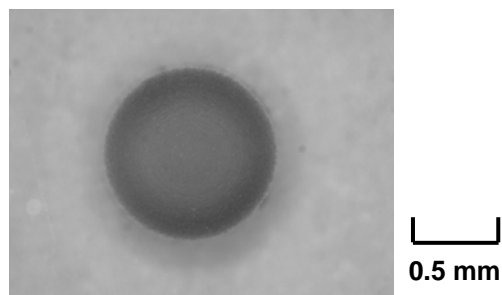
In order to determine parameters for the first stage of force feedback control, the relationship between the crack generation at the bottom face of the machined hole and the depth of the drill hole was examined during blind-hole drilling. Figure 5.10(a) shows the behavior of thrust force and displacement in the drilling process when the depth of the drill hole at the tip of the cutting edge was 1.00 mm (which means that the remaining thickness after the drilling was 0.10 mm). In this test, the flow of thrust force control occurs under the following procedures. First, the search speed (which means the preset value of the feed rate until a thrust force signal crosses the threshold to begin force feedback control) is adjusted to 5 mm/sec. Second, the threshold is 2 N. Third, after the thrust force exceeds the threshold, the thrust force is controlled to proportionally increase from the threshold value of 2 N to 10 N over a span of four seconds, and then the thrust force is kept at a constant 10 N. Finally, when the depth of the drill hole reaches 1.00 mm, the fall of the thrust force from 10 to 0 N is controlled by step response after keeping it at a constant 10 N. The photograph of the machined hole obtained by the test is shown in Fig. 5.10(b). In Fig 5.10(a), the displacement of 0

mm indicates the upper surface of the work-piece. As can be seen from Fig. 5.10(b), which is a photograph of the blind-hole viewed from the back side of the work-piece, the bottom face of the machined hole is transparent without any cracks. Figures 5.11(a) and (b) show another example of the drilling tests. This machined hole was made under the same conditions as in the above-mentioned test, but with a different depth of drill hole. The depth of the drill hole was 1.05 mm (which means that the remaining thickness was 0.05 mm). As is obvious from Fig. 5.11(b), the back side of the work-piece has cracks, and these flaws are very large when compared with the diameter of the machined hole. In Fig. 5.11(a), the fluctuation component included in the thrust force increases sharply at the end of the process. This event was also observed in other processes, with varying degrees of crack generation on the back sides of the work-pieces. These results imply that crack generation at the bottom of the machined hole can be detected by observation of the event, which the fluctuation component included in thrust force increases sharply in the process.

The observational results of machined holes under varying the thrust force and the remaining thickness after the drilling are summarized in Table 5.3. The minimum values of the remaining thickness without cracks at the bottom of the machined hole decrease in correlation with an increase in thrust force. From the results, we believe that force feedback control is effective at preventing crack generation at the bottom of the machined hole. However, when we used continuous feed with force feedback control, we were not able to machine any fine through-holes in the tests, as shown in Table5.3.

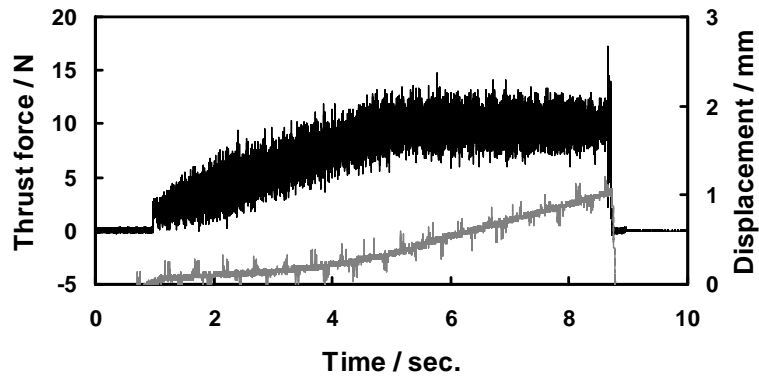


(a) Behavior of thrust force and displacement

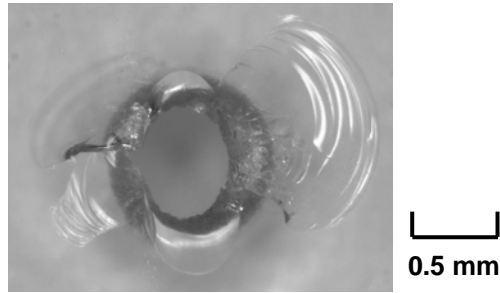


(b) Machined blind-hole viewed from the back side of the work-piece

Fig. 5.10 Result of the drilling test when the remaining thickness after the drilling was 0.10 mm



(c) Behavior of thrust force and displacement



(d) Machined blind-hole viewed from the back side of the work-piece

Fig. 5.11 Result of the drilling test when the remaining thickness after the drilling was 0.05 mm

Table 5.3 Observational results of machined holes under varying conditions

Thrust force [N]	Remaining thickness after the drilling [mm]			
	0	0.05	0.10	$\geq 0.15$
5	Large cracks	Small cracks	No crack	No crack
10	Large cracks	Large cracks	No crack	No crack
15	Large cracks	Large cracks	Large cracks	No crack

Note: large and small represent that the sizes are larger than the hole diameter and smaller than that, respectively.

#### 5.4.2 Examination of through-hole drilling with multistage force control

To drill through holes on plates of borosilicate glass without significant cracks on the exit surfaces, we apply multistage force control to the processes. Figure 5.12 illustrates the flow of multistage thrust-force control in the drilling process, which is designed to prevent crack generation on the exit surface, and the details are as follows. For the first stage of the process, the thrust force and the depth of the drill hole are set at 10 N and 0.95 mm, based on the results in Table 5.3 which were discussed in the preceding section. The set value has some safety margin, and the slope  $S_1$  in the flow is the same as that in the tests to investigate crack generation during blind-hole drilling as described in section 5.4. After the first stage, the remaining feed, which included drilling of the backing plate, is divided into 3 steps, as the second stage. This is because the step-feed is useful at preventing the occurrence of chip packing at the flutes of tools as mentioned in subsection 5.3.2. In addition, the slope  $S_2$  in the flow is set at 2 N/sec.

Figure 5.13 shows the result of the drilling test with the multistage thrust-force control, when the thrust force  $F$  in the flow is set at 3 N. The behavior of the moving-averaged thrust force during the process is also controlled as predetermined values. As can be seen from Fig. 5.13(b), which shows the machined through-hole viewed from the exit surface of the work-piece, small cracks at the circular edge consists of the exit surface and at the side of the machined hole are observed, but the maximum width of cracks to the hole diameter is approximately 3 %. On the other hand, in tests where the thrust force  $F$  in the flow was set at 4 N or more, the maximum widths of cracks to the hole diameter on the exit surface of the machined holes were over 10 %.

These results showed that multistage thrust-force control based on sensor signals from the cutting dynamometer can machine through-holes on plates of borosilicate glass without significant cracks at the circular edge consists of the exit surface or at the side of the machined hole.

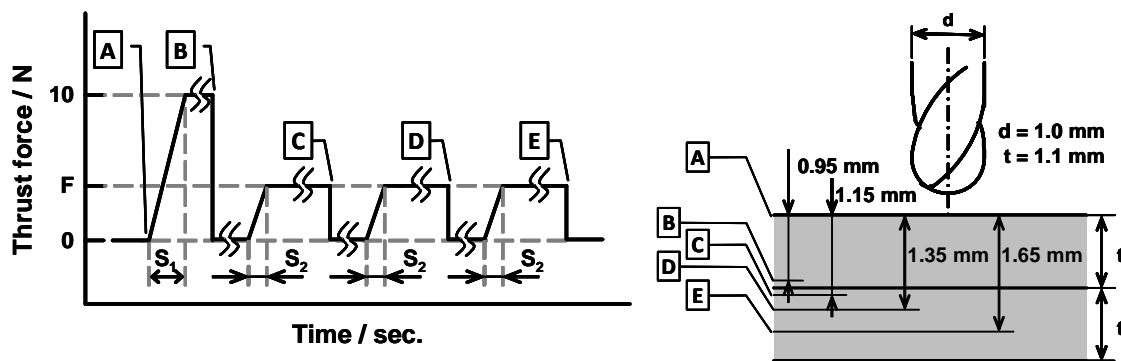
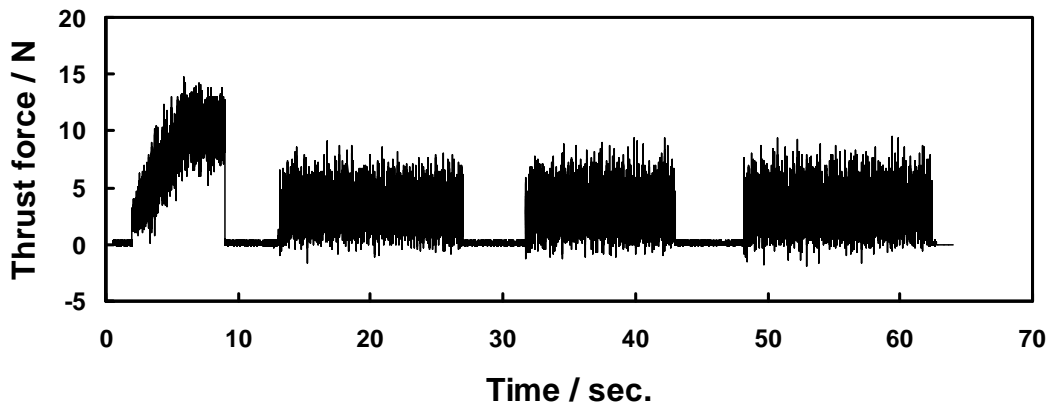


Fig. 5.12 Flow of multistage thrust-force control

## 5.6 Summary of this chapter

In this chapter, we propose to apply feedback control based on thrust force, in order to realize defect-free drilling of borosilicate glass. The key points of our work can be summarized as follows:

- 1) Through drilling and milling tests with our newly developed system, it has been verified that our system can adequately control the cutting force during drilling and milling processes.
- 2) By conducting drilling tests using ball-end mills when making blind-holes on plates of borosilicate glass with the developed machining system, we have confirmed the following: Without allowing for cracks at the bottom of the machined hole, the



(a) Behavior of thrust force



(b) Machined through-hole viewed from the exit surface of the work-piece

Fig. 5.13 Result of the drilling test with the multistage thrust-force control

minimum values of the remaining glass thickness decrease in correlation with an increase in the predetermined thrust force. From the results, we believe that the proposed force-feedback control is effective at preventing crack generation at the bottom of the machined hole.

- 3) Based on the results of drilling tests using ball-end mills when making through-holes, we have verified that, under specific conditions, multistage thrust-force control can machine through-holes on plates of borosilicate glass without significant cracks at

the circular edge consists of the exit surface or at the side of the machined hole.

- 4) From these results, we have confirmed that our proposed feedback control based on thrust force has the possibility of defect-free drilling of borosilicate-glass with our newly developed system.



## **Chapter 6**

# **Drilling of carbon fiber reinforced plastic composites with the developed machining system**

### **6.1 Objectives**

To achieve delamination-free drilling of CFRP composites, one of the most effective and reliable approaches is to control the feed rate or spindle speed based on thrust force, since the degree of thrust force is directly related to the occurrence of delamination. However, the application of the approach to drilling of composite materials has not yet been fully investigated. One exception is a successful study done by Stone and Krishnamurthy, who have developed a neural network thrust force controller designed to minimize delamination while drilling graphite-epoxy laminate [114]. This technique, unfortunately, is not suitable for practical use because the update time for controlling the

feed rate is every 0.276 sec., which means that the controller cannot regulate the feed rate at the exact instant when a machining anomaly occurs.

The objective of the present work is to propose an approach to apply feedback control based on thrust force, in order to realize defect-free drilling of CFRP composites. In this study, by conducting drilling tests with the developed machining system which is fully described in chapter 4, we have investigated the possibility of defect-free drilling of CFRP composites with feedback control based on thrust force. In the drilling tests, we used a conventional twist drill, and the work-piece was a quasi-isotropic laminate composite, which is a stack of unidirectional plies consisting of high-strength carbon fibers T800S and high-toughness matrix resin 3900-2b.

## **6.2 Work-piece material**

Generally, CFRP composite structures are combinations of unidirectional inner plies, to keep weight to a minimum, and woven surface plies, to reduce impact damage or hole preparation damage. But unidirectional fiber materials do offer some benefits over woven materials because of their ability to be oriented in the direction of the structural load, which can keep weight to a minimum [115]. From the standpoint of structural strength, woven surface plies are not indispensable and might be used less in the future. Accordingly, as work-pieces in the drilling tests, we used quasi-isotropic laminate composites, which were a stack of 16 unidirectional plies with the fiber orientation  $[45^{\circ}/0^{\circ}/-45^{\circ}/90^{\circ}]_{2s}$ . No woven surface plies were used. The reinforcing fiber is high-strength carbon fiber T800S, and the matrix is high-toughness resin 3900-2b. The thickness of the work-pieces is approximately 3.0 mm and the mechanical properties are shown in Table 6.1 [116].

Table 6.1 Mechanical properties of the workpiece material

<b>Critical crack propagation energy per unit area in mode I</b> [0] <sub>24</sub>	<b>0.54 kJ/m<sup>2</sup></b>
<b>Young's modulus</b> [45/0/-45/90] <sub>2s</sub>	<b>53.0 GPa</b>
<b>Poisson's ratio</b> [45/0/-45/90] <sub>2s</sub>	<b>0.33</b>
<b>Tensile strength</b> [45/0/-45/90] <sub>2s</sub>	<b>908 MPa</b>

### 6.3 Experimental procedure

In order to investigate the possibility of defect-free drilling of the CFRP composites with feedback control based on thrust force, we carried out drilling tests with our newly developed system. In the drilling tests, thrust force signals for the feedback control were processed by a low-pass filter in the AC servo amplifier for z-axis, and the cutoff frequency was set at 40 Hz in order to eliminate the influence caused by the spindle speed. On the other hand, recorded signals by the data acquisition system were directly acquired. The drilling conditions are shown in Table 6.2. We used diamond-like-carbon (DLC) coated twist-drills with a diameter of 3.0 mm, and the drilling was done under dry conditions. As shown in Fig. 6.1, to prevent drills from colliding with the table of the cutting dynamometer, a jig to fix the work-piece was used.

After the drilling tests, the damaged areas around the holes on the surfaces of the work-pieces were observed and measured using an optical microscope with a CCD camera. In addition, the work-pieces were examined with an X-ray inspection apparatus to detect the extent of inner delamination. To estimate the quality of the machined holes, we used delamination factor  $F_d$ , which was proposed by Chen [117] and has since been

widely used. This factor enables the evaluation and analysis of the extent of delamination in laminated compositions. The value of delamination factor  $F_d$  can be obtained by the following equation, where  $D_{max}$  is the maximum diameter of the damaged zone and  $D$  is the diameter of the hole:

$$F_d = \frac{D_{max}}{D} \quad (6.1)$$

Table 6.2 Drilling conditions

<b>Tool</b>	<b>Diamond-like carbon (DLC) coated carbide twist drill</b> Diameter: 3 mm Number of teeth: 2 Point angle: 120° Helix angle: 38° – 20°, Complex angle
<b>Cutting parameters</b>	Cutting speed: 56.5 – 226.1 m/min. (Spindle speed: 6,000 – 24,000 rpm) Lubrication: Dry

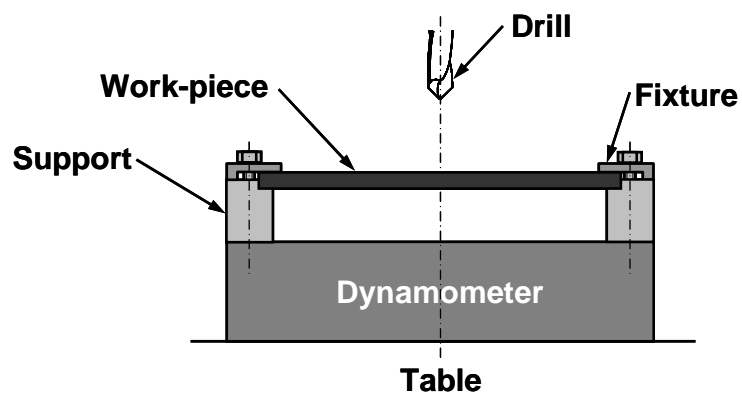


Fig. 6.1 Experimental setup

## 6.4 Examination to reduce machining defects

### on the exit surface

In the practical drilling process of CFRP composites at machining shop, jigs such as a locating plate and a backup plate are commonly utilized not only for positioning holes but for reducing machining defects [115]. But depending on conditions, it is not always possible to set up the jig under a structural component made of CFRP composites when an airframe is being repaired. From this standpoint, it is important to avoid machining defects on the drill-exit surface of CFRP composite. In this section, therefore, we have considered the methodology for controlling thrust force and the optimum cutting speed during the drilling process in order to minimize machining defects on the drill-exit surfaces of CFRP composites.

#### 6.4.1 Methodology for controlling thrust force

To drill through-holes on the CFRP composites without significant machining defects, we apply peck drilling technique to the processes. This technique is a repetitive process of the drill advancing to ever-increasing depths and then withdrawing from the hole to clear the debris and dissipate heat [115].

Analysis of delamination mechanisms during drilling using a Linear Elastic Fracture Mechanics (LEFM) approach has been developed and different models have been presented [87]. The one most referred to is the Hocheng and Dharan delamination model [118]. Figure 6.2 shows the schematic view of delamination in CFRP composites due to drilling. At the propagation of delamination, the drill movement of distance  $dX$  is associated with the work done by the thrust force  $F_A$ , which is used to deflect the plate

as well as to propagate the interlaminar crack. The energy balance equation gives

$$G_{IC}dA = F_A dX - dU \quad (6.2)$$

where  $dU$  is the infinitesimal strain energy,  $dA$  the increase in the area of the delamination crack, and  $G_{IC}$  the critical crack propagation energy per unit area in mode I. Figure 6.3 shows the schematics of delamination. In Fig. 6.3 the center of the circular plate is loaded by a twist drill with a diameter of  $d$ .  $F_A$  is the thrust force,  $X$  is the displacement,  $H$  is the thickness of the work-piece,  $h$  is the uncut depth of the work-piece under tool, and  $a$  is the radius of delamination. The isotropic behavior and pure bending of the laminate are assumed in the model. For a circular plate subject to clamped ends and a concentrated load, the stored strain energy  $U$  is

$$U = \frac{8\pi M X^2}{a^2} \quad (6.3)$$

where

$$M = \frac{Eh^3}{12(1-\nu^2)} \quad (6.4)$$

and the displacement  $X$  is

$$X = \frac{F_A a^2}{16\pi M} \quad (6.5)$$

The critical thrust force for the onset of delamination  $F_{crit}$  can be calculated

$$F_{crit} = \pi \sqrt{32G_{IC}M} = \pi \left[ \frac{8G_{IC}Eh^3}{3(1-\nu^2)} \right]^{1/2} \quad (6.6)$$

where  $E$  is Young's modulus and  $\nu$  is Poisson's ratio.

Since the values of the critical crack propagation energy per unit area in mode I  $G_{IC}$ , Young's modulus  $E$  and Poisson's ratio  $\nu$  of the work-piece material are known as shown in Table 6.1, the value of the critical thrust force for the onset of delamination  $F_{crit}$  can be calculated. Figure 6.4 shows the correlation between the work-piece uncut depth

under tool  $h$  and the calculated critical thrust force for the onset of delamination  $F_{crit}$ .

On the other hand, we examined the minimum value of the thrust force needed to generate a hole with the twist drill during the 2nd step of peck drilling process. Figure 6.5 shows the result when the cutting speed is 56.5 m/min. and the rate of increase in thrust force is 40 N/sec. The signals of thrust force and displacement are processed by a low-pass filter, and the cutoff frequency is set at 40 Hz, since the raw signals include a specific frequency component as described below. The experimental result showed that the minimum value of thrust force required to generate a hole is approximately 17 N when whole cutting edges of the drill nose section contact the work-piece.

Based on the calculated and experimental results, we designed the methodology for controlling thrust force in the drilling process to prevent machining defects caused by delamination, as illustrated in Fig. 6.6. The basic flow is the same as that in Fig. 4.5 in chapter 4 without the holding times at 40 N, 20 N and 10 N. In Fig. 6.6, letters  $A$  to  $F$  in both illustrations represent the connection between the drill position at the pointed end of the twist drill and the thrust force. In the flow of thrust force control, the rate of increase in thrust force  $R$  is set at 40 N/sec. The process from the drill-entry surface to 2.8 mm in depth from the surface is divided into 4 steps, and the keeping thrust force is set at 40 N, which is higher than the minimum value of thrust force needed to generate a hole but lower than the calculated critical thrust force that causes the onset of delamination  $F_{crit}$ . For the fifth step of the process, the thrust force is initially set at 20 N during the motion from 2.8 mm to 3.2 mm in depth. The reason is that the critical thrust force for the onset of delamination  $F_{crit}$  decreases exponentially with a decrease in the work-piece uncut depth under tool  $h$  as shown in Fig. 6.4, while it is necessary to keep the thrust force over 17 N (which is the minimum value of thrust force needed to

generate a hole). After that, the controlling value is reduced to 10 N by step response. This is because the pointed end of the twist drill has by now already exited a fraction from the drill-exit surface of the work-piece. Thus, the thrust force should be reduced as much as possible to prevent the occurrence of delamination. However, when the thrust force is set at 5 N, it is frequently difficult to machine through-holes because of the occurrence of the rubbing phenomenon, during which the cutting edge slips on the surface of the work-piece. Therefore, we have chosen the value of 10 N.

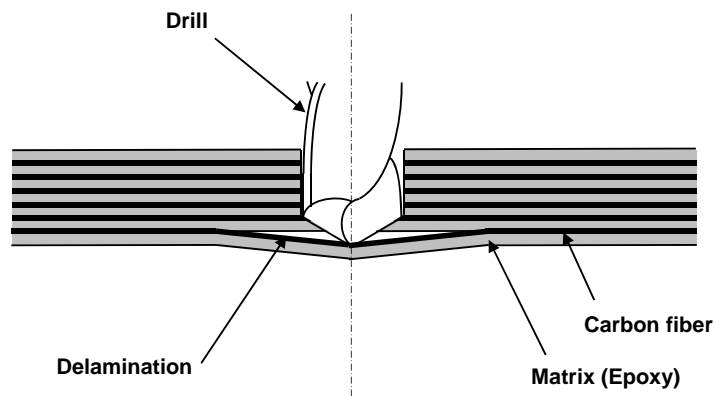


Fig. 6.2 Schematic view of delamination in CFRP composites due to drilling

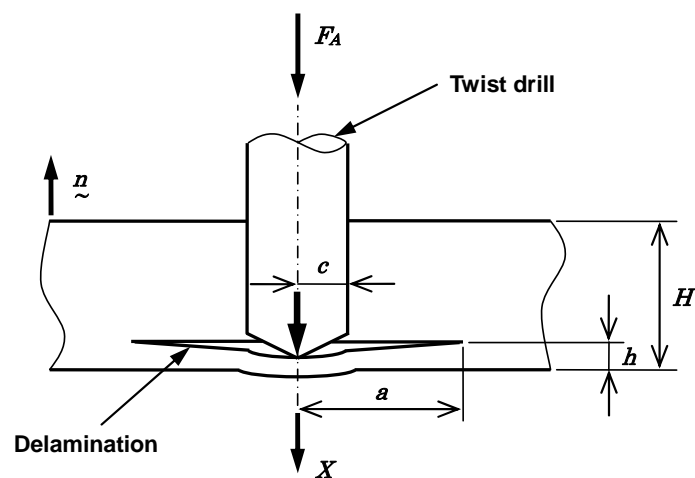


Fig. 6.3 Circular plate model for delamination analysis

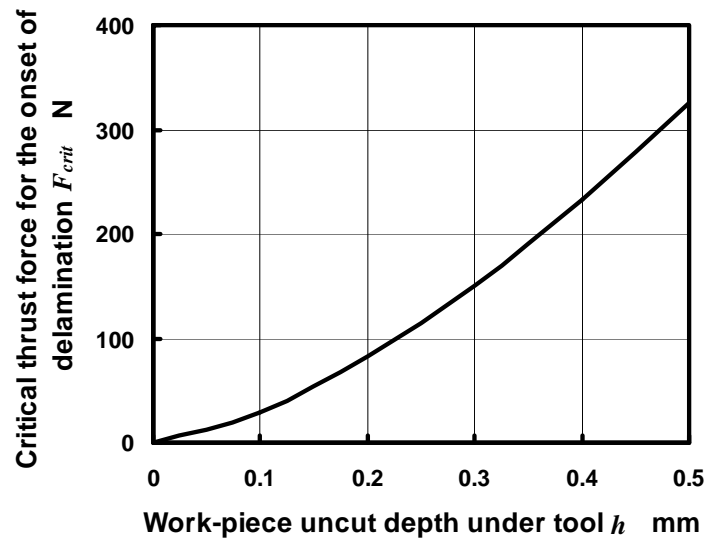


Fig. 6.4 Correlation between the uncut depth  $h$  and the calculated critical thrust force  $F_{crit}$

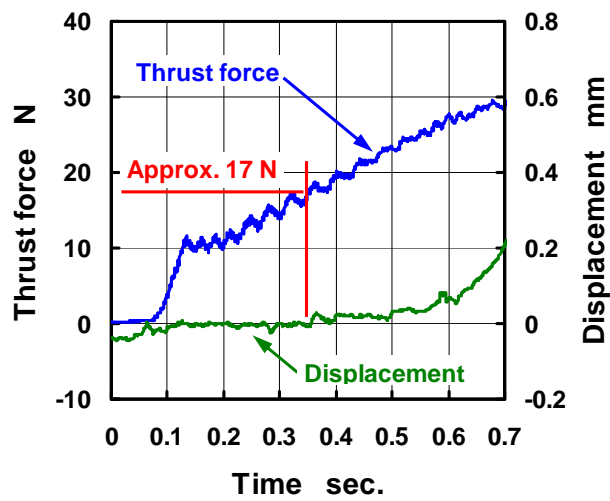


Fig. 6.5 Minimum value of the thrust force to generate a hole  
(Cutting speed: 56.5 m/min.)

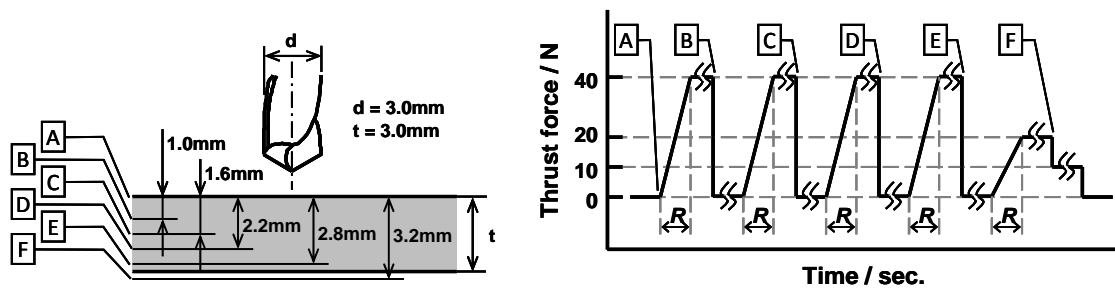
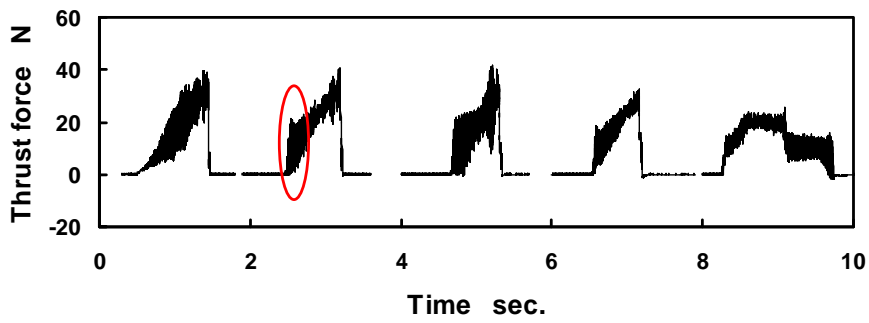


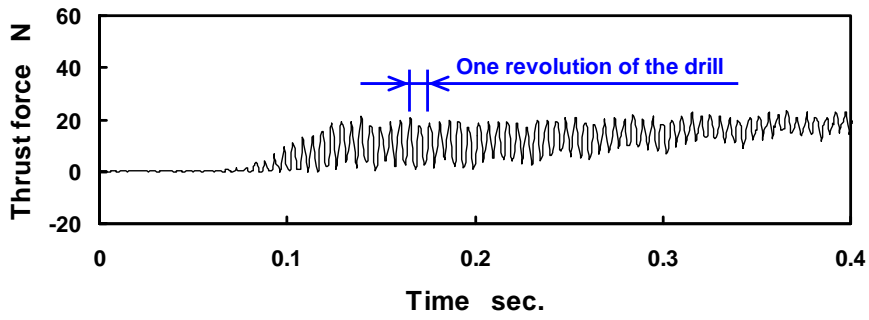
Fig. 6.6 Flow of thrust force control in the drilling process

#### 6.4.2 Behavior of thrust force during the drilling process

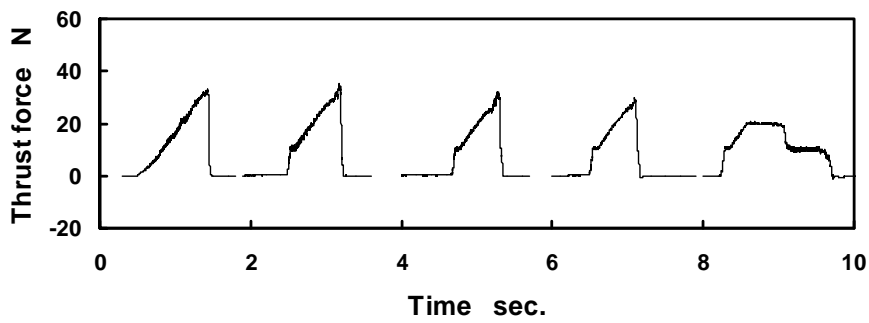
Figure 6.7 shows an example of the behavior of thrust force during the drilling process when the cutting speed was 56.5 m/min. In Fig. 6.7(a), which shows raw signals measured by the cutting dynamometer, the fluctuation component included in the thrust force is observed. To observe the detailed variability over time, a diagram with a magnified time scale in the abscissa is shown in Fig. 6.7(b). The magnified part is circled with a red line in Fig. 6.7(a). From Fig. 6.7(b), the fluctuation component is periodic, and the frequency is 200 Hz, which matched with double that of the frequency caused by the spindle speed of the twist drill. Figure 6.8 represents a schematic view of the cutting mechanism of CFRP composites per single ply. In cross-section A-A, the number of carbon fibers to be cut is the maximum value in the process. With the revolution of the twist drill, the number of carbon fibers to be cut decreases, as shown in cross-section B-B. The minimum value of carbon fibers to be cut in the process is seen in cross-section C-C. With the further revolution of the twist drill, the number of carbon fibers to be cut increases, and then shows the maximum value again when the twist drill



(a) Raw signals



(b) Magnified time scale in the abscissa



(c) Filtered signals (Cutoff frequency: 40 Hz)

Fig. 6.7 Behavior of thrust force during the drilling process  
(Cutting speed: 56.5 m/min.)

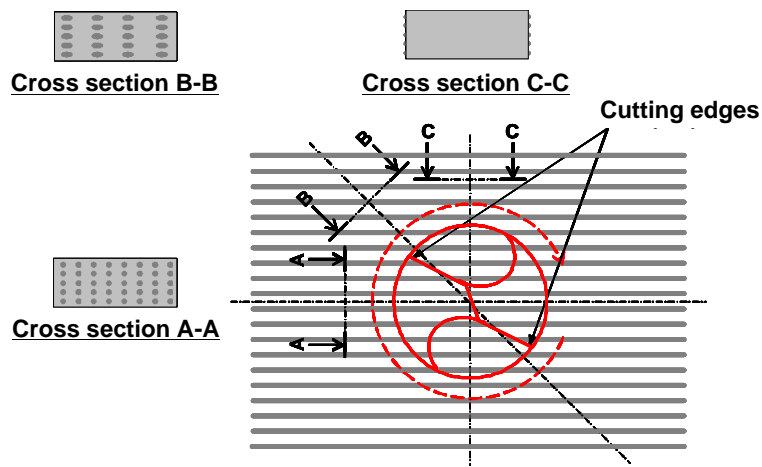


Fig. 6.8 Schematic view of the cutting mechanism of CFRP composites per single ply

rotates 180 degrees with respect to cross-section A-A. The machinability of carbon fibers is inferior as compared with that of matrix resin. Therefore, the behavior of thrust force depends heavily on the number of carbon fibers to be cut, and the frequency of the fluctuation included in the thrust force is synchronized with double that of the spindle speed of the twist drill.

To confirm that the behavior of the thrust force during the drilling process was operated at predetermined values, the raw signals were processed by a low-pass filter program on a computer for which the cutoff frequency was set at 40 Hz. The cutoff frequency is the same as that for the feedback control, and the filtered signals are shown in Fig. 6.7(c). The filtered signals from the first to fourth step do not reach 40 N, which is the preset level of thrust force to be kept constant. The reason is that each cutting to generate the appointed depth of hole is completed when the thrust force is controlled to proportionally increase at 40 N/sec. from 8 N of the threshold to 40 N. As is obvious from Fig. 6.7(a), (b) and (c), the fluctuation component included in the thrust force

caused by the cutting mechanics of CFRP composite is observed, but the filtered thrust force during the process is controlled as a predetermined value.

From the results, it has been verified that our recently developed system can control the thrust force during the drilling process.

#### **6.4.3 Relationship between cutting speed and the quality of the machined hole**

The relationship between cutting speed and the quality of the machined hole has also been investigated and the results are summarized in Table 6.3. The quality of the machined hole is expressed as the delamination factor  $F_d$  of fiber breakout as well as the presence or absence of uncut fiber. With regard to the uncut fiber in the table, "P" and "A" mean the presence and the absence, respectively, and ">" represents the relation between the appearance frequencies. The machining defects were observed and measured from the drill-exit surface of the CFRP composite. In addition, the delamination factor  $F_d$  of inner defects obtained from the X-ray photograph is utilized for evaluating the quality of the machined hole. Figure 6.9 shows typical examples of the machined holes produced when the cutting speeds were 141.3 m/min., 169.6 m/min. and 197.8 m/min. Optical micrographs and X-ray photographs were also taken from the drill-exit surfaces. From Table 6.3, the delamination factor  $F_d$  of fiber breakout decreases slightly with an increase in the cutting speed. But the delamination factor  $F_d$  of inner defects is substantially unaffected by a change of the cutting speed. On the other hand, the occurrence of uncut fiber shows different trends. When the cutting speed is set at 169.6 m/min., we obtained (with some exceptions) machined holes without any uncut fibers on the drill-exit surface. But when the cutting speed is set at other values,

we did not get machined holes without any uncut fibers on the drill-exit surface, with one exception. The exceptional hole was produced when cutting speed is set at 113.0 m/min., but only one hole was obtained.

When the cutting speed is 141.3 m/min. or less, the shape of the uncut fibers is needle-like, as shown in Fig. 6.9(a). And, based on a rough estimate, the volume of the uncut fibers decreases with an increase in the cutting speed. On the other hand, when the cutting speed is 197.8 m/min. or more, locally-deformed matrix resin at the edge of the machined hole is observed as shown in Fig. 6.9(c). The locally-deformed matrix resin is caused by the cutting heat generated during the drilling process, and brings about a different type of delamination.

From Table 6.3 and Fig. 6.9, we have found that the optimum cutting speed is 169.6 m/min. and the resulting delamination factor  $F_d$  of the machined hole is 1.07.

Table 6.3 Relationship between cutting speed and the quality of the machined hole

<b>Cutting speed m/min.</b>	<b>56.5</b>	<b>84.8</b>	<b>113.0</b>	<b>141.3</b>	<b>169.6</b>	<b>197.8</b>	<b>226.1</b>
<b><math>F_d</math> of fiber breakout on drill-exit surface</b>	<b>1.13</b>	<b>1.16</b>	<b>1.13</b>	<b>1.10</b>	<b>1.07</b>	<b>1.07</b>	<b>1.07</b>
<b>Presence (P) or absence (A) of uncut fiber on exit surface</b>	<b>P</b>	<b>P</b>	<b>P &gt; A</b>	<b>P</b>	<b>A &gt; P</b>	<b>P</b>	<b>P</b>
<b><math>F_d</math> of inner delamination observed by X-ray inspection</b>	<b>1.06</b>	<b>1.04</b>	<b>1.06</b>	<b>1.04</b>	<b>1.04</b>	<b>1.06</b>	<b>1.06</b>

#### 6.4.4 Effect of thrust force on the quality of the machined hole

In the fifth step of the process, the controlling value of thrust force is reduced from 20 N to 10 N by step response, when the pointed end of the twist drill exits a fraction

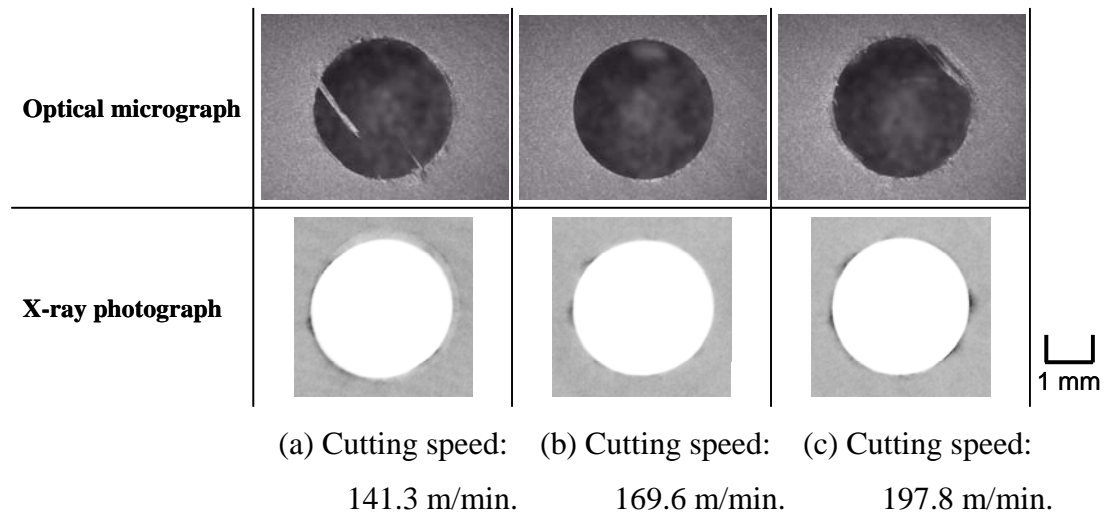


Fig. 6.9 Optical micrographs and X-ray photographs of the machined holes viewed from the drill-exit surfaces

from the drill-exit surface of the work-piece, as described in sub-section 6.4.1. To confirm the effectiveness of the control methodology, we performed drilling tests under following conditions. The cutting speed was set at 169.6 m/min. The flow of thrust force control is the same as that in Fig. 6.6 except for the fifth step. For the fifth step, the thrust force is set at 20 N during the whole process after the increase in thrust force at 40 N/sec.

The machined hole viewed from the drill-exit surface is shown in Fig. 6.10. As is obvious from Fig. 6.10, the quality of the machined hole is low as compared with that in Fig. 6.9(b). The delamination factor  $F_d$  of fiber breakout is 1.11 and uncut fibers are observed. From these results, we confirmed that, after the pointed end of the twist drill exits the drill-exit surface of the work-piece, it is essential to reduce the thrust force as much as possible. Therefore, it may be concluded that the application of feedback

control based on thrust force to drilling of CFRP composites is effective at preventing the occurrence of machining defects.

The results in this section showed that a feedback control process, with the methodology for controlling thrust force as described in sub-section 6.4.1, can machine through-holes without significant machining defects on the CFRP composite when the cutting speed is set at 169.6 m/min.



Fig. 6.10 Machined hole viewed from the drill-exit surface  
(Thrust force for the fifth step: at a constant 20 N, Cutting speed: 169.6 m/min.)

#### **6.4.5 Effect of thrust force on the quality of the machined hole**

To verify the availability of our proposed control methodology, another type of CFRP composites was drilled with the developed machining system. The work-piece is unidirectional laminate composites with a thickness of 2.2 mm. No woven surface plies were used. The reinforcing fiber is high-strength carbon fiber T800S, and the matrix is high-toughness resin 3900-2b. In the drilling tests, the basic methodology for controlling thrust force is the same as that in Fig. 6.6 without the number of steps. The process from the drill-entry surface to 2.0 mm in depth from the surface is divided into 3 steps because of the difference in the thicknesses of the work-pieces. For the fourth

step of the process, the thrust force is initially set at 20 N during the motion from 2.0 mm to 2.3 mm in depth. In the flow of thrust force control, the rate of increase in thrust force  $R$  is set at 80 N/sec.

Figure 6.11 shows an example of the machined holes viewed from the drill-exit surface when the cutting speed was 56.5 m/min. The delamination factors  $F_d$  of fiber breakout on drill-exit surface and inner delamination are 1.06 and 1.03, respectively. And uncut fiber on exit surface is not observed.

Based on the result of the experiment, we have verified the availability of our proposed feedback control methodology to the drilling of various types of CFRP composites.

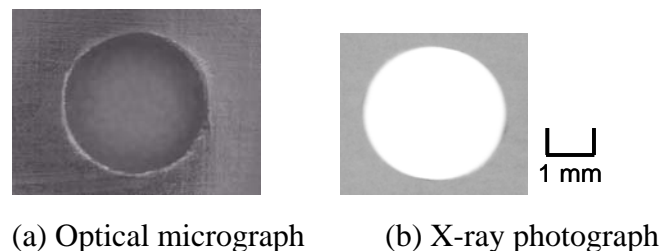


Fig. 6.11 Machined hole viewed from the drill-exit surface  
(Work-piece: Unidirectional laminate composites, Cutting speed: 56.5 m/min.)

## 6.5 Investigation to prevent machining defects on the entry and exit surfaces

In section 6.4, we have confirmed that the feedback control process, with a

methodology for controlling thrust force, can machine through-holes without significant machining defects on the drill-exit surface of CFRP composites. This is because it is not always possible to set up the jig under a structural component made of CFRP composites when an airframe is being repaired. On the other hand, when defect-free drilling of CFRP composites without any jigs on the both surfaces is realized, the process brings benefits such as the quality improvement of products, the cost reduction of manufacturing and so on. We have therefore investigated the methodology of CFRP composites drilling in order to minimize machining defects on the drill-entry and drill-exit surfaces.

First, we examined the influence of thrust force control on delamination factor  $F_d$  under varying conditions. The parameters were the keeping thrust force and the rate of increase in thrust force to the keeping thrust force. In the drilling tests, we used the quasi-isotropic laminate composites described in section 6.2, and the processes made blind-holes with a depth of 1.0 mm by one step. The cutting speed was set at 169.6 m/min. Figure 6.12 shows the influence of thrust force control on delamination factor  $F_d$ . The delamination factor  $F_d$  decreases with decrease in the rate of increase in thrust force. In addition, the decrease of the keeping thrust force has good effect to improve the delamination factor  $F_d$ . But it is necessary to keep the thrust force over 17 N for the first step, as described in 6.4.1. From the results, we designed the methodology for controlling thrust force in the drilling process to prevent machining defects on the both surfaces of CFRP composites, as illustrated in Fig. 6.13. The rate of increase in thrust force is set at 6.7 N/sec., and the keeping thrust force is set at 20 N.

Figure 6.14 (a) shows the machined hole viewed from the both surfaces of CFRP composites. The delamination factors  $F_d$  of fiber breakout on the drill-entry and

drill-exit surfaces are 1.02 and 1.06, respectively. The result showed that thrust force control based on sensor signals measured by the cutting dynamometer can drill through-hole on CFRP composites without significant machine defects on the both surfaces.

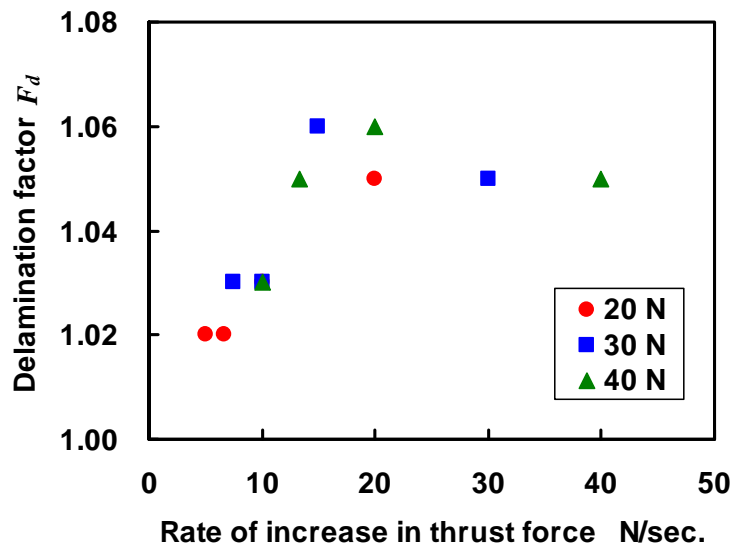


Fig. 6.12 Influence of thrust force control on delamination factor  $F_d$

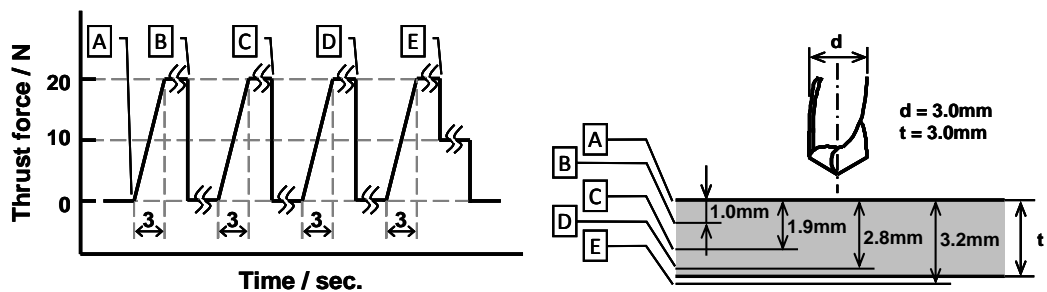


Fig. 6.13 Thrust force control for preventing machine defects on the entry and exit surfaces

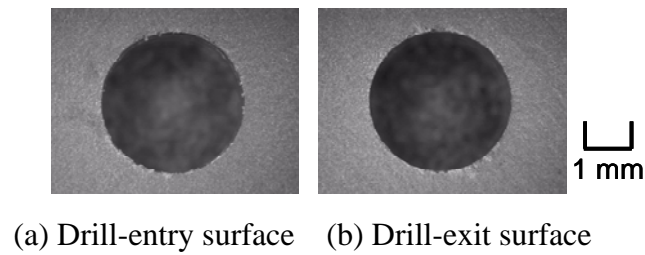


Fig. 6.14 Machined hole viewed from the both surfaces of CFRP composites

Finally, a continuous drilling test was carried out under the same conditions. The relationship between the number of machined holes and cutting time is shown in Fig. 6.15. The cutting time means actual time without the idling period of the main spindle. The cutting time shows a gradual increase up to the 16th hole and then an abrupt increase as shown in Fig. 6.15. Figure 6.16 shows the machined holes which were obtained from 14th to 17th operations in the continuous drilling test. When the 14th hole was drilled, there was no uncut fiber on the drill-entry surface. But a few uncut fibers were observed when the 15th hole was machined. After the drilling, the extent of uncut fibers was increased with increase in the number of machined holes. For reference, the width of flank wear at the cutting edge after the drilling of 20th hole was 0.06 mm on average. The relationship between the remarkable increases in the cutting time and the quality of the machined holes is not full agreement. But it is believe that the relationship has potentially-correlated. To realize the monitoring technology for drilling of CFRP composites with our developed machining system, the further detailed investigation is required as our future work.

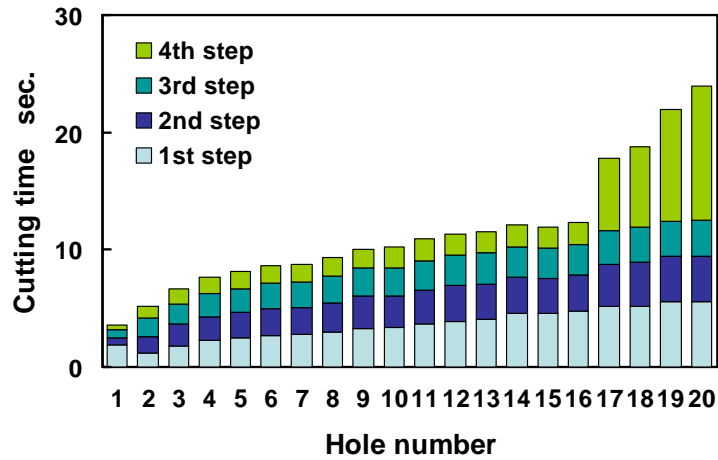


Fig. 6.15 Relationship between the number of machined holes and cutting time

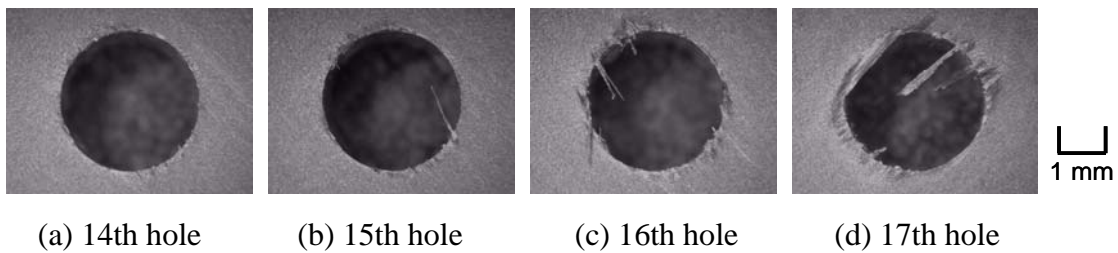


Fig. 6.16 Machined holes viewed from the drill-exit surfaces

## 6.6 Summary of this chapter

To realize defect-free drilling of CFRP composites, we have proposed an approach of applying feedback control based on thrust force, because the degree of thrust force is directly related to machining defects caused by the occurrence of delamination. The key points of our work can be summarized as follows:

- 1) We have come up with a methodology for controlling thrust force to minimize machining defects caused by the occurrence of delamination on the drill-exit surface during the drilling process of CFRP composites.
- 2) The relationship between cutting speed and the quality of the machined hole have been investigated. Consequently, in our drilling tests, we found that the optimum cutting speed is 169.6 m/min.
- 3) In addition, a methodology for controlling thrust force to prevent significant machining defects on the both surfaces of CFRP composites has been proposed.
- 4) Through drilling tests with our newly developed system, we have confirmed that the feedback control process, with two methodologies for controlling thrust force, can machine through-holes without significant machining defects on CFRP composites when the cutting speed is set at 169.6 m/min.

## **Chapter 7**

### **Conclusions**

#### **7.1 Summary**

In this dissertation, we have proposed monitoring and control technologies based on sensor information for milling and drilling processes, in order to provide bases for intelligent machining systems which can automatically recognize the state of the machining process and cope with unforeseen changes in the process or troubles in machining.

In chapter 2, we proposed a method for detecting cutting torque by utilizing the magnetostrictive effect and a sensor system for realizing the method, in order to monitor the milling and drilling processes. Subsequently, a sensor system based on the proposed method, in which a magnetostrictive torque sensor was installed in a tool holder, was developed. In addition, we carried out the static and dynamic evaluation tests of the developed sensor system. Static evaluation tests, including a calibration test and

investigations of the influence of radial force and axial force, confirmed that the developed sensor system had the ability to detect torque. Dynamic evaluation tests showed that the proposed sensor system had the ability to detect cutting torque, through comparison with the dynamic torque measured by a piezoelectric type of dynamometer acting on a workpiece as a standard. From the results it may be concluded that the proposed sensor system can measure the cutting torque with a high degree of accuracy in milling and drilling processes.

In chapter 3, milling and drilling tests were performed, in order to investigate the relationship between tool failure and cutting torque. As the results, the possibility of estimating flank wear during the milling process from cutting torque detected by the proposed sensor system has been recognized, as the maximum value of the cutting torque per revolution increased with increases in flank wear. Also, the possibility of estimating tool fracture during the milling process from cutting torque detected by the proposed sensor system has been recognized because the difference in the values of the maximum cutting torque generated by the two cutting edges consisting of a cutting tool increased when a tool fractured. In addition, a method for estimating abnormal drilling state caused by tool wear is proposed using the standard deviation and the mean value of the cutting torque as indexes, and the validity of the proposed method is confirmed through continuous drilling tests. Also, a method for detecting tool fracture during drilling process is proposed using the frequency component caused by the spindle speed included in the cutting torque as an index. Subsequently, we have developed a monitoring system for cutting processes, which has not only monitoring functions but also database functions to assist in developing monitoring algorithms. The database functions are twofold such as the functions of a threshold database and a sensor signal

database. The threshold database records thresholds, which are used for diagnosis of the state of the cutting process in the monitoring algorithm. The sensor signal database can record raw sensor signals obtained from cutting tests along with the attribute information. And then, the developed system can simulate monitoring algorithm by utilizing the recorded sensor signals, in order to examine the propriety of the monitoring algorithm.

In chapter 4, to realize defect-free cutting of difficult-to-cut materials, namely, borosilicate glass and carbon fiber reinforced plastic (CFRP) composites, we propose to apply feedback control based on cutting force, because the degree of thrust force is directly related to the occurrence of machining defects. Therefore, we have developed a machining system which can be operated at a predetermined cutting force by changing the feed rate based on cutting force signals measured by a piezoelectric cutting dynamometer, and the basic performances of the developed system have been confirmed through evaluation tests.

In chapter 5, cutting tests of borosilicate glass with the developed machining system were carried out, in order to consider the possibility of the defect-free cutting with feedback control based on cutting force. By conducting drilling tests with ball-end mills when making blind-holes on plates of borosilicate glass, we have confirmed the following: Without allowing for cracks at the bottom of the machined hole, the minimum values of the remaining glass thickness decrease in correlation with an increase in the predetermined thrust force. From the results, we believe that the proposed force-feedback control is effective at preventing crack generation at the bottom of the machined hole. Based on the results of drilling tests with ball-end mills when making through-holes, we have verified that, under specific conditions, multistage

thrust-force control can machine through-holes on plates of borosilicate glass without significant cracks at the circular edge consists of the exit surface or at the side of the machined hole. From these results, we have confirmed that our proposed feedback control based on thrust force has the possibility of defect-free drilling of borosilicate-glass with our newly developed machining system.

In chapter 6, to realize defect-free drilling of CFRP composites, we also studied the approach of applying feedback control based on thrust force. First, we have come up with a methodology for controlling thrust force to minimize machining defects caused by the occurrence of delamination on the drill-exit surface during the drilling process of CFRP composites. The relationship between cutting speed and the quality of the machined hole have been investigated. In the drilling tests, we used a conventional twist drill, and the work-piece was a quasi-isotropic laminate composite, which is a stack of unidirectional plies consisting of high-strength carbon fibers T800S and high-toughness matrix resin 3900-2b. Consequently, in our drilling tests, we found that the optimum cutting speed is 169.6 m/min. In addition, a methodology for controlling thrust force to prevent significant machining defects on the both surfaces of CFRP composites has been proposed. Through drilling tests with our recently developed machining system, we have confirmed that the feedback control process, with two methodologies for controlling thrust force, can machine through-holes without significant machining defects caused by the occurrence of delamination on CFRP composites when the cutting speed is set at 169.6 m/min.

## **7.2 Future work**

In this study, we have developed a sensor system based on the magnetostrictive effect

which is installed in a tool holder for sensing cutting torque, and then a monitoring system for cutting processes based on cutting torque from the developed sensor system has been developed. In addition, we have developed a machining system which can be operated at a predetermined cutting force by changing the feed rate based on cutting force signals measured by a piezoelectric cutting dynamometer. This is because cutting processes need to be made more autonomous due to the shortage of skilled operators in recent years, to improve the quality of products, to reduce the production cost, etc.

The developed monitoring system has database functions to assist in developing monitoring algorithms as well as the functions for monitoring tool fracture in the end-milling and drilling processes. However, the monitoring algorithms in the monitoring system require preparatory cutting tests to set a suitable threshold which is utilized for judging the state of cutting process. To dispense with the time-consuming cutting tests, further studies which included the development of cutting simulation system are needed. We think the development is one of key points for achieving the practical use of monitoring systems for cutting processes.

Concerning our newly developed machining system with feedback control based on cutting force, we have confirmed that the system can control the predetermined force. In addition, we have verified that the feedback control process can machine through-holes without causing significant machining defects on difficult-to-cut materials, namely, borosilicate glass and CFRP composites. We have also touched on the potentiality of cutting process monitoring with the machining system just a little. But the machining system does not have any functions for monitoring the state of cutting process at present.

A genuine intelligent machining system, which can manufacture goods

autonomously, requires both monitoring and control functions. In addition, the integration technology of those functions is needed. Further studies are required as our future work, in order to realize the genuine intelligent machining system.

# Acknowledgment

It is my great pleasure to acknowledge all persons who concern this work.

First I would like to express my deep gratitude to Professor Fumihito Arai, Department of Mechanical Science and Engineering, Nagoya University, Japan for his warm advice and guidance. And, I would like to extend to Professor Toshio Fukuda in Department of Micro-Nano Systems Engineering, Professor Eiji Shamoto in Department of Mechanical Science and Engineering, and Associate Professor Tadashige Ikeda in Composite Engineering Research Center, my sincere thanks for kindly agreeing with being my doctoral committee member. Their comments were very helpful in improving my dissertation.

I would also like personally thank to Associate Professor Yoko Yamanishi, Dr. Hisataka Maruyama, Dr. Tmohiro Kawahara, Dr. Taisuke Masuda and Dr. Akihiro Ichikawa in Arai laboratory for constant support. I would like to extend my thanks to all the laboratory member.

In addition, I gratefully acknowledge the member of “Sensor Fused Intelligent Monitoring System for Machining” project which was supported by the Intelligent Manufacturing Systems Program as well as my colleagues at the previous company Mitsubishi Materials Corporation and the present company Kistler Japan Co., Ltd.

Finally, I would like to make a most cordial acknowledgment to my parents and my wife for their kind support.

Hiroo OZEKI



## References

- [1] Edited by Mitsubishi Materials Corporation, IMS Program Report on Sensor Fused Intelligent Control System for Optimizing Machining Processes –Project No. 9506– (in Japanese), IMS Promotion Center, (1996), p. 1.
- [2] Byrne, G., Dornfeld, D., Inasaki, I., Ketteler, G., Koenig, W., and Teti, R., Tool Condition Monitoring - The Status of Research and Industrial Application (Keynote paper), *Annals of the CIRP*, Vol. 44, No. 2 (1995), pp. 541-567.
- [3] Moriwaki, T., Intelligent Machine Tool: Perspective and Themes for Future Development, *ASME Manufacturing Science and Engineering*, Vol. 2, PED-Vol. 68-2 (1994), pp. 841-849.
- [4] Moriwaki, T., Intelligent Machine Tools, *Journal of the Japan Society of Mechanical Engineers* (in Japanese), Vol. 96 (1993), pp. 1010-1014.
- [5] Ohzeki, H. and Mashine, A., SIMON – Sensor Fused Intelligent Monitoring System for Machining, *Proceedings of Symposium on the Current Status and the Future of IMS Program* (in Japanese), The Japan Society for Precision Engineering, (2001), pp. 35-39.
- [6] Edited by Mitsubishi Materials Corporation, IMS Program Report on Sensor Fused Intelligent Monitoring System for Machining –Project No. 9806– (in Japanese), IMS Promotion Center, (1999), pp. 19-25.
- [7] Edited by the Japan Society for Precision Engineering, Handbook of Precision Machining (in Japanese), Corona Publishing, (1992), pp. 1316-1321.
- [8] Dimla, E. and Dimla, Snr., Sensor Signals for Tool-Wear Monitoring in Metal Cutting Operations—A Review of Methods, *International Journal of Machine Tools & Manufacture*, 40 (2000) pp. 1073–1098.
- [9] Hatamura, Y., Force and Torque Sensors, *Journal of the Japan Society of Mechanical Engineers* (in Japanese), Vol. 89 (1986), pp. 1055-1058.

- [10] Ikezaki, Y., Takeuchi, Y., and Sakamoto, M., Measurement of Cutting Forces in Rotating Tool by Means of Optical Data Transmission ( 2nd Report ), *Journal of the Japan Society for Precision Engineering* (in Japanese), Vol. 53 (1987), pp. 755-761.
- [11] Cselle, T., and Stirnimann, J., Cutting Force Measurements on Rotating Tools, *Technical Report of Kistler*, 20.163e 7.94 (1994).
- [12] Kirchiheim, A., Stirnimann, J. and Veselovac, D., H3 – High Performance, High Accuracy and High Frequency, *CIRP International Conference on High Performance Cutting*, (2006).
- [13] Brinksmeier, E., Prediction of Tool Fracture in Drilling, *Annals of the CIRP*, Vol. 39 (1990), pp. 97-100.
- [14] Sasada, I., Suzuki, N., Mizogami, K., and Toda, K., Basic Study for Detection of Cutting Torque Using Shape Magnetic Anisotropy from the Shape of a Twist Drill, *Proceeding of IEE Japan Working Group on Magnetics* (in Japanese), MAG-93-280 (1993), pp. 99-106.
- [15] Sasada, I., Recent Developments of Magnetostrictive Torque Sensors, *Transactions of IEE Japan* (in Japanese), Vol. 114-A, No. 4 (1994), pp. 277-281.
- [16] Edited by the Japan Society for Precision Engineering, *Handbook of Manufacturing System*, Corona Publishing, (1997), pp. 2-11.
- [17] Edited by the Japan Society for Precision Engineering, *Handbook of Precision Machining*, Corona Publishing, (1992), pp. 1369-1391.
- [18] Choi, D., Kwon, W.T. and Chu, C.N., Real-Time Monitoring of Tool Fracture in Turning Using Sensor Fusion, *International Journal of Advanced Manufacturing Technology*, 15 (5), (1999), pp. 305–310.
- [19] Blum, T. and Inasaki, I., A Study on Acoustic Emission from the Orthogonal Cutting Process, *ASME Trans. Journal of Engineering for Industry* 112 (3) (1990) 203–211.
- [20] Moriwaki, T. and Tobito, M., A New Approach to Automatic Detection of Life of Coated Tool Based on Acoustic Emission Measurement, *ASME Trans. Journal of Engineering for Industry* 112 (3) (1990) 212–218.
- [21] Roget, J., Souquet, P. and Gsib, N., Application of Acoustic Emission to the

- Automatic Monitoring of Tool Condition during Machining, *ASNDT Materials Evaluation* 46 (1988) 225–229.
- [22] Tansel, I.N. and McLaughlin, C., On-Line Monitoring of Tool Breakage with Unsupervised Neural Network, *Trans. NAMRI/SME* (1991) 364–370.
- [23] Lee, L.C., Lee, K.S. and Gan, C.S., On the Correlation Between Dynamic Cutting Force and Tool Wear, *International Journal of Machine Tools and Manufacture* 29 (3) (1989) 295–303.
- [24] Kakade, S., Vijayaraghavan, L. and Krishnamurthy, R., In-Process Tool Wear and Chip-Form Monitoring in Face Milling Operation Using Acoustic Emission, *Journal of Material Processing Technology* 44 (1994) 207–214.
- [25] Zheng, S.X., McBride, R., Barton, J.S., Jones, J.D.C., Hale, K.F. and Jones, B.E., Intrinsic Optical Fiber Sensor for Monitoring Acoustic Emission, *Sensors and Actuators, A: Physical* 31 (1992) 110–114.
- [26] Koenig, W., Kutzner, K. and Schehl, U., Tool Monitoring of Small Drills with Acoustic Emission, *International Journal of Machine Tools and Manufacture* 32 (4) (1992) 487–493.
- [27] Edited by the Japan Society for Abrasive Technology, *Dictionary of cutting, grinding and polishing items* (in Japanese), Kogyo Chosakai Publishing, (1995), p. 11.
- [28] Szecsi, T., A DC Motor Based Cutting Tool Condition Monitoring System, *Journal of Materials Processing Technology*, 92-93 (1999), pp. 350-354.
- [29] Kurada, S. and Bradley, C., A review of Machine Vision Sensors for Tool Condition Monitoring, *Computers in Industry*, 34, (1997), pp. 55-72.
- [30] Liang, S.Y., Hecker R.L. and Landers, R.G., Machining process monitoring and control: the state-of-the-art, *Transactions of the ASME: Journal of Manufacturing Science and Engineering*, Vol. 126–2, (2004), pp. 297-310.
- [31] Zuperl, U., Cus, F. and Reibenschuh, M., Review: Neural Control Strategy of Constant Cutting Force System in End Milling, *Robotics and Computer-Integrated Manufacturing*, 27, (2011), pp. 485–493.
- [32] Ibaraki, S. and Shimizu, T., A long-term control scheme of cutting forces to regulate tool life in end milling processes, *Precision Engineering*, 34, (2010), pp.

675–682.

- [33] Kim, D. and Jeon, D., Fuzzy-logic Control of Cutting Forces in CNC Milling Processes Using Motor Currents as Indirect Force Sensors, *Precision Engineering*, 35, (2011), pp. 143–152.
- [34] Kurihara, D., Kakinuma, Y. and Katsura, S., Cutting Force Control Applying Sensorless Cutting Force Monitoring Method, *Journal of Advanced Mechanical Design, Systems, and Manufacturing*, Vol.4, No.5, (2010), pp.955-965.
- [35] Altintas, Y., Prediction of Cutting Forces and Tool Breakage in Milling from Feed Drive Current Measurements, *ASME, Journal of Engineering for Industry*, Vol. 114 (1992), pp. 386-392.
- [36] Konig, W., Langhammer, K. and Schemmel, H.U., Correlation Between Cutting Force Components and Tool Wear, *Annals of CIRP*, 21, (1972), pp. 19-20.
- [37] Tlustý, J. and Andrews, G.C., A Critical Review of Sensors for Unmanned Machining, *Annals of CIRP*, 32, (1983), pp. 563-572.
- [38] Lindstrom, B. and Lindberg, B., Measurement of Dynamic Cutting Forces in the Cutting Process, A New Sensor for In-process Measurement, *Proceedings of 24th International Machine Tool Design and Research Conference*, (1983), pp. 137-147.
- [39] Takeyama, H., Doi, Y., Mitsuoka T. and Sekiguchi, H., Sensors of Tool Life for Optimization of Machining, *Proceedings of 8th International Machine Tool Design and Research Conference*, (1967), pp. 191-208.
- [40] Stoferle, T.H. and Bellmann, B., Continuous Measuring of Flank Wear, *Proceedings of 16th International Machine Tool Design and Research Conference*, (1975), pp. 573-578.
- [41] Ravindra, H.V., Srinivasa, Y.G. and Krishnamurthy, R., Modelling of tool wear based on cutting forces in turning, *Wear*, 169 (1993), pp. 25–32.
- [42] Dimla Snr, D.E., Tool wear monitoring using cutting force measurements, *in: 15th NCMR: Advances in Manufacturing Technology XIII*, (1999), pp. 33–37.
- [43] Bayramoglu, M. and Döngel, U., A systematic investigation on the use of force ratios in tool condition monitoring for turning operations, *Trans. Institute of Measurement and Control*, 20 (2), (1998), pp. 92–97.

- [44] Ko, T.J. and Cho, D.W., Cutting state monitoring in milling by a neural network, *International Journal of Machine Tools and Manufacture*, 34 (5), (1994), pp. 659–676.
- [45] Purushothaman, S. and Srinivasa, Y.G., A back-propagation algorithm applied to tool wear monitoring, *International Journal of Machine Tools and Manufacture*, 34 (5), (1994), pp. 625–631.
- [46] Tarng, Y.S., Hseih, Y.W. and Hwang, S.T., Sensing tool breakage in face milling with a neural network, *International Journal of Machine Tools and Manufacture*, 34 (3), (1994), pp. 341–350.
- [47] Dornfeld, D.A., Neural network sensor fusion for tool condition monitoring, *Annals of the CIRP*, 39 (1), (1990), pp. 101–105.
- [48] Lee, K.S., Lee, L.C. and Teo, S.C., On-line tool wear monitoring using a PC, *Journal of Material Processing Technology*, 29, (1992), pp. 3–13.
- [49] Marques, M.J.M. and Mesquita, R.M.D., Monitoring the wear of sintered high-speed steel tools, *Journal of Material Processing Technology* 25 (1991), pp. 195–213.
- [50] Kim, J.S. and Lee, B.H., An analytical model of dynamic cutting forces in chatter vibration, *International Journal of Machine Tools and Manufacture*, 31 (3), (1991), pp. 371–381.
- [51] Oraby, S.E. and Hayhurst, D.R., Development of models for tool wear force relationships in metal cutting, *International Journal of Machine Tools and Manufacture*, 33 (2), (1991), pp. 125–138.
- [52] Yao, Y., Fang, X.D. and Arndt, G., Comprehensive tool wear estimation in finish-machining via multivariate timeseries analysis of 3-D cutting forces, *Annals of the CIRP*, 39 (1), (1990), pp. 57–60.
- [53] Yao, Y. and Fang, X.D., Modeling of multivariate time series for tool wear estimation in finish-turning, *International Journal of Machine Tools and Manufacture*, 32 (4), (1992), pp. 495–508.
- [54] Shi, T. and Ramalingam, S., Real-time flank wear sensing, *Winter Annual Meeting of the ASME, PED 43*, (1990), pp. 157–170.
- [55] Lee, L.C., Lam, K.Y. and Liu, X.D., Characterisation of tool wear and failure,

*Journal of Materials Processing Technology*, 40, (1994), pp. 143–153.

- [56] Lee, K.J., Lee, T.M. and Yang, M.Y., Tool wear monitoring system for CNC end milling using a hybrid approach to cutting force regulation, *International Journal of Advanced Manufacturing Technology*, 32 (1), (2007), pp. 8–17.
- [57] Harz, M. and Engelke, H., Curvature Changing or Flattening of Anodically Bonded Silicon and Borosilicate Glass, *Sensors and Actuators*, A55, (1996), pp. 201-209.
- [58] Schjolberg-Henriksen, K., Jensen, G.U., Hanneborg, A. and Jakobsen, H., Anodic Bonding for Monolithically Integrated MEMS, *Sensors and Actuators*, A114, (2004), pp. 332-339.
- [59] Murai, J., Introduction of Glass Substrate for Anodic Bonding and the Market View, *New Glass* (in Japanese), Vol. 20, No. 2, (2005), pp. 58-62.
- [60] Bu, M., Melvin, T., Ensell, G.J., Wilkinson, J.S. and Evans, A.G.R., A New Masking Technology for Deep Glass Etching and Its Microfluidic Application, *Sensors and Actuators*, A115, (2004), pp. 476-482.
- [61] Park, J.H., Lee, N.-E., Lee, J. Park, J.S. and Park, H.D., Deep Dry Etching of Borosilicate Glass Using SF<sub>6</sub> and SF<sub>6</sub>/Ar Inductively Coupled Plasmas, *Microelectronic Engineering*, 82, (2005), pp. 119-128.
- [62] Iliescu, C., Tay, F.E.H. and Miao, J., Strategies in Deep Wet Etching of Pyrex Glass, *Sensors and Actuators*, A133, (2007), pp. 395-400.
- [63] Belloy, E. et al., Powder Blasting for Three-Dimensional Microstructuring of Glass, *Sensors and Actuators*, 86, (2000), pp. 231–237.
- [64] Hidai, H., Itoh, S., Tokura, H., Nagasawa, S. and Tachikawa, S., High-Aspect-Ration Microdrilling with UV Laser Ablation. I – Drilling Holes with an Aspect-Ratio of 190 in Bolosilicate Glass –, *Jounarl of the Japan Society for Presision Engineering* (in Japanese), Vol. 76, No. 10, (2010), p. 1161-1165.
- [65] Hidai, H., Itoh, S. and Tokura, H., High-Aspect-Ration Microdrilling with UV Laser Ablation. II – Influence of Beam Parameters on Hole Profile –, *Jounarl of the Japan Society for Presision Engineering* (in Japanese), Vol. 76, No. 11, (2010), p. 1266-1270.

- [66] Hidai, H., Itoh, S. and Tokura, H., High-Aspect-Ration Microdrilling with UV Laser Ablation. III – Influence of Pulse Width on Hole Profile –, *Journal of the Japan Society for Precision Engineering* (in Japanese), Vol. 76, No. 12, (2010), p. 1383-1387.
- [67] Park, B.J., Choi, Y.J. and Chu, C. N., Prevention of Exit Crack in Micro Drilling of Soda-Lime Glass, *Annals of the CIRP*, Vol. 51, Issue 1 (2002), pp. 347-350.
- [68] Mizobuchi, A., Ogawa, H. and Masuda, M., Drilling Conditions and Crack Restraint of Step Drilling Method in Through-Hole Drilling of Glass Plate, *Journal of the Japan Society for Precision Engineering* (in Japanese), Vol. 77, No. 3, (2011), pp. 296-300.
- [69] Bouras, N., Madjoubi, M.A., Kolli, M., Benterki, S. and Hamidouchi, M., Thermal and Mechanical Characterization of Borosilicate Glass, *Physics Procedia*, Vol. 2, Issue 3 (2009), pp. 1135-1140.
- [70] Moriwaki, T., Shamoto, E. and Inoue, K., Ultraprecision Ductile Cutting of Glass by Applying Ultrasonic Vibration, *Annals of the CIRP*, Vol. 41 (1), (1992), pp. 141-144.
- [71] Shamoto, E., Ma, C.X. and Moriwaki, T., Ultraprecision Ductile Cutting of Glass by Applying Ultrasonic Elliptical Vibration Cutting, *Proceedings of 1st International Conference and General Meeting of EUSPEN*, (1999), pp. 408-411.
- [72] Lee, J., Lee, D., Jung, Y. and Chung, W., A Study on Micro-Grooving Characteristics of Planar Lightwave Circuit and Glass Using Ultrasonic Vibration Cutting, *Journal of Materials Processing Technology*, 130-131, (2002), pp. 396-400.
- [73] Yan, B.H., Wang, A.C., Huang, C.Y. and Huang, F.Y., Study of Precision Micro-Holes in Borosilicate Glass Using Micro EDM combined with Micro Ultrasonic Vibration Machining, *International Journal of Machine Tools & Manufacture*, 42, (2002), pp. 1105-1112.
- [74] Matsumura, T. and Ono, T., Effect of Cutter Axis Inclination on Brittle Fracture in Glass Machining, *Proceedings of the Abrasive Technology Conference 2007* (in Japanese), (2007), pp.5-6.
- [75] Matsumura, T. and Ono, T., Cutting process of glass with inclined ball end mill,

- Journal of Materials Processing Technology*, 200, (2008), pp.356-363.
- [76] Ono, T. and Matsumura, T., Influence of tool inclination on brittle fracture in glass cutting with ball end mills, *Journal of Materials Processing Technology*, (2008), 202, pp.61-69.
- [77] Foy, K., Wei, Z., Matsumura, T. and Huang, Y., Effect of Tilt Angle on Cutting Regime Transition in Glass Micromilling, *International Journal of Machine Tools & Manufacture*, 49, (2009), pp. 315-324.
- [78] Iizuka, T., Ductile-Mode Cutting for Glass, *Journal of the Japan Society of Mechanical Engineers* (in Japanese), Vol. 111, No. 1074, (2008), p. 449.
- [79] Iizuka, T., Ductile-Mode Cutting for Glass, *Journal of the Japan Society for Abrasive Technology* (in Japanese), Vol. 52, No. 11, (2008), pp. 634-637.
- [80] Mizobuchi, A. and Ogawa, H., Crack size and processing efficiency in through hole drilling of glass plate using an electroplated diamond tool, *Journal of the Japan Society for Abrasive Technology* (in Japanese), Vol. 54, No. 3, (2010), pp. 145-150.
- [81] Mizobuchi, A., Ogawa, H. and Sasaoka, T., Grinding Force and Crack Size on Through-Hole Drilling of Glass Plate Used Electroplated Diamond Tool in Helical Drilling, *Journal of the Japan Society for Abrasive Technology* (in Japanese), Vol. 54, No. 12, (2010), pp. 731-736.
- [82] Izui, H., New Materials and Manufacturing Technologies Required for Next-Generation Aircraft, *Journal of the Japan Society for Precision Engineering* (in Japanese), Vol. 75, No. 8, (2009), pp. 937-940.
- [83] Denkena, B., Boehnke, D. and Dege, J.H., Helical Milling of CFRP-Titanium Layer Compounds, *CIRP Journal of Manufacturing Science and Technology*, 1, (2008), pp. 64-69.
- [84] Yonezawa, T. and Inasaki, I., Cutting of Composite Material with Ultrasonic Vibration, *Transactions of the Japan Society of Mechanical Engineers Series C* (in Japanese), Vol. 69, No. 682, (2003), pp. 243-248.
- [85] Shyha, I.S., Aspinwall, D.K., Soo, S.L. and Bradley, S., Drilling Geometry and Operating Effects when Cutting Small Diameter Holes in CFRP, *International Journal of Machine Tools & Manufacture*, 49 (2009), pp. 1008–1014.

- [86] Hocheng, H. and Tsao, C.C., The Path Towards Delamination-Free Drilling of Composite Materials, *Journal of Materials Processing Technology*, 167 (2005), pp. 251–264.
- [87] Marques, A.T., Durão L.M., Magalhães, A.G., Silva, J.F. and Tavares, J.M.R.S., Delamination Analysis of Carbon Fiber Reinforced Laminates: Evaluation of a Special Step Drill, *Composites Science and Technology*, 69 (2009), pp. 2376–2382.
- [88] Hanasaki, S., Fujiwara, J., Kawai, T., Nomura, M. and Miyamoto, T., Study on Tool Wear Mechanism of CFRP Cutting II, *Transactions of the Japan Society of Mechanical Engineers Series C* (in Japanese), Vol. 71, No. 702, (2005), pp. 365-370.
- [89] Nakajima, M., Manufacturing Technology of Aircraft Airframe Structure, *Journal of the Japan Society for Precision Engineering* (in Japanese), Vol. 75, No. 8, (2009), pp. 941-944.
- [90] Lee, Y.S., Ben, G. and Lee, S.H., Effect of the Hole on the Tensile Fatigue Properties of CFRP Laminates, *Advanced Composite Materials*, 18, (2009), pp. 43-59.
- [91] Abrão, A.M., Faria, P.E., Campos Rubio, J.C., Reis, P. and Paulo Davim, J., Drilling of Fiber Reinforced Plastics: A Review, *Journal of Materials Processing Technology*, 186 (2007), pp. 1–7.
- [92] Tsao, C.C. and Hocheng, H., Taguchi Analysis of Delamination Associated with Various Drill Bits in Drilling of Composite Material, *International Journal of Machine Tools & Manufacture*, 44, (2004), pp. 1085–1090.
- [93] Hocheng, H. and Tsao, C.C., Effects of Special Drill Bits on Drilling-Induced Delamination of Composite Materials, *International Journal of Machine Tools & Manufacture*, 46 (2006), pp. 1403–1416.
- [94] Hocheng, H. and Tsao, C.C., Comprehensive Analysis of Delamination in Drilling of Composite Materials with Various Drill Bits, *Journal of Materials Processing Technology*, 140 (2003), pp. 335–339.
- [95] Tsao, C.C. and Hocheng, H., Evaluation of Thrust Force and Surface Roughness in Drilling Composite Material Using Taguchi Analysis and Neural Network, *Journal of Materials Processing Technology*, 203 (2008), pp. 342–348.

- [96] Tsao, C.C., Investigation into the Effects of Drilling Parameters on Delamination by Various Step-Core Drills, *Journal of Materials Processing Technology*, 206 (2008), pp. 405–411.
- [97] Tsao, C.C. and Hocheng, H., Effect of Eccentricity of Twist Drill and Candle Stick Drill on Delamination in Drilling Composite Materials, *International Journal of Machine Tools & Manufacture*, 45 (2005), pp. 125–130.
- [98] Tsao, C.C., Effect of Deviation on Delamination by Saw Drill, *International Journal of Machine Tools & Manufacture*, 47 (2007), pp. 1132–1138.
- [99] Tsao C.C., Effect of Pilot Hole on Thrust Force by Saw Drill, *International Journal of Machine Tools & Manufacture*, 47 (2007), pp. 2172–2176.
- [100] Tsao, C.C. and Hocheng, H., Effects of Exit Back-Up on Delamination in Drilling Composite Materials Using a Saw Drill and a Core Drill, *International Journal of Machine Tools & Manufacture*, 45 (2005), pp. 1261–1270.
- [101] Durão, L.M.P., Gonçalves, D.J.S., Tavares, J.M.R.S., Albuquerque, V.H.C., Vieira, A. A. and Marques, A. T., Drilling Tool Geometry Evaluation for Reinforced Composite Laminates, *Composite Structures*, 92 (2010), pp. 1545–1550.
- [102] Gaitonde, V.N., Karnik, S.R., Rubio, J.C., Correia, A.E., Abrão, A.M. and Davim, J.P., *Journal of Materials Processing Technology*, 203 (2008), pp. 431–438.
- [103] Davim, J.P. and Reis, P., Study of Delamination in Drilling Carbon Fiber Reinforced Plastics (CFRP) Using Design Experiments, *Composite Structures*, 59 (2003), pp. 481–487.
- [104] Davim, J.P. and Reis, P., Drilling Carbon Fiber Reinforced Plastics Manufactured by Autoclave – Experimental and Statistical Study, *Materials and Design*, 24 (2003), pp. 315–324.
- [105] Wang, X., Wang, L.J. and Tao, J.P., Investigation on Thrust Force in Vibration Drilling of Fiber-Reinforced Plastics, *Journal of Materials Processing Technology*, 148 (2004), pp. 239–244.
- [106] Zhang, L.B., Wang, L.J., Liu, X.Y., Zhao, H.W., Wang, X. and Luo, H.Y., Mechanical Model for Predicting Thrust and Torque in Vibration Drilling

- Fiber-Reinforced Composite Materials, *International Journal of Machine Tools & Manufacture*, 41 (2001), pp. 641–657.
- [107] Koenig, W., Wulf, C., Grass, P. and Willerscheid, H., Machining of Fiber Reinforced Plastics, *Annals of the CIRP*, 34 (1985), pp. 537–548.
- [108] Hauptmann, P., *Sensors (Principles & Applications)*, Prentice Hall, (1991), pp. 178-180.
- [109] Iwai, R., Force Control Servo System to Realize High Precision and High-Speed Response, *Press Forming Journal* (in Japanese), Vol. 3, No. 1 (2004), pp. 41–48.
- [110] Nagamatsu, A., *Introduction to Modal Analysis*, (1993), Corona Publishing, pp. 66-78.
- [111] Tamura, S., Nishiyama, M. and Tazawa, T., “MINAS<sup>TM</sup> A4 Series” AC Servo Motor and Amplifier, *Matsushita Technical Journal*, Vol. 51, No. 1, (2005), pp. 13-16.
- [112] Information on [http://www.kistler.com/mediaaccess/5015A\\_BP\\_\\_000-297e-01.10.pdf](http://www.kistler.com/mediaaccess/5015A_BP__000-297e-01.10.pdf), (information acquisition on Jun. 10, 2011)
- [113] Information on <http://www.schott.com/borofloat/english/attribute/mechanical/index.html>, (information acquisition on Apr. 15, 2010).
- [114] Krishnamurthy, K. and Stone, R., A Neural Network Thrust Force Controller to Minimize Delamination during Drilling of Graphite-Epoxy Laminate, *International Journal of Machine Tools & Manufacture*, Vol. 36, No. 9 (1996), pp. 985–1003.
- [115] Miracle, D.B. and Donaldson, S.L., *ASM Handbook Vol. 21: Composites*, (2001), pp. 646–650, ASM International.
- [116] Japan Aerospace Exploration Agency, Advanced Composites Database System (online in Japanese), available from <<http://www.jaxa-acdb.com>>, (accessed 2011-7-17)
- [117] Chen, W.C., Some Experimental Investigations in the Drilling of Carbon Fiber Reinforced Plastic (CFRP) Composite Laminates, *International Journal of Machine Tools & Manufacture*, 37 (1997), pp. 1097–1108.
- [118] Hocheng, H. and Dharan, C.K.H., Delamination during Drilling in Composite

Laminates, *Transaction of the ASME: Journal of Engineering for Industry*, 112 (1990), pp. 236-239.

# List of accomplishments

## Papers published in scholarly journal

- [119] Aoyama, H., Inasaki, I., Ohzeki, H. and Machine, A., Cutting Force Sensing by Utilizing Magnetostrictive Effect, *The International Journal for Manufacturing Science & Production*, Vol.1, No.1 (1997), pp. 27-32.
- [120] Ohzeki, H., Machine, A., Aoyama, H. and Inasaki, I., Development of a Magnetostrictive Torque Sensor for Milling Process Monitoring, *Transactions of the ASME: Journal of Manufacturing Science and Engineering*, Vol.121 (1999), pp. 615-622.
- [121] Hagiwara, M., Mano, Y., Hamada, M., Nunogami, K., Ohzeki, H. and Ito, S., Development of a New Testing Machine for Torque/Clamp Force Testing for Threaded Fasteners in Accordance with ISO 16047, *Journal of Advanced Mechanical Design, Systems, and Manufacturing*, Vol.3, No.4, (2009), pp. 324-332.
- [122] Ohzeki, H. and Arai, F., Drilling of Borosilicate Glass with Feedback Control Based on Cutting Force, *Advanced Materials Research*, Vol.325 (2011), pp. 442-448.
- [123] Ohzeki, H. Hoshi, H. and Arai, F., Drilling of Carbon Fiber Reinforced Plastic Composites with Feedback Control Based on Cutting Force, *Journal of Advanced Mechanical Design, Systems, and Manufacturing*, Vol.6, No.1 (2012), pp. 52-64.

## Proceedings of International conference

- [124] Aoyama, H., Ohzeki, H., Machine, A. and Takeshita, J., Cutting Force Sensing in Milling Process, *International CIRP/VDI-Conference on Monitoring of Machining and Forming Processes*, (1995), pp. 319-333.

- [125] Aoyama, H., Inasaki, I., Ohzeki, H. and Machine, A., Development of a Sensor Utilizing a Magnetostrictive Effect for Detecting Cutting Torque in the Milling Process, *2nd International Abrasive Technology Conference*, (1995), pp. 428-433.
- [126] Ohzeki, H., Machine, A., Aoyama, H. and Inasaki, I., Development of a Magnetostrictive Torque Sensor for Milling Process Monitoring, *1997 ASME International Mechanical Engineering Congress and Exposition*, MED-Vol.6-1 (1997), pp. 129-136.
- [127] Aoyama, H., Suda, I., Inasaki, I., Ohzeki, H. and Machine, A., Monitoring of Tool Wear and Tool Failure by Cutting Torque in Milling Process, *International Conference on Manufacturing Milestones toward the 21st Century*, (1997), pp. 101-106.
- [128] Aoyama, H., Inasaki, I., Suda, I. and Ohzeki, H., Prediction of Tool Wear and Tool Failure in Milling by Utilizing Magnetostrictive Torque Sensor, *26th North American Manufacturing Research Conference*, (1998), pp. 125-130.
- [129] Aoyama, H., Inasaki, I., Ohzeki, H. and Suda, I., Modeling of the Milling Processes Based on the Form-Shaping Theory, *CIRP International Workshop on Modeling of Machining Operations*, (1998), pp. 387-395.
- [130] Ohzeki, H., Suda, I. and Machine, A., Monitoring of Tool Failure in Drilling by Utilizing Magnetostrictive Torque Sensor, *Second International Workshop on Intelligent Manufacturing Systems 1999*, (1999), pp. 787-794.
- [131] Aoyama, H., Murashita, H., Ishii, T. and Ohzeki, H., Basic Research on Development of Magnetostrictive Sensor for Detecting Cutting Force, *14th American Society for Precision Engineering Annual Meeting*, Vol.20 (1999), pp. 256-259.
- [132] Aoyama, H., Amemiya, A., Inasaki, I. and Ohzeki, H., Basic Study on Development of Sensor to Detect Cutting Force Components Based on Villari Effect, *28th North American Manufacturing Research Conference*, (2000), pp. 323-328.
- [133] Hagiwara, M., Mano, Y., Hamada, M., Nunogami, K. and Ohzeki, H., Development of a New Torque Cell System for Torque/clamp Force Testing for Threaded Fasteners in accordance with ISO 16047, *The 3rd International*

*Conference on Manufacturing, Machine Design and Tribology*, (2009), p. 35.

- [134] Ohzeki, H. and Arai, F., Basic Study on Feedback Control of Glass Cutting Processes Based on Cutting Forces, *4th CIRP International Conference on High Performance Cutting*, Vol.1 (2010), pp. 85-90.
- [135] Ohzeki, H., Hoshi, H., Hasumi, Y. and Arai, F., Drilling of CFRP laminate with feedback control based on cutting force, *The 4th International Conference on Manufacturing, Machine Design and Tribology*, (2011), pp. 53-54.
- [136] Ohzeki, H. and Arai, F., Drilling of Borosilicate Glass with Feedback Control Based on Cutting Force, *14th International Symposium on Advances in Abrasive Technology*, (2011), pp. 442-448.

